

EFFECTS OF NUMERICAL WEATHER PREDICTIONS
ON WIND POWER FORECASTS

A THESIS SUBMITTED TO
THE GRADUATE SCHOOL OF NATURAL AND APPLIED SCIENCES
OF
MIDDLE EAST TECHNICAL UNIVERSITY

BY

İREM IŞIK ÇETİN

IN PARTIAL FULFILLMENT OF THE REQUIREMENTS
FOR
THE DEGREE OF MASTER OF SCIENCE
IN
EARTH SYSTEM SCIENCE

JUNE 2018

Approval of the thesis:

**EFFECTS OF NUMERICAL WEATHER PREDICTIONS
ON WIND POWER FORECASTS**

submitted by **İREM İŞİK ÇETİN** in partial fulfillment of the requirements for the degree of **Master of Science in Earth System Science, Middle East Technical University** by,

Prof. Dr. Halil Kalıpçılar
Dean, Graduate School of **Natural and Applied Sciences**

Prof. Dr. Can Bilgin
Head of Department, **Earth System Science**

Prof. Dr. İsmail Yücel
Supervisor, **Civil Engineering Dept./
Earth System Science, METU**

Prof. Dr. Ramazan Sarı
Co-Supervisor, **Business Administration Dept./
Earth System Science, METU**

Examining Committee Members:

Assoc. Prof. Dr. Mustafa Tuğrul Yılmaz
Civil Engineering Department, METU

Prof. Dr. İsmail Yücel
Supervisor, Civil Engineering Department /
Earth System Science, METU

Assist. Prof. Dr. Hakan Aksu
Meteorological Engineering Department, Ondokuz Mayıs
University

Date: 22.06.2018

I hereby declare that all information in this document has been obtained and presented in accordance with academic rules and ethical conduct. I also declare that, as required by these rules and conduct, I have fully cited and referenced all material and results that are not original to this work.

Name, Last Name: İrem IŞIK ÇETİN

Signature

ABSTRACT

EFFECTS OF NUMERICAL WEATHER PREDICTIONS ON WIND POWER FORECASTS

Işık Çetin, İrem
M.S., Department of Earth System Science
Supervisor: Prof. Dr. İsmail Yücel
Co-Supervisor: Prof. Dr. Ramazan Sarı

June 2018, 183 pages

Wind energy investments are rapidly increasing in Turkey. The prediction of the electrical power generated from the wind is also gaining importance in this field because of the complexity of meteorological parameter wind. In this context, Wind Energy Monitoring and Forecasting Center (RITM) project has been initiated within the scope of the General Directorate of Renewable Energy (YEGM), in 2010. The final hourly wind energy predictions are generated by using the combination of the production data from Wind Power Plants and different numerical weather prediction models with this project. In this Thesis Study, 6 Wind Power Plants are selected according to their high wind potential and their terrain structure (complex or flat) from 3 geographical regions (Marmara, Mediterranean, Aegean) in Turkey. The terrain structures of Wind Power Plants are determined by using Geographical Information System Models which give two maps: digital elevation and roughness.

The long term (3-4 year) observed wind speed data of the wind power plants from each region are compared with 3 different Meso Scale Numerical Weather Forecast Model (ECMWF, GFS, ALADIN) outputs and final wind power predictions which mean a combination of RITM power forecast system, compared to actual energy productions. The analyses are made for diurnal, seasonal, monthly basis and different grid points

that belongs to each NWP model. Obtained results which is determined by using RMSE, bias and Correlation Coefficients for each time scales are used for determining best grid points for each model. This study aims to compare the performance of each Numerical Weather Prediction Models in the RITM system which has different terrain and climate structures, at different time scales and at different energy thresholds. In addition to numerical weather prediction analysis, Turkish Electricity Market prices according to Renewable Energy Supporting Mechanism and Day Ahead Market Prices have also been calculated for 6 wind power plants in this study in order to research effects of wind power forecasts to the income and market prices. It is foreseen that the study will research and analyze the performance of different numerical weather forecasts in the wind forecasting system of different climate and terrain conditions and importance of wind power forecasts in electricity market.

Keywords: Wind power, short term wind power forecast, numerical weather prediction, renewable energy

ÖZ

SAYISAL HAVA TAHMİNLERİNİN RÜZGAR ENERJİ TAHMİNLERİNE ETKİLERİ

Işık Çetin, İrem
Yüksek Lisans., Yer Sistem Bilimleri Bölümü
Tez Yöneticisi: Prof. Dr. İsmail Yücel
Ortak Tez Yöneticisi: Prof. Dr. Ramazan Sarı

Haziran 2018, 183 sayfa

Ülkemizde rüzgar enerjisi yatırımları hızla artmaktadır. Karmaşık meteorolojik bir parametre olan rüzgârdan üretilen elektriksel güç tahminleri de bu alanda önem kazanmaktadır. Bu kapsamda 2010 yılında Yenilenebilir Enerji Genel Müdürlüğü (YEGM) bünyesinde Rüzgar İzleme ve Tahmin Merkezi (RITM) projesi başlatılmıştır. Bu proje ile rüzgar santrallerine ait üretim verileri ve farklı sayısal hava tahmin modelleri kullanılarak bu modellerin kombinasyonu ile saatlik nihai tahminler üretilmektedir. Bu tez çalışmasında Türkiye’de bulunan rüzgar potansiyeli yüksek ve farklı iklim durumlarına sahip 3 coğrafi bölgeden (Marmara, Ege, Akdeniz Bölgeleri), arazi yapısına göre kompleks ve düz arazi durumları olmak üzere 2’şer örnek Rüzgar Enerjisi Santrali seçilmiştir. Santrallerin arazi yapıları bir CBS (Coğrafi bilgi Sistemi) yazılımından pürüzlülük ve digital yükseklik haritaları çıkartılarak belirlenmiştir. Her bir bölgeden seçilen santrallerin uzun dönem (3-4 yıllık) üretim verileri, RITM sistemindeki 3 farklı Orta Ölçekli Sayısal Hava Tahmin Modeli (ECMWF, GFS, ALADIN) girdileri sonucu üretilen rüzgar hızları gerçek ölçüm verileri ve RITM tahminleri sonucu elde edilen nihai güç tahminleri gerçek üretim (MW) verileri ile karşılaştırılmıştır. Karşılaştırmalar aylık, mevsimsel, günlük ve saatlik bazda farklı grid noktaları için yapılmıştır.

Her bir zaman dilimi için hesaplanan RMSE, bias ve korelasyon katsayılarından elde edilen sonuçlar her modele ait en iyi gridi belirlemede kullanılmıştır. Bu çalışma ile RITM sistemindeki her bir Sayısal Hava Tahmin Modelinin farklı arazi ve iklim yapılarında, farklı mevsimsel dönemlerde ve değişen enerji eşik değerlerindeki başarılarının karşılaştırılması amaçlanmaktadır. Sayısal hava tahminlerinin analizlerine ilave olarak, rüzgar güç tahminlerinin gelir ve piyasa fiyatlarına olan etkilerini araştırmak amacıyla bu çalışmada yer alan 6 Rüzgar Enerji Santrali için Yenilenebilir Enerji Kaynaklarını Destekleme Mekanizmasından ve Gün öncesi piyasadan kazandıkları gelirleri de ayrıca hesaplanmıştır. Çalışma ile farklı sayısal hava tahmin verilerinin farklı iklim ve arazi koşullarındaki rüzgar tahmin sistemindeki performansının araştırılması ve rüzgar tahminlerinin piyasadaki öneminin analiz edilmesi öngörülmektedir.

Anahtar Kelimeler: Rüzgar enerjisi, kısa dönem rüzgar enerji tahminleri, sayısal hava tahmini, yenilenebilir enerji

ACKNOWLEDGEMENTS

I would like to thank my supervisor, Prof. Dr. İsmail YÜCEL, for his patience, guidance and support. I would have never been able to complete the study without his precious contributions and encouragement. I would like to thank to my co-supervisor Prof. Dr. Ramazan SARI for his comments and advices on my thesis.

I would like to express my gratitude and appreciation to General Directorate of Renewable Energy. I would like to thank members of RITM Project that gave me the opportunity to collect data for my graduate study.

I would like to thank my sister, Göksu IŞIK, for her support, critical comments and always being there for me. I also would like to thank my husband Sinan ÇETİN for his patience and support. I would like to thank my parents Ertan IŞIK and Hatice IŞIK for their encouragements and supports.

The wind power production, prediction and numerical weather prediction data (GFS, ECMWF and ALADIN) data were received from GDRE. Due to the agreement between WPP owners and GDRE names of WPPs weren't shared.

to my family

TABLE OF CONTENTS

ABSTRACT.....	v
ÖZ	vii
ACKNOWLEDGEMENTS	ix
DEDICATION	x
TABLE OF CONTENTS.....	xi
LIST OF TABLES	xiv
LIST OF FIGURES	xv
LIST OF ABBREVIATIONS	xix
CHAPTERS	
1. INTRODUCTION	1
1.1. Formation of Winds.....	3
1.2. Wind Power.....	5
1.3. Wind Power Forecasts.....	5
1.3.1. Methods.....	7
1.3.2. Wind Power Monitoring and Forecasting Center in Turkey.....	10
1.4. Turkish Electricity Market	13
1.5. Literature Review of Relevant Topics.....	18
1.6. The significance of the study.....	21
1.7. The Thesis format.....	21
2. METHODS AND DATA.....	23
2.1. General Information	23

2.2. Data.....	24
2.2.1. Numerical Weather Prediction Data	24
2.2.2. Observation Data	25
2.2.3. Power Data.....	26
2.3. Methods and Software	28
2.4. General Characteristics of Wind Power Plants in This Study.....	30
2.4.1. Climate and Wind Potential of Turkey	31
2.4.2. Aegean Region.....	32
2.4.3. Marmara Region	40
2.4.4. Mediterranean Region.....	49
3. DATA ANALYSIS AND RESULTS	59
3.1. WPP-1.....	60
3.1.1. Evaluation of Wind Speeds at Monthly, Daily, and Hourly Time Scales.....	60
3.1.2. Diurnal Variation.....	70
3.1.3. Energy Comparison.....	75
3.2. WPP-2.....	78
3.2.1. Evaluation of Wind Speeds at Monthly, Daily, and Hourly Time Scales.....	78
3.2.2. Diurnal Variation.....	88
3.2.3. Energy Comparison	92
3.3. WPP-3.....	95
3.3.1. Evaluation of Wind Speeds at Monthly, Daily, and Hourly Time Scales.....	96
3.3.2. Diurnal Variation.....	104
3.3.3. Energy Comparison.....	108
3.4. WPP-4.....	111

3.4.1. Evaluation of Wind Speeds at Monthly, Daily, and Hourly Time Scales	111
3.4.2. Diurnal Variation	120
3.4.3. Energy Comparison	124
3.5. WPP-5	127
3.5.1. Evaluation of Wind Speeds at Monthly, Daily, and Hourly Time Scales	127
3.5.2. Diurnal Variation	137
3.5.3. Energy Comparison.....	141
3.6. WPP-6	144
3.6.1. Evaluation of Wind Speeds at Monthly, Daily, and Hourly Time Scales.....	145
3.6.2. Diurnal Variation	153
3.6.3. Energy Comparison.....	158
4. REGIONAL AND GENERAL EVALUATION OF ALL WPPS.....	163
5. EVALUATION OF INCOME AND WIND POWER FORECASTS.....	171
5.1. Diurnal Variation of Income	171
5.2. Monthly Variation of Income	173
6. SUMMARY, CONCLUSIONS and RECOMMENDATIONS.....	175
REFERENCES.....	179

LIST OF TABLES

Table 1-1 Annex-1 of the Law [40].....	16
Table 1-2 Annex II of the Law [40]	17
Table 2-1 General Information about WPPs	23
Table 2-2 Grid Point Heights above the Sea Level for all NWP Models.....	25
Table 2-3 WOS Parameters and Measurement Heights	26
Table 2-4 Data Availability	27
Table 2-5 Turbine Characteristics about WPPs.....	28
Table 2-6 WPP-1 Data information.....	34
Table 2-7 Meteorological Parameters	35
Table 2-8 WPP-2 Data information.....	38
Table 2-9 Meteorological Parameters of WPP-2.....	39
Table 2-10 WPP-3 Data information.....	43
Table 2-11 Meteorological Parameters of WPP-2.....	43
Table 2-12 WPP-4 Data Information	47
Table 2-13 Meteorological Parameters for WPP-4	48
Table 2-14 Data Information for WPP-5.....	52
Table 2-15 Meteorological Parameters for WPP-5	52
Table 2-16 Data Information for WPP-6.....	56
Table 2-17 Meteorological Information for WPP-6.....	57
Table 3-1 Seasonal bias, RMSE and Correlation Coefficients for all models and grids from hourly data.....	69
Table 3-2 Seasonal bias, RMSE and Correlation Coefficients for all models and grids from hourly data.....	87
Table 3-3 Seasonal bias, RMSE and Correlation Coefficients for all models and grids from hourly data.....	103
Table 3-4 Seasonal bias, RMSE and Correlation Coefficients for all models and grids from hourly data.....	119
Table 3-5 Seasonal bias, RMSE and Correlation Coefficients for all models and grids from hourly data.....	136
Table 3-6 Seasonal bias, RMSE and Correlation Coefficients for all models and grids from hourly data.....	152
Table 4-1 Summary of all results for each WPP	169

LIST OF FIGURES

Figure 1.1 World and Turkey Wind Energy Growth between 2012 and 2017 [3] [4].....	2
Figure 1.2 Earth's Wind Patterns [9].....	4
Figure 1.3 The Architecture of the RITM Project [31].....	11
Figure 1.4 Turkish Electricity Market Structure	14
Figure 2.1 Turbine Power Curve [9].....	30
Figure 2.2 Koppen Climate Specification [58].....	31
Figure 2.3 Turkey Wind Speed Potential Distribution Map at 100 m.a.g.l [59].....	32
Figure 2.4 Elevation Map of WPP-1.....	33
Figure 2.5 Roughness Map of WPP-1	33
Figure 2.6 Wind Rose for WPP-1	35
Figure 2.7 Location of WPP-1 turbines, Grid Points and WOS	36
Figure 2.8 Elevation Map for WPP-2	37
Figure 2.9 Roughness Map for WPP-2	37
Figure 2.10 Wind Rose for WPP-2	39
Figure 2.11 Location of WPP-2 Turbines, Grid Points and WOS	40
Figure 2.12 Elevation Map for WPP-3	41
Figure 2.13 Roughness Map for WPP-3	42
Figure 2.14 Wind Rose for WPP-3	44
Figure 2.15 Location of WPP-3 turbines, Grid Points and WOS	45
Figure 2.16 Elevation Map for WPP-4	46
Figure 2.17 Roughness Map for WPP-4	46
Figure 2.18 Wind Rose for WPP-4	48
Figure 2.19 Location of WPP-4 turbines, Grid Points and WOS	49
Figure 2.20 Elevation Map for WPP-5	50
Figure 2.21 Roughness Map for WPP-5	51
Figure 2.22 Wind Rose for WPP-5	53
Figure 2.23 Location of WPP-5 turbines, Grid Points and WOS	54
Figure 2.24 Elevation Map for WPP-6	55
Figure 2.25 Roughness Map for WPP-6	55
Figure 2.26 Wind Rose for WPP-6	57
Figure 2.27 Location of WPP-6 turbines, Grid Points and WOS	58
Figure 3.1 Seasonal Wind Rose from observed data (WPP-1)	61
Figure 3.2 Wind Rose for all Grids (WPP-1).....	62
Figure 3.3 Monthly Wind Speed Profile (WPP-1).....	63
Figure 3.4 Daily Avg. Scatter Plot for ALADIN Predictions (WPP-1).....	64
Figure 3.5 Daily Avg. Scatter Plot for GFS Predictions (WPP-1).....	65

Figure 3.6 Daily Avg. Scatter Plot for ECMWF Predictions (WPP-1).....	66
Figure 3.7 Daily Avarage Time Series of all NWP and Observation data (WPP-1).....	67
Figure 3.8 Diurnal Temperature by seasonally for the best grids (WPP-1)	71
Figure 3.9 Diurnal Wind Speed by Seasonally for the best grids (WPP-1)	72
Figure 3.10 Diurnal Cycles for RMSE of Wind Speed (WPP-1).....	73
Figure 3.11 Diurnal Cycles for bias of Wind Speed (WPP-1)	74
Figure 3.12 Diurnal Cycles for Correlation Coefficient of Wind Speed and Predictions (WPP-1).....	75
Figure 3.13 The Relationship between Observed Wind Speed and Produced Power (WPP-1)	76
Figure 3.14 Diurnal Cycle for Energy and Wind Speed (WPP-1)	77
Figure 3.15 Monthly RMSE for Wind Speed Predictions (WPP-1).....	78
Figure 3.16 Seasonal Wind Rose (WPP-2)	79
Figure 3.17 Wind Rose for all Grids (WPP-2).....	80
Figure 3.18 Monthly Average Wind Speed Profile (WPP-2).....	81
Figure 3.19 Daily Avg. Scatter Plot for ALADIN Predictions (WPP-2)	82
Figure 3.20 Daily Avg. Scatter Plot for GFS Predictions (WPP-2)	83
Figure 3.21 Daily Avg. Scatter Plot for ECMWF Predictions (WPP-2).....	84
Figure 3.22 Daily Avarage Time Series of all NWP and Observation data (WPP-2).....	85
Figure 3.23 Diurnal Temperature by seasonally for the best grids (WPP-2)	88
Figure 3.24 Diurnal Wind Speed by Seasonally for the best grids (WPP-2)	89
Figure 3.25 Diurnal Cycles for RMSE of Wind Speed (WPP-2).....	90
Figure 3.26 Diurnal Cycles for bias of Wind Speed (WPP-2)	91
Figure 3.27 Diurnal Cycles for Correlation Coefficient of Wind Speed and Predictions (WPP-2).....	92
Figure 3.28 Relationship between Observed Wind Speed and Produced Power (WPP-2)....	93
Figure 3.29 Diurnal Cycle for Energy and Wind Speed (WPP-2)	94
Figure 3.30 Monthly RMSE for Wind Speed Predictions (WPP-2).....	95
Figure 3.31 Seasonal Wind Rose (WPP-3)	96
Figure 3.32 Wind Rose for All Grids (WPP-3).....	97
Figure 3.33 Monthly Average Wind Speed Values (WPP-3)	98
Figure 3.34 Daily Avg. Scatter Plot for ALADIN Predictions (WPP-3)	99
Figure 3.35 Daily Avg. Scatter Plot for GFS Predictions (WPP-3)	99
Figure 3.36 Daily Avg. Scatter Plot for ECMWF Predictions (WPP-3).....	100
Figure 3.37 Time Series of all NWP and Observation data (WPP-3).....	101
Figure 3.38 Diurnal Temperature by seasonally for the best grids (WPP-3)	104
Figure 3.39 Diurnal Wind Speed by Seasonally for the best grids (WPP-3)	105
Figure 3.40 Diurnal Cycles for RMSE of Wind Speed (WPP-3).....	106
Figure 3.41 Diurnal Cycles for Bias of Wind Speed (WPP-3).....	107

Figure 3.42 Diurnal Cycles for Correlation Coefficient of Wind Speed and Predictions (WPP-3)	108
Figure 3.43 The Relationship between Observed Wind Speed and Produced Power (WPP-3)	109
Figure 3.44 Diurnal Cycle for Energy and Wind Speed (WPP-3).....	110
Figure 3.45 Monthly RMSE for Wind Speed and Energy Predictions (WPP-3).....	111
Figure 3.46 Seasonal Wind Rose (WPP-4).....	112
Figure 3.47 Wind Rose for All Grids (WPP-4)	113
Figure 3.48 Monthly Average Wind Speeds (WPP-4).....	114
Figure 3.49 Daily Avg. Scatter Plot for ALADIN Predictions (WPP-4).....	115
Figure 3.50 Daily Avg. Scatter Plot for GFS Predictions (WPP-4).....	115
Figure 3.51 Daily Avg. Scatter Plot for ECMWF Predictions (WPP-4).....	116
Figure 3.52 Time Series of all NWP and Observation data (WPP-4).....	117
Figure 3.53 Diurnal Temperature by seasonally for the best grids (WPP-4).....	120
Figure 3.54 Diurnal Wind Speed by Seasonally for the best grids (WPP-4).....	121
Figure 3.55 Diurnal Cycles for RMSE of Wind Speed (WPP-4)	122
Figure 3.56 Diurnal Cycles for bias of Wind Speed (WPP-4).....	123
Figure 3.57 Diurnal Cycles for Correlation Coefficient of Wind Speed and Predictions (WPP-4)	124
Figure 3.58 The Relationship between Observed Wind Speed and Produced Power (WPP-4)	125
Figure 3.59 Diurnal Cycle for Energy and Wind Speed (WPP-4).....	126
Figure 3.60 Monthly RMSE for Wind Speed and Energy Predictions (WPP-4).....	127
Figure 3.61 Seasonal Wind Rose (WPP-5).....	128
Figure 3.62 Wind Rose for All Grids (WPP-5)	129
Figure 3.63 Monthly Average Wind Speed Values (WPP-5)	130
Figure 3.64 Daily Avg. Scatter Plot for ALADIN Predictions (WPP-5).....	131
Figure 3.65 Daily Avg. Scatter Plot for GFS Predictions (WPP-5).....	132
Figure 3.66 Daily Avg. Scatter Plot for ECMWF Predictions (WPP-5).....	133
Figure 3.67 Time Series of all NWP and Observation data (WPP-5).....	134
Figure 3.68 Diurnal Temperature by seasonally for the best grids (WPP-5).....	137
Figure 3.69 Diurnal Wind Speed by Seasonally for the best grids (WPP-5).....	138
Figure 3.70 Diurnal Cycles for RMSE of Wind Speed (WPP-5)	139
Figure 3.71 Diurnal Cycles for bias of Wind Speed (WPP-5).....	140
Figure 3.72 Diurnal Cycles for Correlation Coefficient of Wind Speed and Predictions (WPP-5)	141
Figure 3.73 The relationship between Observed Wind Speed and Produced Power (WPP-5)	142
Figure 3.74 Diurnal Cycle for Energy and Wind Speed (WPP-5).....	143

Figure 3.75 Monthly RMSE for Wind Speed and Energy Predictions (WPP-5)	144
Figure 3.76 Seasonal Wind Rose (WPP-6)	145
Figure 3.77 Wind Rose for All Grids (WPP-6)	146
Figure 3.78 Monthly Average Wind Speed Values (WPP-6)	147
Figure 3.79 Daily Avg. Scatter Plot for ALADIN Predictions (WPP-6)	148
Figure 3.80 Daily Avg. Scatter Plot for GFS Predictions (WPP-6)	149
Figure 3.81 Daily Avg. Scatter Plot for ECMWF Predictions (WPP-6).....	149
Figure 3.82 Time Series of all NWP and Observation data (WPP-6)	150
Figure 3.83 Diurnal Temperature by seasonally for the best grids (WPP-6)	153
Figure 3.84 Diurnal Wind Speed by Seasonally for the best grids (WPP-6)	155
Figure 3.85 Diurnal Cycles for RMSE of Wind Speed (WPP-6).....	156
Figure 3.86 Diurnal Cycles for bias of Wind Speed (WPP-6)	157
Figure 3.87 Diurnal Cycles for Correlation Coefficient of Wind Speed and Predictions (WPP-6).....	158
Figure 3.88 The relationship between Observed Wind Speed and Produced Power (WPP-6)	159
Figure 3.89 Diurnal Cycle for Energy and Wind Speed (WPP-6)	160
Figure 3.90 Monthly RMSE for Wind Speed and Energy Predictions (WPP-6)	161
Figure 4.1 Regional Evaluation for all WPPs	164
Figure 4.2 Daily Average RMSE for the best grids for all WPPs	165
Figure 4.3 Daily Average Bias for the best grids for all WPPs.....	166
Figure 4.4 Daily Average NRMSE for Wind Power.....	167
Figure 4.5 Diurnal NRMSE for all WPPs	167
Figure 4.6 Diurnal NBias for All WPPs.....	168
Figure 5.1 Diurnal Variation of Market Prices (2012-2017).....	172
Figure 5.2 Diurnal Variation of Income for all WPPs.....	173
Figure 5.3 Monthly Average Variation of Income	174

LIST OF ABBREVIATIONS

- ALADIN: Meso-scale Numerical Weather Prediction Model from Meteo-France
- CFD: Computational Fluid Dynamics
- DAMP: Day Ahead Market Prices
- ECMWF: The European Centre for Medium-Range Weather Forecasts
- EMRA: Energy Market Regulatory Authority (Republic of Turkey)
- EPIAS: Energy Exchange Istanbul
- EXIST: Energy Exchange Istanbul
- GDRE: Republic of Turkey General Directorate of Renewable Energy
- GFS: Global Forecast System
- GHG: Greenhouse Gases
- IPCC: Intergovernmental Panel on Climate Change
- m.a.g.l.: meter above the ground level
- m.a.s.l: meter above the sea level
- MCP: Market Clearing Price
- NRMSE: Normalized Root Mean Square Error
- NWP: Numerical Weather Prediction
- PBL: Planetary Boundary Layer
- RITM: Wind Power Monitoring and Forecasting Center in Turkey (Rüzgar İzleme ve Tahmin Merkezi)
- RMSE: Root Mean Square Error
- SCADA: Supervisory Control and Data Acquisition
- SMP: System Marginal Prices
- SRTM: Shuttle Radar Topography Mission
- TEIAS: Transmission Operator in Turkey
- TUBITAK: The Scientific and Technological Research Council of Turkey
- WOS: Wind Observation Station
- WPP: Wind Power Plant

WRF: Weather Research and Forecast

YEKDEM: Renewable Energy Resources Supporting Mechanism

YSU: Yonsei University

CHAPTER 1

1. INTRODUCTION

Increasing CO₂ emissions lead to Climate Change and especially in the last decades, government policies have started to change in order to reduce Green House Gas emissions. Researches and technological developments show that canalizing renewables instead of fossil fuels are apt to decrease CO₂ emissions. The report of IPCC: Renewable Energy Sources and Climate Change Mitigation advise that for decreasing GHG emissions Wind Energy has important potential and smaller environmental footprint when compared to other resources. In addition, many studies have investigated and different scenarios for a long term have been evaluated by IPCC and it is agreed that wind energy will have a great role in the future to reduce GHG emissions. If it is thought that not only electricity supply and demand but also CO₂ and GHG emissions will increase in the near future. Integrating renewables to the traditional grids is difficult because of the unavailability of the resource [1].

It is estimated that wind energy will be significant for many countries in the future since the current electricity systems depend mostly on conventional power plants. There are big differences between wind and these other resources. The unification of wind into the traditional electricity systems requires more significant disputes [2]. However, wind energy share in the electricity markets is dramatically increasing both in the World and in Turkey. Figure 1.1 shows the Total Installed Capacity of the World and Turkey that increased rapidly from 2012 to 2017 [3]. Today, Turkey's installed wind power capacity is approximately 6872 MW by the end of 2017 [4]. Besides, Turkey's total installed energy capacity is 83275 MW and the share of wind energy is approximately % 8 of total installed capacity [5]. The installed capacity of the wind energy has started to increase dramatically in the last decade similarly to the world trends. According to Electricity Energy Market and Security of Supply Strategy

Document, Turkey aims to reach to 20000 MW installed wind energy capacity in 2023 [6].

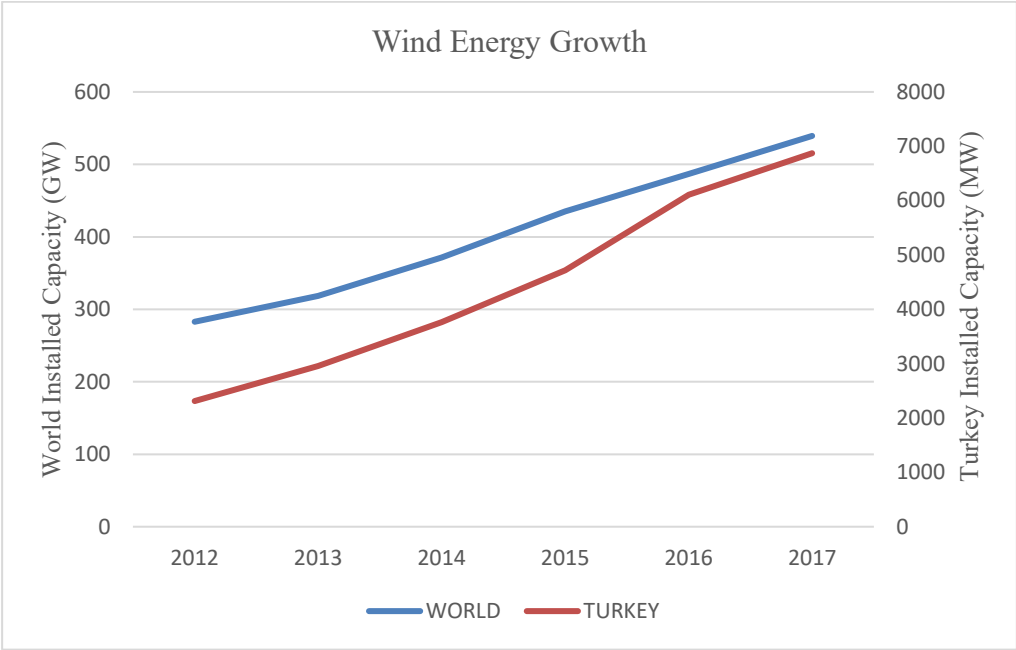


Figure 1.1 World and Turkey Wind Energy Growth between 2012 and 2017 [3], [4]

Integration of wind energy to the electricity systems has to be taken into account for trustworthy and economic grid management due to the nature of wind. According to IPCC Special Report, these three challenges have to be considered for integration:

- Regional wind resource effects and effects of wind resource over not only continental wind power plants but also offshore wind power plants transmission
- Instable wind energy production on a different time scale
- High error rates on forecasting wind power output compared to other energy resources.

Wind farms that is located in several different locations effects the instability of wind energy. It means if the wind farms are far away from each other, it will be expected

that their production relationship could not be so relevant. Besides, longer time variability could have more predictable output than a shorter time variability. In order to manage reliable and more economical electric transmission, wind resource has to be determined by using modern simulation models [1].

Short term wind power forecasts which made for day ahead markets are significant for stakeholders of wind power systems. Better forecasts are required for supply security and operational costs and the grid managers, public authorities, electrical distributors, wind power owners and electricity dealers [7].

For the reasons that mentioned above, Turkey has developed a project for predicting and monitoring all wind power plants in Turkey. This study aims to analyze Turkish Wind Power Monitoring and Forecasting Center's predictions for selected 6 Wind Power Plants which have the longest data, are distributed over different geographical regions and different complexity. The study mostly focuses on Numerical Weather Prediction Model outputs which are used in RITM Prediction System.

1.1. Formation of Winds

The synthesis of both meteorology and practice of climatology and geophysical fluid dynamics expressed the forecasted power which is produced by wind energy [8]. The Sun is the initial source for wind and other renewable energies [9]. The reason is irregular heating of earth surface that causes different pressure sources. The equator region absorbs more global radiation than Polar Regions because of incoming solar radiation [9], [10]. Solar radiation and rotation of the earth are the two primary components of the general circulation of the atmosphere [11]. These circulations have an impact on pressure differences which move from high pressure to low pressure areas. Figure 1.2 explains the earth's wind circulation; surface winds are affected by these wind patterns according to their surface structure. "*Pressure forces*", the "*Coriolis force*" (reasoned from earth's rotation), "*inertial forces due to large-scale*

circular motion”, and “*frictional forces at the earth’s surface*” are the four atmospheric forces that drive the motion of winds [9].

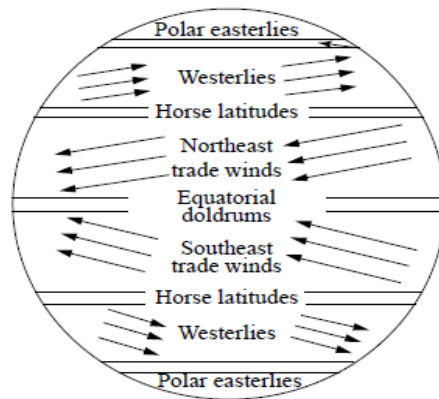


Figure 1.2 Earth's Wind Patterns [9]

In addition to this global circulation pattern, earth geographical structure which includes continental and aquatic surfaces are significantly impact the distribution of atmospheric circulation. The motion of atmosphere has been affected by these surfaces through three different ways:

- 1) Pressure differences
- 2) Solar radiation absorption
- 3) Available humidity in the air

Smaller circulations such as hurricanes; monsoon circulation and extratropical cyclones take place due to the heat changes at high and low pressure centers. Land and sea breezes; valley and mountain winds; monsoon-like flow; foehn winds; thunderstorms; tornadoes come off from local winds on a smaller scale. These types of motions arise from heating of surfaces due to the topographic structure at smaller time scale [9]. For example, land breeze occurs at night time for the reason that the land cooling is quicker than the sea. Cooler air on the land moves over the land from

the sea. Sea breeze also occurs vice versa. These motions are resulted from regional winds [10].

Topography affects the wind, which is closer to earth surface. “*Orography, roughness and shelter*” are three important components of these effects [8]. Roughness generally refers to vegetation of a terrain. Obstacles are the reasons of lower wind speed on a terrain which means shelter [12].

1.2. Wind Power

Following equation explains available wind power and the relationship between the wind speed and the produced power of the wind energy. The P (kW) in the equation is power, A (m²) is an area where the rotor of turbine detected and V (m/s) is wind speed and the ρ (kg/m³) density of the air.

$$P = \frac{1}{2} \times A \times \rho \times V^3 \quad (1)$$

This equation indicates that the wind power is proportional to the increase in the density of the air and the area swept by the rotor. Past studies show the wind speed dominates the produced power. It is also seen that wind speed of the air is the most effective source of wind power [9].

1.3. Wind Power Forecasts

Traditional power plants produce energy based on the demand, however, wind power plants produce energy according to the existence of wind, which leads to instability on the power outputs. The most significant distinction between wind and traditional energy resources could be explained in this way. Hence, balancing supply and demand becomes important for large penetrated wind energy electricity systems [13].

Wind Power Forecasts have become important because of the managing electrical grids and operational planning. It is hard to manage embedded Wind Energy systems due to the complex nature and variability of the wind. Reduced wind power forecast errors provides a better planning for transmission managers and power system integrations of wind reduce the risks [14]. It is a well-known fact that precise and steady wind power forecasts help to improve enhancing installed wind power [15]. “Day ahead forecast”, “day ahead market”, “unit commitment”, “real time operation” and “market settlement” are 5 components of classical operation for an electricity system. Day ahead market and forecast requires hourly predictions one day before. Unit commitment requires planning and real time operation requires regulating real power as in daytime [16]. Intra day and day ahead markets could be more comprehensive with well-developed wind forecasting technology [15].

As a result of that, many research done and applications have been performed during last decades wind penetrated market and transmission design techniques [16], [17], [18], [19]. Many countries which already have large wind penetration have improved their wind power forecasting methods and systems by using different approaches to control and manage their system and grids [13].

Wind power forecasts are evaluated in the literature according to four time scales. [20], [21], [22],[23]. *Ultra-short term forecasts* produce their forecasts within a few minutes that expands to 1 hour at most. This type of wind energy forecasts is mostly used for “electricity market clearing”, “real time grid operations” and “regulation actions”. Secondly, *Short Term Forecasts* range from 1 hour to several hours. The application areas of short term forecasts are “economic load dispatch planning”, “load reasonable decisions”, “operational security in electricity markets”. Thirdly, *Medium Term Forecasts* are used for “unit commitment decisions”, “reserve requirement decisions” and “generator online/offline decisions”. The range of medium term forecasts expands to several hours to a week. Finally, Long Term wind power forecasts that predict to wind from 1 week to 1 year or more, are used to “maintain planning”, “operation

management”, “optimal operating costs” and “feasibility study for design of the wind farm” [23].

1.3.1. Methods

This study aims to focus mostly on short term wind forecasts which are up to 48 hours for the day ahead markets. Therefore short term prediction methods in the literature are explained below.

1.3.1.1. Statistical Models

Statistical Methods are used for short term wind energy forecasting [15]. These models examine a large amount of data and do not determine atmospheric conditions elaborately. In addition, using recorded power data to predict wind energy power based on the relationship between power and meteorological data. The initial data could be transformed into power output through the statistical method. Thus, these methods are named as “black box”. Some of the statistical methods are as in the following: autoregressive (AR), moving average (MA), autoregressive moving average model (ARMA) and autoregressive integrated moving average model (ARIMA), the Box-Jenkins methodology and Kalman filtering, artificial neural networks (ANN), fuzzy systems, gray predictors or support vector machines (SVM). ANN and SVM methods use learning approach method which profit from predicted wind and historical power relationship [14].

1.3.1.2. Physical Models

Atmospheric and geological conditions such as terrain, obstacle, pressure, and temperature are used in these models to predict wind speed. They could sometimes use statistical model as input to predict the wind energy [24].

Physical models are based mostly on observed meteorological data or weather prediction outputs, which require more technological systems. The lower atmosphere should be evaluated exhaustively for predicting wind power[14]. Because of the high resolution of Numerical Weather Prediction (NWP) models, in order to predict better the local effects coming from orography, roughness, near-by obstacles and the presence of other wind turbines they have to be taken into account [8]. For modeling irregular landscape, wind algorithms could be examined under two subcategories; dynamic and climatic models which are not successful to figure out clearly momentum and energy equations. Another physical model is Computational Fluid Dynamics (CFD) that is used to set regional situation on a terrain [14].

1.3.1.3. Hybrid Models

Hybrid Models aim to utilize advantages of other models (statistical, physical etc.) and acquire most favorable universal prediction accomplishment. Hybrid Models are aggregation of various types of forecasting models. These types could be explained by 3 categories; namely, combination of physical and statistical approaches, combination of models for the short term and medium term, and combination of alternative statistical models [15].

1.3.1.4. Numerical Weather Prediction Models

Since atmospheric scientists have started to use Numerical Weather Prediction (NWP) models by predicting macro or meso-scale weather events, the use of short term generated wind power prediction becomes challenging. Therefore, while the NWP models solve the conservation and momentum equations computationally, topographic information should be used in NWP models to get better description of land-surface atmosphere interaction. On the other hand, model output statistics could be applied to the outputs of NWP Models [24].

NWP models takes into account many effects over a wind farm. For example; they are obstacles, roughness, orography, speed up or down, scaling of the local wind speed within wind farms, wind farm layouts, and wind turbines power curves [15].

Wind speed predictions for enclosing grid points over the wind power plant are supplied by NWP systems. Due to the large spatial resolution of NWP Models, wind speed forecasts have to reduce the micro scale of the wind farm (downscaling). The downscaling provided by meso-scale or micro scale model from the physical method can further improve wind power forecasts around the wind power plant. These types of models also need terrain information of a modeled wind farm. More complex flow models such as CFD or MM5 (Mesoscale Model) are used to calculate wind speed predictions and they give a better solution for modeling wind flow [25].

Three main components are included in NWP models; “the dynamic center”; “the physical equations” and “the information gathering software code”. Adiabatic non-viscous flows are described in the dynamic center, meteorological variability processes and information gathering software code are represented in the physical equations. This means that all atmospheric information at a given time is represented in the NWP models. Not only electrical industry utilizes NWP Models, but also a variety of industries, sectors and public utilities utilize the outputs of NWP Models.

Many NWP model have been developed according to regional weather conditions. These are ETA model (hydrostatic), HIRLAM, ALADIN and MM5 and the Weather Research and Forecast (WRF) Model, HRM, COSMO [26].

1.3.2. Wind Power Monitoring and Forecasting Center in Turkey

Turkey's Wind Power Monitoring and Forecasting Center project (shortly called RITM with Turkish Acronym) has been started in 2010 within the scope of Ministry of Energy and Natural Resources/GDRE. The Scientific and Technological Research Council of Turkey (TUBITAK), Turkish State of Meteorology and General Directorate of Renewable Energy are the stakeholders of the project [27]. RITM legislation was published in February 2015 and has imposed an obligation for all Wind Power Plants (WPPs), which have 10 MW or higher installed capacity to connect the RITM system [28]. Currently, 148 WPPs have been integrated into RITM system. While the total installed capacity of Turkey is 6872 MW, RITM has 6518 MW installed capacity which means that nearly all wind power generations have been integrated to the center. Integrating macro-scale wind farms to the project are the major purpose of the project [27].

The targets of the project are to integrate all wind power plants in Turkey to the RITM system, provide forecasts for their wind power, and minimizing prediction error. RITM serves to transmission system operators and also WPP owners and public authorities with the other different similar regional forecast and control centers. Short term and very short term forecasts are produced by RITM system via using several data and forecasting modules [29].The stakeholder of system could reach the monitoring and forecasting data through the internet [30].

1.3.2.1. Forecast system of RITM Project

Terciyani et al (2013) describes the RITM System as three main parts; *Data Acquisition, Data Storage and Processing, Data Presentation: Graphical User Interface*. Figure 1.3 explains the main forecast structure of RITM forecast system [31]. *Data Acquisition*; Four different resources send their data to the center. These data are; NWP output data from three different sources, Supervisory Control and Data Acquisition (SCADA) data, and Meteorological Observation data from 6 Wind Observation Stations (WOS) and Wind Power Data from wind power analyzers [29], [31]. European Center of Medium Range Weather Forecasting (ECMWF) and Global Forecast System (GFS) data are used as an initial condition of Weather Research and Forecast Model (WRF) and ALADIN Model output data come from the Turkish State of Meteorology. The servers located in General Directorate of Renewable Energy (GDRE) both stores the data coming from ALADIN and WRF. Data Storage and Processing and includes several hybrid forecasting algorithms that are kept operational. The final part provides an easier utilization of outputs for the described RITM users [31].

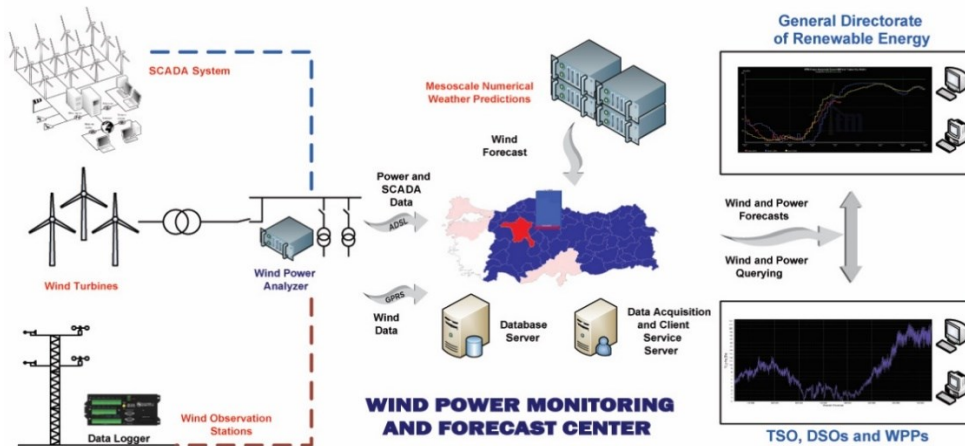


Figure 1.3 The Architecture of the RITM Project [31]

Figure 1.3 also explains that each WPP sends their real time power data through the SCADA system or Power Quality Analyzer (PQA) device which is developed by TUBITAK. SCADA system includes wind velocity, wind direction, turbine status and power data. PQA includes wind power and other electrical power data. Meteorological masts also send their wind velocity, wind direction, pressure, relative humidity and temperature values [31]. However, Meteorological Masts are not compulsory for wind farms. 7 meteorological towers were built at first phase of the project for 7 wind farms. Those data are also used for research and validation purposes of model outputs.

1.3.2.2. Forecast Modules on RITM System

Because of the significant usage areas of forecasts, RITM system has designed the combination of many forecast models [32],[33],[34],[35]. The day-ahead market, intra-day market and real-time load balancing are the areas of usage for RITM forecasts [31].

In Forecast modules, the outputs of Global Forecast System (GFS) and ECMWF atmospheric circulation models are used to provide initial and boundary conditions for Weather Research and Forecast Model (WRF). ALADIN Model outputs are also used for power predictions. ALADIN model is operated at Turkish State of Meteorology (MGM with Turkish Acronym) servers and its outputs come directly from there while WRF Model is configured in RITM servers and run four times a day[31], [32].

The results of the NWP models are evaluated and clustered through the k-means algorithm that is called Statistical Hybrid Wind Power Forecast (SHWIP). The SHWIP is based on a calculation of Normalized Mean Absolute Error (NMAE) for wind speed over 100 grids points around each WPP for which a power curve is assigned. The power curve of each WPP is obtained from physical model (based on computational fluid dynamics) and SHWIP model is used for choosing best grid point which has the lowest NMAE that has been chosen according to historical data. The details of model are explained in [32].

At the same time ANN, SVM and linear regression models are run [35]. Finally, hybrid forecasts are produced by using all of the model outputs. All models are combined based on the three combination methods; Lp-norm, FSS (Fuzzy Soft Sets) and tree based combination [34].

According to the first results of the project; an error rate per WPP is changing between 8-16 % NMAE and yearly performance of all WPPs is approximately 5 % NMAE [31]. In addition to the short term forecasts, “very short term forecasts” are produced for every hour by using direct time series models for intra-day market purposes [36].

All of this algorithms and system structure were built by TUBITAK MAM Institute of Energy. The aim of this study is to evaluate and compare the performances of three different NWP Models of RITM system in forecasting the wind power.

The detailed information and studies about the project are explained in [29] ~ [37].

1.4. Turkish Electricity Market

Turkish Electricity Market contains Production, Transmission, Distribution, Wholesale and Retail, Market Operating, Import and Export Activities. Both public and private legal entities that have a licence could make production activities. TEIAS (Turkey Electricity Transmission Joint Stock Company-Turkish acronym) is responsible for transmission activities. Distribution activities are carried out by distribution companies who have a licence for their local regions. Wholesale and Retail activities are managed by production and supply companies. Operating Market activities are carried out by EXIST. (Energy Exchange İstanbul). While the import activities are followed by supply and production companies, export activities could be supervised by supply companies [38].

Turkish Electricity Market is managed by two operators; System Operator which is called TEIAS and market operator; named EXIST. These two operators are determined by Electricity Market Law as it mentioned above. TEIAS is responsible for investments about electricity transmissions, planning, distribution of loads and

frequency control, operating balancing power market and international interconnection workings. EXIST has been dependently settling down purview of Law on Electricity Market and Law on Turkish Trade at 18 March 2015 [38]. According to Balancing and Reconciliation Regulation: TEIAS and EXIST carry out balancing mechanism activities and necessary procedures and principles for these activities in order to balance the supply and demand of electricity by providing all necessary coordination and communication. [39]

Turkey’s Electricity Market Structure is made up of three different markets; a day ahead, intraday and Balancing Power Market. EXIST is responsible for the day ahead and intraday markets and their balance, TEIAS is responsible for real time balancing. Electricity trade is started one day before in Day Ahead Market; also market prices are determined according to supply demand balances [39]. Figure 1.4 explains the market structure of Turkish Electricity Market. Market Clearing Price (MCP) is determined according to the demand and supply balance.

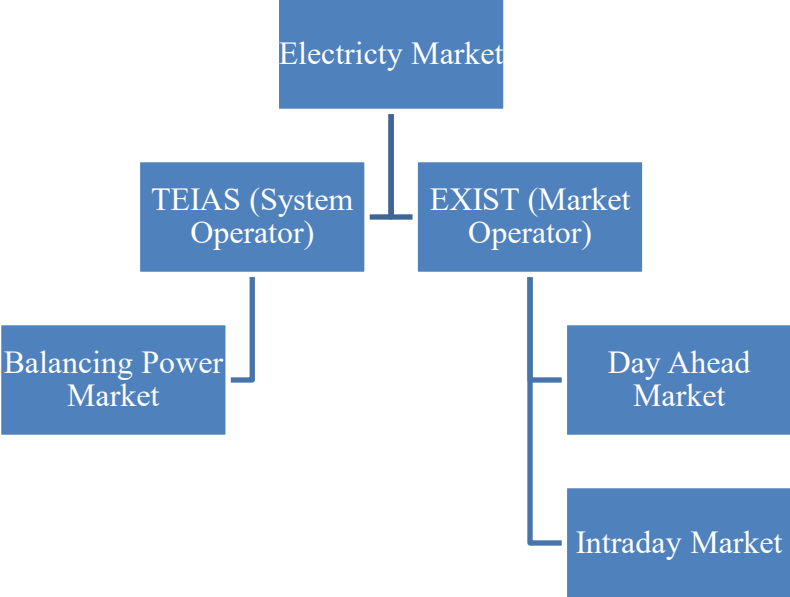


Figure 1.4 Turkish Electricity Market Structure

Electricity trades on Electricity Markets occur in Day Ahead and Intraday Market.

Day Ahead Market: Electricity trade is occurred one day before. A day ahead market include hourly offers which start at 00:00 am and finishes at 00:00 am every day for the next day. Each participant makes their offer until 11:30 am for next day [39]. The market based on Balancing and Reconciliation Regulation.

Intraday Market: The electricity spot price is set on an hourly basis. It starts every day at 00:00 am and ends at 00:00 am. It is a continuous type of market [39].

Supporting Mechanism of Renewable Energy Resources

Renewable energy resources are evaluated in a different type of supporting mechanism according to Law on Utilization of Renewable Energy Sources for The Purpose of Generating Electrical Energy. The purpose of this law ***“is to expand the utilization of renewable energy sources for generating electric energy, to benefit from these resources in a secure, economic and qualified manner, to increase the diversification of energy resources, to reduce greenhouse gas emissions, to assess waste products, to protect the environment and to develop the related manufacturing industries for realizing these objectives”*** [40]. Due to the law, Renewable Energy Resources certification has been given to the electricity producer in order to determine the type of resources. Moreover, production companies which are subject to Supporting Mechanism of Renewable Energy Resources that is called YEKDEM (Turkish Acronym) have electricity sales guarantee according to the prices Annex-1 of the Law depending on their resources for a period of 10 years. Table 1.1. explains these prices and shows the Wind Power Production companies that could sell their electricity from 7.3 Dollar cent/kWh.

Table 1-1 Annex-1 of the Law [40]

Annex-I	
Type of Production Facility Based on Renewable Energy Resources	Prices Applicable (US Dollar cent/kWh)
a. Hydroelectric production facility	7,3
b. Wind power based production facility	7,3
c. Geothermal power based production facility	10,5
d. Biomass based production facility (including landfill gas)	13,3
e. Solar power based production facility	13,3

In addition to these prices, the prices that join in Annex-2 are supplemented in the event that the wind turbine/renewable energy resource unit components are domestically produced. Table 1.2 shows the additional prices for wind power based production facilities. For example if a wind farm is included in YEKDEM and used domestic wing in their facility, this WPP could sell their electricity (7.3 + 0.8) 8.1 Dollar cent / kWh. According to EMRA (Energy Market Regulatory Authority) data, 151 WPPs will benefit from YEKDEM prices during 2018 [40].

Table 1-2 Annex II of the Law [40]

Annex II		
(Provision of the law dated 29/12/2010 and numbered 6094)		
Type of Facility	Domestic Production	Domestic Contribution (US Dollar cent/kWh)
B- Wind power based production facility	1- Blade	0,8
	2- Generator and power electronics	1,0
	3- Turbine tower	0,6
	4- All of the mechanical equipment in rotor and nacelle groups (excluding payments made for the wing group and the generator and power electronics.)	1,3

The details of supporting renewables in Turkey are regulated by **Regulation on Certification and Support of Renewable Energy Resources**. The income of each production facility has been calculated according to given formula [41]

$$YEKBED_i = \sum_{b=1}^n \sum_{t=1}^l \sum_{u=1}^k (UEVM_{i,b,u} \times [(YEKF_{i,b} \times KUR_u) - PTF_{t,u} \times j]) \quad (2)$$

[41]

YEKBED_i: For an invoicing period, the price of the Renewable Energy Resources that will be paid to the participant or to the market operator by the participant. **UEVM_{i,b,u}**: the amount of power supply which is produced by “b” power supply/draw unit based on reconciliation within the scope of YEKDEM and which belongs to “i” YEKDEM participant for “u” reconciliation period (MWh). **YEKF_{i,b}**: the price that will apply “I” YEKDEM participant for “b” power supply/draw unit based on reconciliation

(USD/MWh), KUR_u : The current CBRT foreign exchange buying rate on the day when the “u” settlement period is included. $PTF_{t,u}$: Market Clearing Price that belongs to “t” offer region and “u” reconciliation period (TL/MWh). k : number of settlement periods that belongs to the bill region. l : number of offer region. j : tolerance coefficient which is determined by EMRA. n : number of power supply/draw unit based on reconciliation within the scope of YEKDEM which belongs to I YEKDEM participant [41].

The income of an electricity production facility within the corps of YEKDEM started to be calculated according to the formula above with the changes made by the regulation that is published on 29th of April 2016. As the plants that have been included into YEKDEM are over 15 GW now, the income formula of YEKDEM is changed as in the following, in order for the party, which caused the imbalance, to take the responsibility for it and in order to minimize these imbalances, which could occur within the system. According to that, j coefficient is to be fixed by EMRA. “ j ” is updated as 0.97 in 2018 after the publication of regulation, at the time of which it was 0.98 [42].

All WPPs in this study are participants of YEKDEM. For this reason, income calculations of WPPs have been made according to the formula above. Market clearing and system marginal prices have been taken from EPIAS. YEKDEM and Day-Ahead Market Prices (DAMP) have been calculated and evaluated in Chapter 5.

1.5. Literature Review of Relevant Topics

The following literature is summarized as they are found the most relevant studies to the study performed in this thesis:

- ***Dabernig, M. (2013). Comparison of different numerical weather prediction models as input for statistical wind power forecasts (Doctoral dissertation, University of Innsbruck).***

Three different NWP models (deterministic and probabilistic ECMWF and GEFS from Austria) were compared by applying MOS (Model Output Statistics) to results of selected 7 turbines in Austria. MOS methods were used for minimizing NWP errors, Fitted regression as a MOS method were applied by using real measurement data and NWP model outputs. In order to determine the differences on NWP models, revenue on Austria Energy Market, RMSE that belongs to each WPP were calculated. Deterministic and probabilistic ECMWF results found better values than GEFS model. It was also concluded that performance of MOS depends on initial weather data. Revenue showed different results than RMSE, nearly all NWP models had same revenue. However, revenue with two ECMWF models were found better than GEFS [43].

- ***Bielecki M.F., “Statistical Characterization of Errors in Wind Power Forecasting,” 2010.***

WPP production and commercial deterministic prediction data were compared in a selected WPP in Northwestern United States. Ramp events are also examined by using RAMP identification algorithm. In order to evaluate wind power forecasts, traditional error analysis was made (mean bias, mean absolute error, and root mean square of the error) and discussed. In addition to this, error metrics, delta pdf, correlation coefficient are also presented and discussed [44].

- ***SĪLE, T., et al. Verification of numerical weather prediction model results for energy applications in Latvia. Energy Procedia, 2014, 59: 213-220.***

WRF Model outputs for 172 grid points in central Latvia were compared to 24 observation stations in between May and November 2013. GFS data had been used for

initial data of WRF. Bias and RMSE were used to compare differences between model and observation. Model outputs were mostly resulted as overestimated [45].

- ***ALESSANDRINI, S.; SPERATI, S.; PINSON, Pierre. A comparison between the ECMWF and COSMO Ensemble Prediction Systems applied to short-term wind power forecasting on real data. Applied energy, 2013, 107: 271-280.***

The performances of two different NWP initial data (COSMO LEPS and ECMWF EPS) were compared. NWP data are used in a real wind power forecast in Southern Italy. Wind power forecasts had been made by using probabilistic forecast system. MOS is also applied to model outputs. Brier score and RMSE were used to evaluate the results. Cosmo LEPS showed better performance than ECMWF EPS [46].

- ***LANGE, Matthias, et al. On the uncertainty of wind power predictions-Analysis of the forecast accuracy and statistical distribution of errors. Transactions of the ASME-N-Journal of Solar Energy Engineering, 2005, 127.2: 177-184.***

Short term wind power forecasts errors and wind speed errors were evaluated in this study by using RMSE, bias. Short term forecasts had made by using NWP data and nonlinear power curve of turbine. 6 onshore WPPs had been used for this study. A relationship is found between bias and terrain type. bias showed a negative variation at a complex terrain and showed positive values at flat terrains on this study. That means, forecast errors were underestimated for complex terrain or vice versa. The most important result of this study is that relative error of power forecasts increases at the rate of 1.8–2.6 by comparing to wind speed forecasts [47].

- ***HOLTTINEN, Hannele; MIETTINEN, Jari; SILLANPÄÄ, Samuli. Wind power forecasting accuracy and uncertainty in Finland. Espoo, VTT, 2013.***

Short term wind power forecast errors and costs in the electricity market were calculated in this study. Different NWP models were combined for 6 different sites in Finland. Combination methods were also examined. Cumulative density function and

kernel densities were used for evaluation of uncertainties. The study gave an idea on the aspect of wind farm owners and an overview on informed transmission operators [48].

1.6. The significance of the study

The aim of the study is analyzing different numerical weather prediction models in a wind power forecast system and investigating behavior of the models at different time scales (diurnal, daily, monthly and seasonal). Currently wind power forecasts are performed by using 3 NWP model in RITM system, however model performances in a wind power forecast system have never been examined before in Turkey. Wind power forecast accuracy mostly depended on reliable wind speed forecasts. Therefore, determining better NWP models for different regions and time scales would be important for power forecast systems.

1.7. The Thesis format

First chapter explains the methodology about wind power forecasts and wind power monitoring and forecasting center in Turkey. Chapter 2 gives information about 6 wind power plant from 3 different geographical region. Each wind farm is evaluated in terms of data availability, elevation, roughness, regional climate conditions and installed capacity etc. Data Analyses and Results has been given in Chapter 3. Each wind farm has been evaluated at monthly, daily and diurnal time scales and energy prediction and production values have been compared to wind speeds. The results have been interpreted at Chapter 4. Chapter 5, Turkish Electricity Market prices according to Renewable Energy Supporting Mechanism and Day Ahead Market Prices have also been calculated for 6 wind power plants in this study in order to research effects of

wind power forecasts to the income and market prices. Finally, conclusions and recommendations of each analysis belongs to 6 WPP have been summarized in Chapter 6.

CHAPTER 2

2. METHODS AND DATA

2.1. General Information

Wind Power Plants (WPP) were chosen from Marmara, Aegean and Mediterranean Region in Turkey for this study. The WPPs were selected according to geographical locations, data availabilities and observation stations. Table 2.1 shows the geographical regions, installed capacities and number of turbines of each wind farm.

Table 2-1 General Information about WPPs

WPP	Installed Capacity (MW)	Geographical Region	Number of Turbines
WPP 1	120	Aegean	46
WPP 2	240	Aegean	169
WPP 3	10.2	Marmara	17
WPP 4	15	Marmara	5
WPP 5	48	Mediterranean	16
WPP 6	135	Mediterranean	54

The installed capacity of wind farms change in between 15 and 240 MW. Hub heights of turbines change in between 46 and 85 m for turbines that are used in WPPs.

2.2. Data

2.2.1. Numerical Weather Prediction Data

All NWP and observation data have been obtained from RITM Project Forecast system servers. The WRF model with the initial conditions from ECMWF and GFS is run daily in RITM system. Turkish State of Meteorology also sends daily NWP outputs through ALADIN model for 48 hours from their server to GDRE servers [31],[32]. Numerical weather prediction data had been obtained according to 4 grids which are closest to WOSs. Data times and formats were converted from Unix Time (date format that used in unix systems) to real time. Data were arranged according to WOS data. Missing values were removed in order to compare real and prediction data truly. Duplicated values for 48 hours had been removed since last 24 hours' prediction data have been updated every day.

Turkish State of Meteorology predictions are made by using ALADIN NWP Model which benefits from MeteoFrance [49]. These predictions contain wind speed, wind direction, temperature, and pressure parameters are received four times a day (00:00; 06:00, 12:00; 18:00 GMT) for 48 hours. ALADIN predictions have been made in 5 different vertical levels of atmosphere. Level 2 (approximately 100 m.a.g.l) prediction values have been used in RITM system and in this study to determine the accuracy of the forecasts.

In addition to ALADIN data, two different prediction data, WRF with initial conditions from GFS and WRF with initial conditions from ECMWF are used. A single domain covering the the entire Turkey at 6 km x 6 km grid resolution had been used for WRF predictions. YSU (Yonsei University) Planetary Boundary Layer Scheme has been used for WRF predictions which are first option of PBL options in physics for WRF [50]. WRF forecasts have also been run for 4 times a day for 48 hours similar to ALADIN forecasts [31],[32]. However, only 00:00 am predictions are used for power forecasts. WRF outputs contain many meteorological variables. Wind direction was

calculated from U and V wind speed for each grid point. RITM forecast method uses best grid selection according to the historical power data, 4 grids have been compared for available years. Table 2.2 shows the ALADIN, WRF and WOS heights above the sea level. The italic values show the nearest heights for WOS. It could be seen from the table that the highest power station is WPP-6 and the lowest power station is WPP-3, which is located on the sea level.

Table 2-2 Grid Point Heights above the Sea Level for all NWP Models

WPP	ALADIN Grid Points Heights (m.a.s.l)				WRF Grid Points Heights (m.a.s.l)				WOS Heights (m.a.s.l)
	Grid1	Grid2	Grid3	Grid4	Grid1	Grid2	Grid3	Grid 4	WOS
WPP-1	584	398	572	307	546	492	540	413	598
WPP-2	804	636	522	478	724	650	615	789	701
WPP-3	57	0	0	0	2	0	0	0	11
WPP-4	254	11	95	80	170	6	76	0	244
WPP-5	824	545	320	846	667	750	733	327	626
WPP-6	1063	1140	1025	924	1038	788	901	913	1021

2.2.2. Observation Data

The six WOSs had been established in the first phase of RITM Project. The position of each WOS corresponds to the location of each WPP. The two of them have been damaged by the extreme weather conditions. WOS have included; *Temperature, Pressure, Wind Speed, Wind Direction, Relative Humidity* at different heights. Table 2.3 shows the sensor heights from the ground. 5 of WOSs Wind Speed sensor have been located in same heights (80; 50; 65). Hub height of turbines that are used in those

wind farms are nearly 80 m, except for the WPP-2, which has 65 m hub height and WPP-3 45 m hub height. The data from sensors have been chosen according to those hub heights.

Table 2-3 WOS Parameters and Measurement Heights

Parameter	WPP-1	WPP-2	WPP-3	WPP-4	WPP-5	WPP-6
Temperature	7;80 m	9 m	7 m	9 m	10 m	10;80 m
Pressure	7 m	7 m	7 m	7 m	9 m	9 m
Wind Speed	80;50;65 m	80;50;65 m	45;30 m	80;50;65	80;50;65	80;50;65
Wind Direction	78;48 m	78 m	43;28 m	78 m	78 m	48;78 m
RH	7;80 m	9 m	7 m	9 m	10 m	10;80 m

2.2.3. Power Data

Power production data were taken from RITM main servers. Due to the fact that forecast system has not been stored in servers for power production for each NWP separately, initial data based power values could not be used in this study.

Table 2.4 shows the available data for 6 WPPs. Although prediction and production data are available for all years, all data are adjusted according to measured data, in order to compare real and prediction values truly. WPP-1 and WPP-2 have the shortest record length data since the observation station of WPP-1 has been toppled down due to the weather conditions.

Table 2-4 Data Availability

WPP	Percentage of Available Data	Available Years
WPP-1	% 51	2013, 2014, 2015, 2016
WPP-2	% 66	2012, 2013, 2014, 2015, 2016
WPP-3	% 74.6	2012, 2013, 2014, 2015, 2016
WPP-4	% 88	2012, 2013, 2014, 2015, 2016
WPP-5	% 84	2013, 2014, 2015, 2016
WPP-6	% 83	2013, 2014, 2015, 2016

Each WPP has different type of Turbine. Turbine types change according to the manufacturer, hub height, rotor diameter, turbine power and other characteristics. Table 2.5 explains the turbine power and some technical information about turbines which are used in those wind farms.

Table 2-5 Turbine Characteristics about WPPs

	Power (KW)	Hub Height (m)	Rotor Diameter (m)	Rated Wind Speed (m/s)	Cut-in Wind Speed (m/s)	Cut-out Wind Speed (m/s)
WPP 1	2500	80	90	13	3	25
WPP 2	900	65	44	17	3	25
WPP 3	600	46	40	13	3	25
WPP 4	3000	80	90	15	4	25
WPP 5	3000	80	90	17	4	25
WPP 6	2500	85	100	13.5	3.5	25

2.3. Methods and Software

In order to compare complexity of each WPP, elevation and roughness values have been determined. Geographical information has been determined by using SRTM data from approximately 30 m resolution. SRTM data have been regulated in Global Mapper arranged 20 x 20 km area [53]. Then converted grid.gws file into WindSIM version of 6.2.0 [54]. Roughness maps have been determined by using Corine 2006 land cover data and calculated with the same size as geographical data [51]. Roughness and elevation maps have been coupled up by using WASP Map Editor [52] and used in WindSIM. WindSIM calculates the roughness lengths by using information from the grid.gws files [54].

In order to understand which prediction type is better at which time, error rates belongs to NWP models have been determined. RMSE and bias calculations have been made for observation versus NWP model outputs for each NWP grid and for predicted power output versus power production values for each WPP. RMSE and bias values have been calculated for hours of the day, daily and monthly averages.

RMSE has been calculated by using wind speeds monthly, daily and diurnal averages. Equation 3 explains the RMSE formula which includes “*a*” that is an actual value (production), “*f*” is a forecasted value; “*n*” is the number of data. RMSE is widely used for Wind Forecast Accuracy studies in literature; this is because of the fact that square values of errors show bigger errors with bigger values [44]. The weight of errors is increased by using RMSE. It has also been normalized by using installed capacity of wind farms for power prediction error [48].

$$RMSE = \sqrt{\frac{1}{n} \sum_{i=1}^n (a - f)^2} \quad (3)$$

Equation 4 defines bias for forecasted and actual values. Bias is also defined as an average error. Bias shows the average difference of forecast from actual values. It determines over-under estimations [44].

$$BIAS = \sum_{i=1}^n (f - a) \quad (4)$$

Equation 5 defines correlation coefficient for two variables. It is used for determining the linear relationship between two variables [44].

$$r = \frac{\sum((a_i - \bar{a}) \times (f_i - \bar{f}))}{\sqrt{\sum (a_i - \bar{a})^2 \times \sum (f_i - \bar{f})^2}} \quad (5)$$

In order to determine the accuracy of forecasts for different time horizons; seasonal and grid comparisons have been made for this study. Both average values for time series and RMSE and bias have been calculated and compared seasonally and diurnally. In order to determine the best grid for all prediction methods; correlation coefficients have been calculated. Observation values have been also used for determining characteristics of wind farm locations.

Seasonal variation of wind speed and errors is obviously most important characteristic in Turkey. Because of this diurnal variations are examined seasonally in this chapter.

Electricity production from the wind energy totally depends on the wind speed. Therefore, energy and wind speed relationships are also examined in this study. Each wind turbine has their own power curve by depending on turbine producers. Figure 2.1 is a typical power curve of a wind turbine, it gives an idea about the produced power based on wind speed values. Cut in wind speed means required minimum wind speed to producing energy from a turbine. Rated wind speed indicates required maximum power that will be produced by the turbine. Cut out wind speed means generally harmful for the design and turbine has to be closed [9].

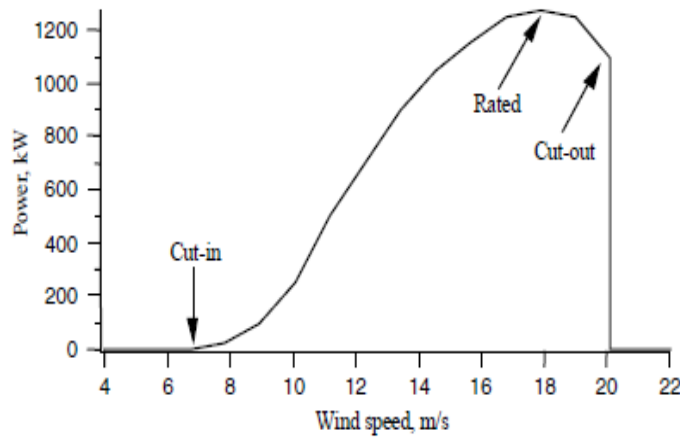


Figure 2.1 Turbine Power Curve [9]

Global Mapper, WindSIM version 6.2.0 and WASP Map Editor were used for elevation and roughness information [54]. The software licenses was procured by the General Directorate of Renewable Energy under an agreement between the GDRE, TUBITAK and the software developer. R project was used for calculating statistical and graphical results. R is an open source and a free software [55]. Windographer Version 4.0.28 trial version was used for some statistical graphical and results [56].

2.4. General Characteristics of Wind Power Plants in This Study

2.4.1. Climate and Wind Potential of Turkey

Turkey is located in subtropical zone and under the effect of Mediterranean climate type site due to geographical location. Polar air masses effects to Turkey in winter times and tropical air masses effect to Turkey in summer times. These polar and tropical air masses are localized due to both their topographical structure and marine and continental effect [57]. Figure 2.2 illustrates the Köppen Climate Classification for Turkey. All of the geographical regions in this study are in Csa type according to Köppen. It means warm winters and dry and hot summers. Generally, Köppen classifies the climates zones by taking into account monthly mean temperature and annual precipitation [58].

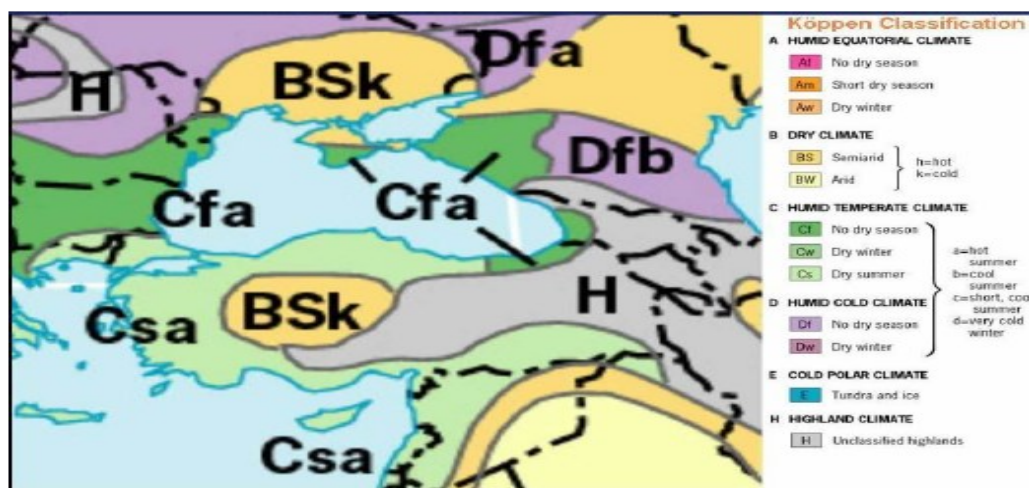


Figure 2.2 Köppen Climate Specification [58]

The following figure shows the Wind Energy Potential Atlas of Turkey annually, which was made by GDRE in 2006 [59]. The map shows the yearly mean wind speed distribution. The Northwest part of Turkey has higher wind potential when compared to other regions. WPP-1, WPP-3 and WPP-4 are in this region. All seasons have higher than 7 m/s yearly mean except spring for those WPPs [59].

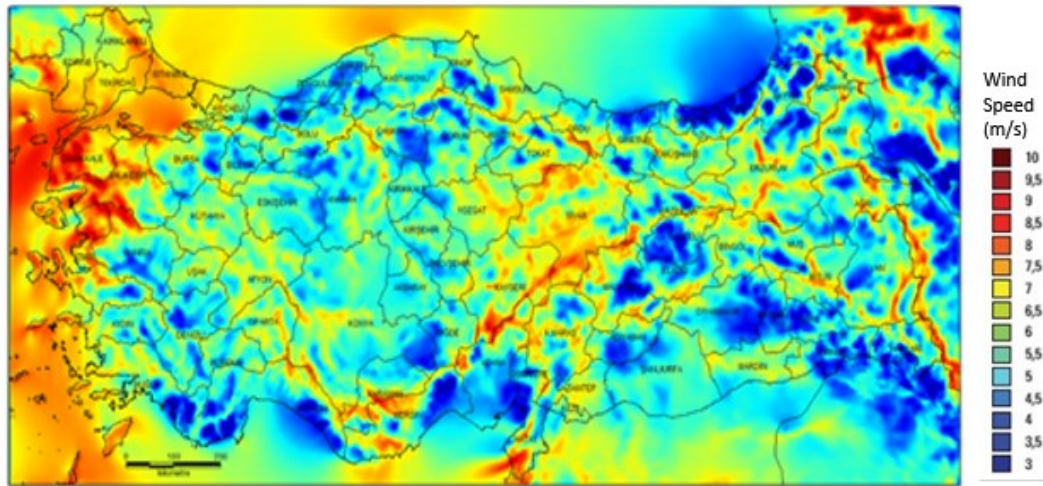


Figure 2.3 Turkey Wind Speed Potential Distribution Map at 100 m.a.g.l [59]

2.4.2. Aegean Region

Aegean Region has the highest wind energy potential in Turkey. According to Wind Energy Potential Atlas (REPA with Turkish acronym) the region has 14907 MW wind energy potential which has higher than 7.5 m/s at 50 m height above the ground [59]. Turkey has different climate types which change from region to region due to the topography. Aegean region receives more rainfall in winter times and has dry and hot summers [60]. According to Turkey Wind Energy Association, Aegean Region has 2684.25 MW installed wind power capacity at the end of 2017 which is 39 % of all over Turkey [4].

2.4.2.1. WPP-1

WPP 1 is located in Aegean Region of Turkey. Figure 2.4 and 2.5 indicate the elevation and roughness maps for WPP-1. Center of maps is WOS station.

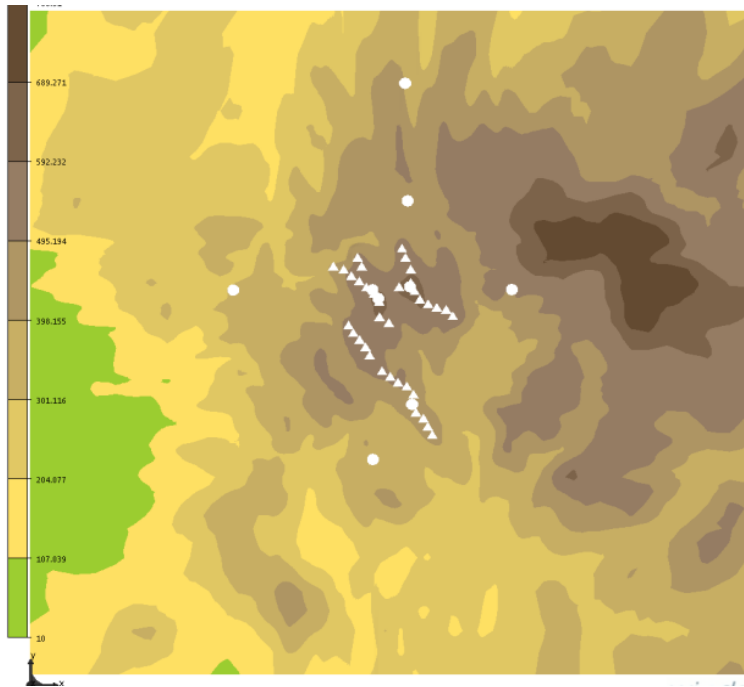


Figure 2.4 Elevation Map of WPP-1



Figure 2.5 Roughness Map of WPP-1

WPP-1 has been located in an area that is 495-689 m above the sea level. The triangles show the turbine locations and circles show the grid point locations on elevation map.

Terrain of the wind farm lacks of vegetation, and roughness height of WPP 1 changes between 0, 0001 and 0.4 m (Figure 2.4).

Meteorological averages have been obtained from WOS. The installed capacity of WPP is 120 MW which consists of 46 wind turbines. Table-2.6 gives summary information about the WPP-1, The WPP-1 has 27 months available data with 60 minutes time interval. The wind farm is located at 598 m elevation above the sea level, which influences the density of air and pressure. Available data starts from 1 Jan. 2013 during the 27 months.

Table 2-6 WPP-1 Data information

Variable	Value
Elevation	598 m
Data period	1 January 2013 00:00 15 April 2015 20:00
Duration	27 months
Length of time step	60 minutes
Mean Wind Speed	6,61 m/s

Mean, maximum and minimum values of Temperature, Air Pressure and air density could be seen from the Table 2.7. Air density has been calculated by using ideal gas equation.

$$P = \rho \cdot R \cdot T \quad (6)$$

Within the equation; P is pressure, T is temperature, R is the universal gas constant (8.314472 m³·kPa·K⁻¹·kmol⁻¹)

Table 2-7 Meteorological Parameters

	Mean	Min	Max
Temperature (°C)	13,6	-9,5	32,6
Pressure(mbar)	953,4	934,5	970
Air Density (kg/m ³)	1,16	1,08	1,28

The wind rose for WPP-1 could be seen from Figure 2.6 that explains the frequency of wind speed by 18 directions. The prevailing wind direction is NE for WPP-1 which is calculated from all WOS wind direction data.

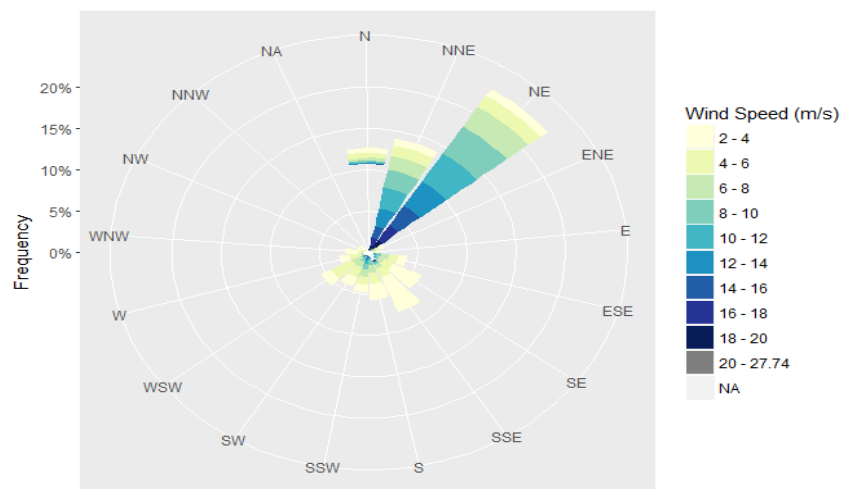


Figure 2.6 Wind Rose for WPP-1

As RITM forecast system uses nearest neighbor method for 4 grid points, Figure 2.7 shows 4 ALADIN and 4 WRF grid locations together with WOS (Obs) and turbine locations. The location of observation station is 598 m above the sea level and ALADIN Grid 1 and WRF Grid 1 have the nearest height for observation station.

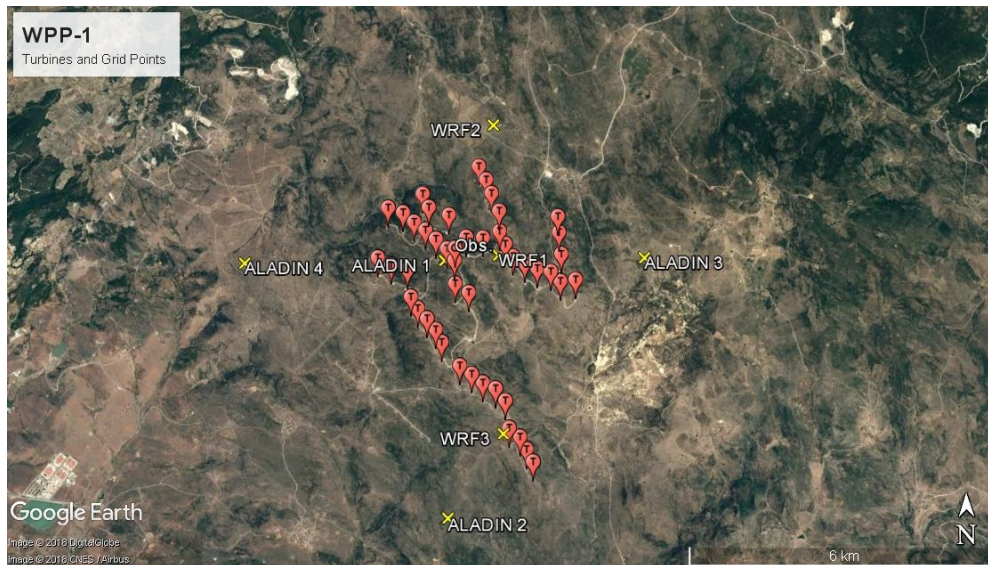


Figure 2.7 Location of WPP-1 turbines, Grid Points and WOS

2.4.2.2. WPP-2

WPP-2 is located in Aegean Region of Turkey. Figure 2.8 and 2.9 shows the elevation and roughness maps for WPP-2. Center of maps is WOS station.

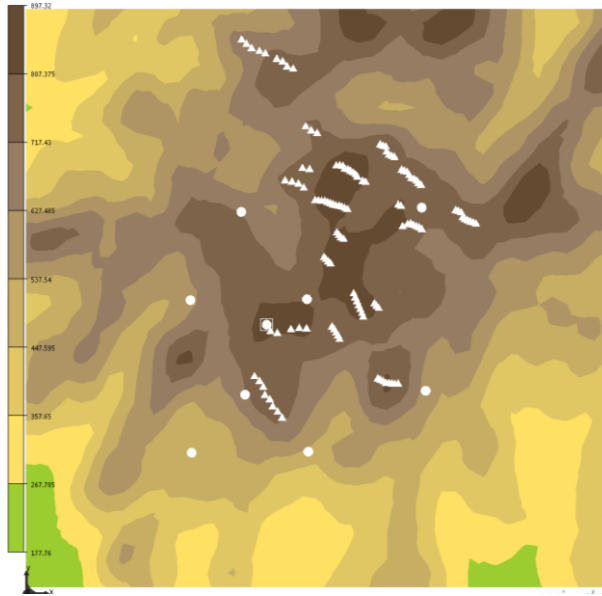


Figure 2.8 Elevation Map for WPP-2

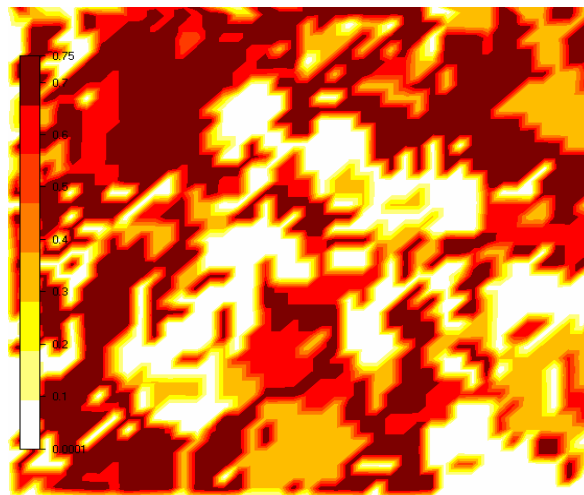


Figure 2.9 Roughness Map for WPP-2

WPP-2 turbines have been distributed over a terrain whose elevation changes between 600 and 900 m above the mean sea level. The triangles show the turbine locations and circles show the Grid point locations on elevation map (Figure 2.8). Roughness length of WPP-2 changes between 0.1-0.75 m (Figure 2.9). The roughness of WPP-2 is flexible but it is more complex than WPP-1.

The installed capacity of WPP is 240 MW which consists of 169 wind turbines. Table 2-8 gives summary information about the WPP-2, The WPP-2 has 4.1 year data with 60 minutes time interval. The WPP is located at 701 m elevation above the sea level.

Available data starts from 7 November 2012 and continues for next 4.1 years. Table 2-8 gives detailed information about WPP-2 data. WPP-2 has more available data than WPP-1.

Table 2-8 WPP-2 Data information

Variable	Value
Elevation	701 m
Data period	7 November 2012 15:00 31 December 2016 01:00
Duration	4,1 years
Length of time step	60 minutes
Mean Wind Speed	7,77 m/s

Mean, maximum and minimum values of Temperature, Air Pressure and air density could be seen from the Table 2.9.

Table 2-9 Meteorological Parameters of WPP-2

	Mean	Min	Max
Temperature (°C)	11,4	-11,2	32,0
Pressure(mbar)	922,0	899,9	938,6
Air Density (kg/m ³)	1,13	1,05	1,24

The prevailing wind direction is NNE for WPP-2 which is calculated from all WOS wind direction data. However, in contrast to WPP-1, there are different wind directions for WPP-2. It can be seen from the Figure 2.9 that, South and North directions have a low percentage but available wind speeds of this direction changes from 2 to 8 m/s which is fair enough for power production.

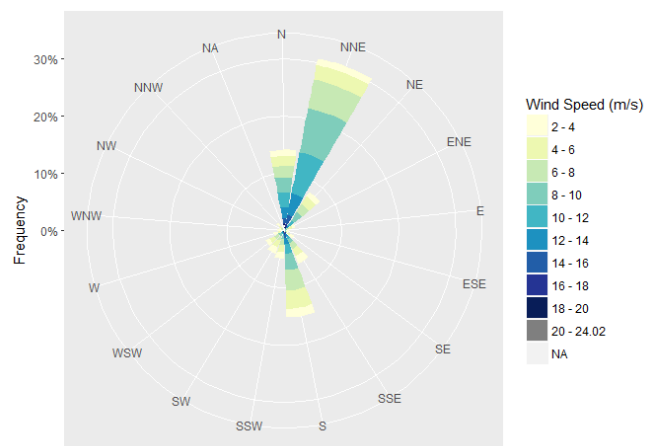


Figure 2.10 Wind Rose for WPP-2

Figure 2.11 illustrates 4 ALADIN and 4 WRF grid locations that have been pointed according to Observation Station and turbine locations. The location of observation station is 701 m above the sea level and ALADIN Point 2 and WRF Point 1 have the nearest height for observation station.

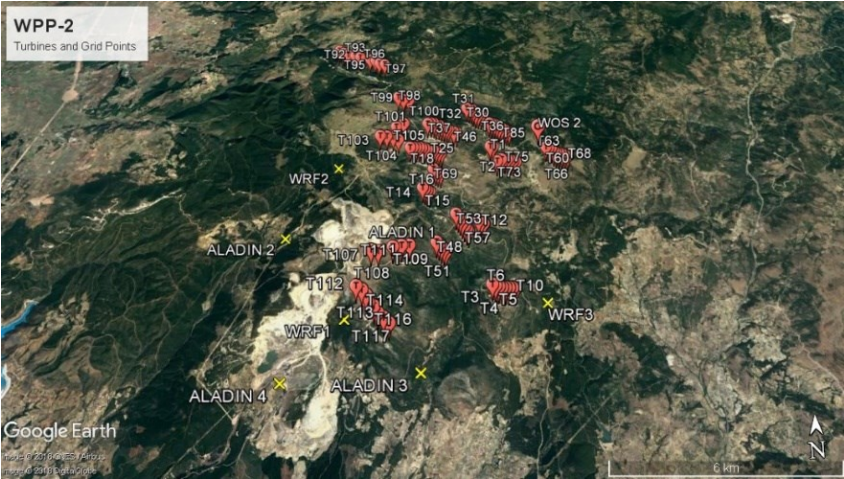


Figure 2.11 Location of WPP-2 Turbines, Grid Points and WOS

2.4.3. Marmara Region

Marmara Region has the second highest wind energy potential in Turkey. According to REPA the region has 12704 MW wind energy potential which has higher than 7.5 m/s wind speed at 50 m height above the ground [59]. Marmara region has Csa type climate according to Koppen Climate Classification [60]. According to Turkey Wind Energy Association report, Marmara Region has 2318.40 MW installed wind power capacity which is approximately 33 % of the entire Turkey [60].

2.4.3.1. WPP-3

WPP-3 is located in Marmara Region of Turkey. Figure 2.12 and 2.13 show the elevation and roughness maps for WPP-3. Center of maps is WOS station which is 10 km far away from the border of the map.

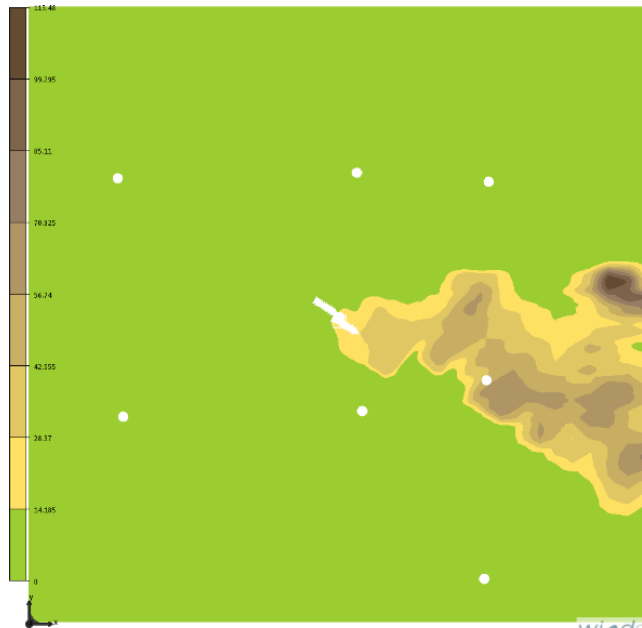


Figure 2.12 Elevation Map for WPP-3

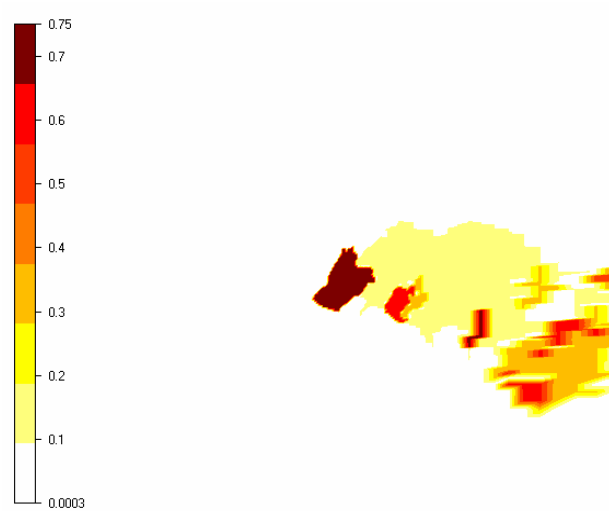


Figure 2.13 Roughness Map for WPP-3

WPP-3 is located at 0-30 m height. The triangles show the turbine locations and circles show the Grid point locations on elevation map. Roughness length of WPP-3 changes between 0.7-0.75 m. WPP-3 is near the sea level and it is quite a flat terrain.

The installed capacity of WPP-3 is 10.2 MW which consists of 17 wind turbines. Table 2-11 gives summary information about the WPP-3. The WPP-3 has 4-year available data. The data starts from 2 May 2012 and continues next 4 years. The table gives detailed information about WPP-3 data.

The wind farm is located in 45 m elevation above the sea level, which is directly influenced by the density of air and pressure. Standard sea level pressure 1013.25 mb and mean pressure of WPP-3 is 1008 mb which is closer to this value. It is already obvious that WPP-3 is located almost at the sea level.

Table 2-10 WPP-3 Data information

Variable	Value
Elevation	45 m
Data period	2 May 2012 10:00 25 April 2016 19:00
Duration	4 years
Length of time step	60 minutes
Mean Wind Speed	7.53 m/s

Mean, maximum and minimum values of Temperature, Air Pressure and air density could be seen from the Table 2-12.

Table 2-11 Meteorological Parameters of WPP-2

	Mean	Min	Max
Temperature (°C)	17,6	-4,6	34,2
Pressure(mbar)	1008,1	958,8	1031,7
Air Density (kg/m ³)	1.21	1.13	1.34

The prevailing wind direction is N for WPP-3 which is calculated from all WOS wind direction data. WPP-3's wind blows dominantly from the north as seen in Figure 2.14 and the frequency of blowing winds from the North is over the 30 %.

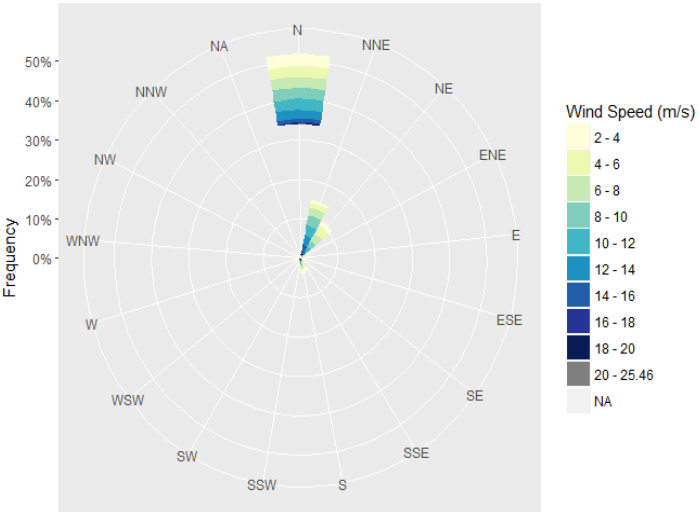


Figure 2.14 Wind Rose for WPP-3

Figure 2.15 shows that 4 ALADIN and 4 WRF grids have been pointed according to WOS and turbine locations. The location of observation station is 45 m above the sea level and nearly all points are at the sea level except ALADIN Grid 1.

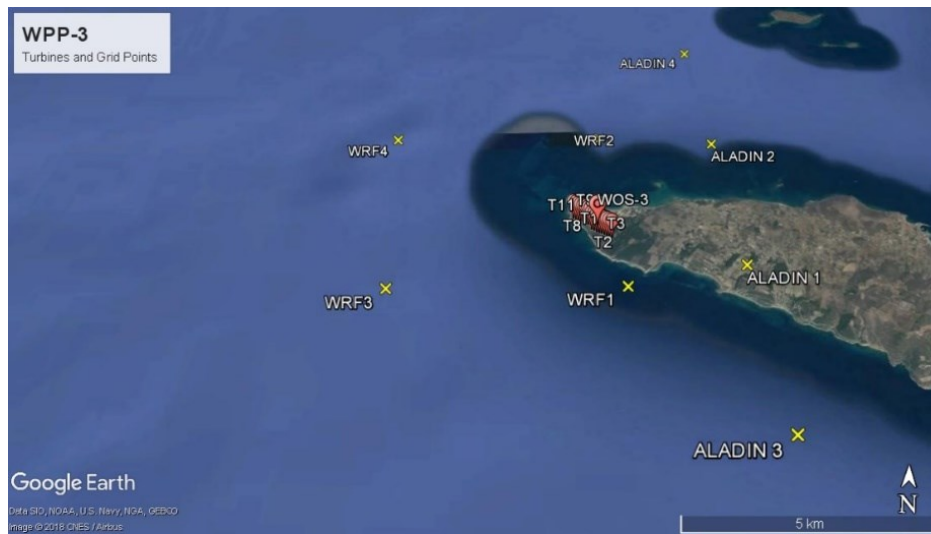


Figure 2.15 Location of WPP-3 turbines, Grid Points and WOS

2.4.3.2. WPP-4

WPP-4 is located in Marmara Region of Turkey. Figure 2.16 and 2.17 shows the elevation and roughness maps for WPP-4 respectively. Center of maps is WOS station which is 10 km far away from the border of the map.

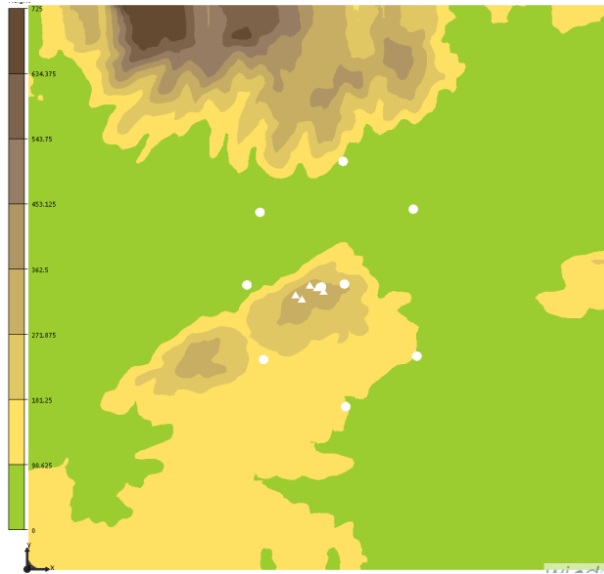


Figure 2.16 Elevation Map for WPP-4

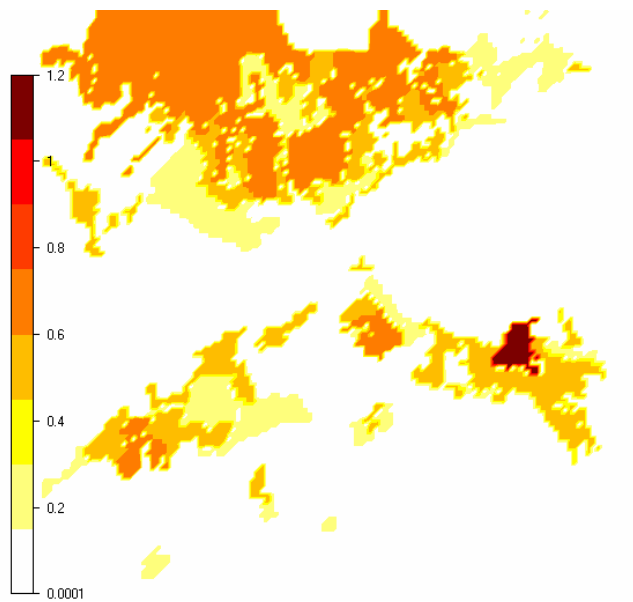


Figure 2.17 Roughness Map for WPP-4

WPP-4 is located at 240-365 m height. The triangles show the turbine locations and circles show the Grid point locations on elevation map. Roughness length of WPP-4 changes between 0.0001-0.2 m. WPP-4 is near the sea like WPP-3, but while WPP-3 is located in sea level and it has high roughness length, WPP-4 is located in higher

than the sea level but it has low roughness length. It should be noted that WPP-4 has more complex terrain than WPP-3.

The installed capacity of WPP-4 is 15 MW which consists of 5 wind turbines. Table 2-13 gives a summary information about the WPP-4. The wind farm has 4.7-year available data which have 60 minutes time interval. The data starts from 24 April 2012 and ends on 31 December 2016. The wind farm is located at 244 m elevation above the sea level.

Table 2-12 WPP-4 Data Information

Variable	Value
Elevation	244 m
Data Period	24 April 2012 11:00 31 December 2016 01:00
Duration	4.7 years
Length of time step	60 minutes
Mean Wind Speed	7,70 m/s

Mean, maximum and minimum values of Temperature, Air Pressure and air density could be seen from the Table 2.13.

Table 2-13 Meteorological Parameters for WPP-4

	Mean	Min	Max
Temperature (°C)	16,2	-5,4	32,8
Pressure(mbar)	998,1	974,7	1021,1
Air Density (kg/m ³)	1.20	1.13	1.33

The prevailing wind directions are NE and NW for WPP-4 as it is illustrated in Figure 2.18. WPP-4 has 2 different prevailing wind direction. This will be taken into account in evaluating the results.

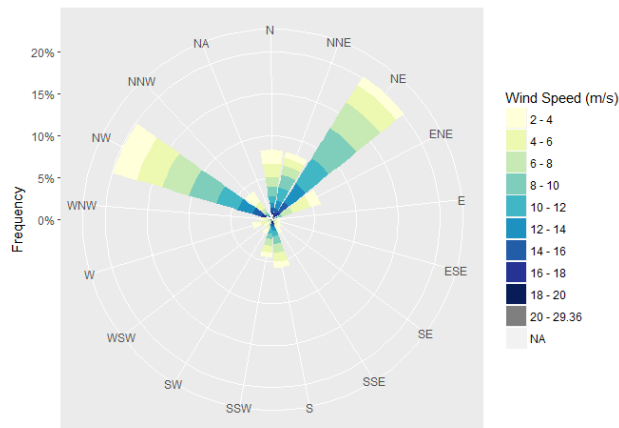


Figure 2.18 Wind Rose for WPP-4

Figure 2.19 shows that 4 ALADIN and 4 WRF grids have been pointed according to Observation Station (WOS-4) and turbine locations. The location of observation station is 244 m above the sea level. ALADIN and WRF grid 1s are closer to the location of WOS.

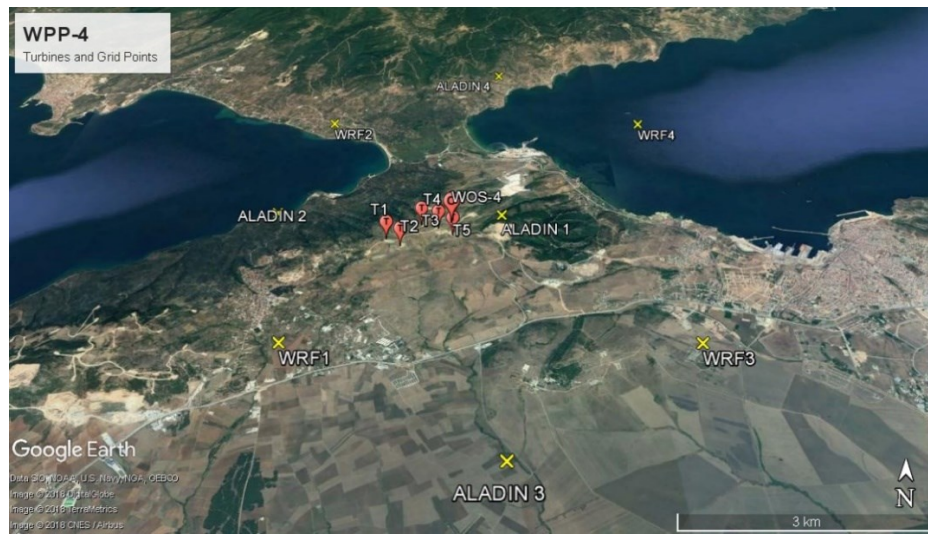


Figure 2.19 Location of WPP-4 turbines, Grid Points and WOS

WPP-4 has different geographic structure. The sea effect might be seen from NE and NW direction of the wind farm which could be explained the 2 prevailing wind directions.

2.4.4. Mediterranean Region

Mediterranean Region has the third highest wind energy potential in Turkey. According to REPA the region has 5335 MW wind energy potential which has higher than 7.5 m/s wind speed at 50 m height above the ground [59]. The region has Csa type climate according to Koppen Climate Classification [60]. Turkey Wind Energy Association report indicates that Mediterranean Region has 919.30 MW installed wind power capacity which is 13,37 % of the entire Turkey [4].

2.4.4.1. WPP-5

WPP-5 is located in Mediterranean Region of Turkey. Figure 2.20 and 2.21 shows the elevation and roughness maps for WPP-5. Center of the map is WOS station which is 10 km far away from the border of the map.

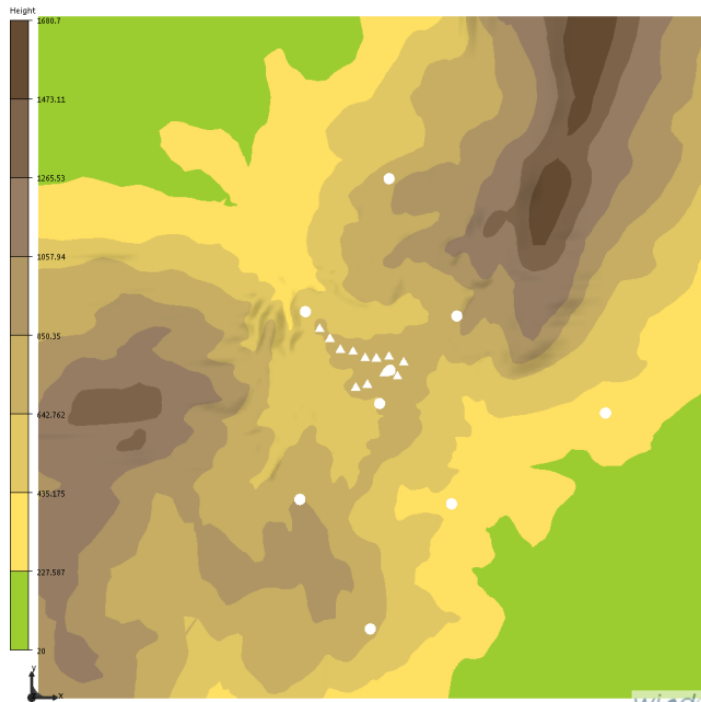


Figure 2.20 Elevation Map for WPP-5

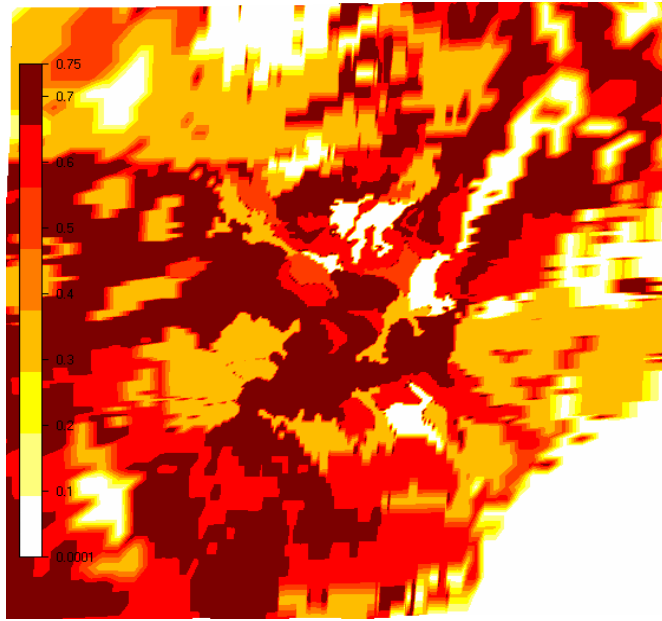


Figure 2.21 Roughness Map for WPP-5

WPP-5 is located at 640-850 m height. The triangles show the turbine locations and circles show the grid point locations on elevation map (Figure 2.20). Roughness height of WPP-5 changes between 0.6-0.75 m (Figure 2.21). WPP-5 is also surrounded by two high hills from west and southeast that are approximately over 1400 m above the sea level.

The installed capacity of WPP-5 is 48 MW which consists of 16 wind turbines. Table 2.15 gives summary information about the WPP-5 data. The wind farm has 4-year available data which have 60 minutes time interval. Available data starts from 24 April 2012 and ends on 31 December 2016.

Table 2-14 Data Information for WPP-5

Variable	Value
Elevation	626 m
Data period	1 January 2013 00:00 31 December 2016 01:00
Duration	4 years
Length of time step	60 minutes
Mean Wind Speed	8,41

Mean, maximum and minimum values of Temperature, Air Pressure and air density could be seen from the Table 2-15.

Table 2-15 Meteorological Parameters for WPP-5

	Mean	Min	Max
Temperature (°C)	14,8	-7	34
Pressure(mbar)	922,1	902,1	935,9
Air Density (kg/m ³)	1,12	1,04	1,21

The prevailing wind direction is NW for WPP-5 which is illustrated in Figure 2.22.

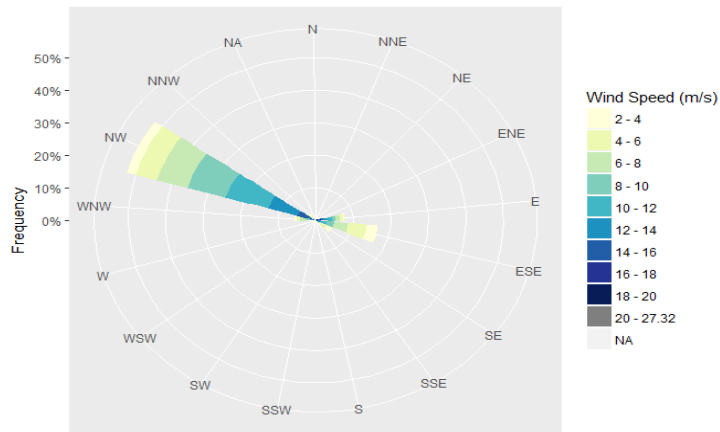


Figure 2.22 Wind Rose for WPP-5

Figure 2.23 shows that 4 ALADIN and 4 WRF grid locations have been pointed according to WOS and turbine locations in Google Earth. The location of observation station is 626 m above the sea level. ALADIN 2 and WRF 1 grid points are closer to the location of WOS. However, WOS and closest prediction points are in a kind of valley. The terrain of the wind farm is surrounded by the forest and valleys.



Figure 2.23 Location of WPP-5 turbines, Grid Points and WOS

2.4.4.2. WPP-6

WPP-6 is located in Mediterranean Region of Turkey. Figure 2.24 and 2.25 shows the elevation and roughness maps for WPP-6. Center of maps is WOS station which is 10 km far away from the border of the map.

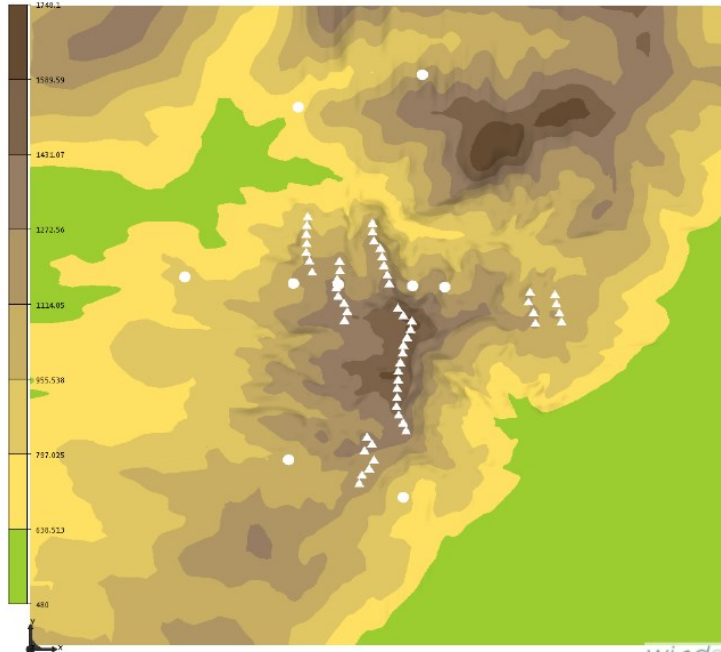


Figure 2.24 Elevation Map for WPP-6

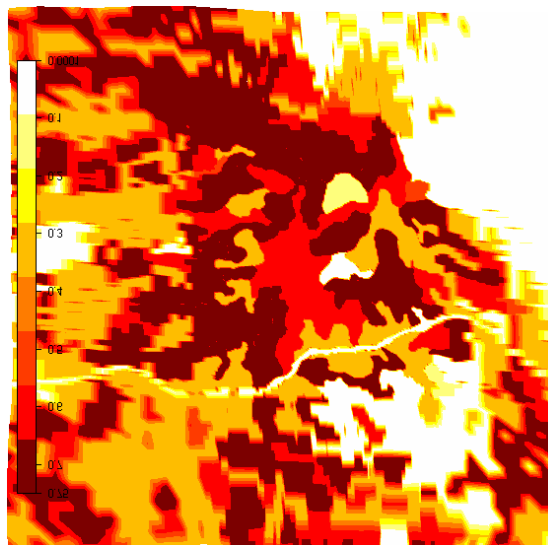


Figure 2.25 Roughness Map for WPP-6

WPP-6 is located at 790-1590 m height which is the highest WPP in this study. The triangles show the turbine locations and circles show the grid point locations on elevation map (Figure 2.24). Roughness length of WPP-6 changes between 0,5-0,75

m (see fig. 2.25). There is also a high hill which has height over the 1600 m located in the North-eastern part of the wind farm. WPP-6 is the most complex terrain and it has the highest roughness height.

The installed capacity of WPP-6 is 135 MW which consists of 54 wind turbines. Table 2-17 gives summary information about the WPP-6. The wind farm has 3.6-year available data which have 60 minutes time interval. Available data starts from 1 January 2013 and ends on 31 July 2016.

The wind farm is located in 1021 m elevation above the sea level. WPP-6 is also located in the highest terrain above the sea level in this study which means the lowest density and means pressure.

Table 2-16 Data Information for WPP-6

Variable	Value
Elevation	1021 m
Start date End date	1 January 2013 00:00 31 July 2016 14:00
Duration	3,6 years
Length of time step	60 minutes
Mean Wind Speed	5,87 m/s

Mean, maximum and minimum values of Temperature, Air Pressure and air density could be seen from the Table 2-17.

Table 2-17 Meteorological Information for WPP-6

	Mean	Min	Max
Temperature (°C)	12,8	-7,4	32,2
Pressure(mbar)	892,5	871,5	906,1
Air Density (kg/m ³)	1,09	1,02	1,17

The prevailing wind direction is W for WPP-6 which is calculated from all WOS wind direction data by using R Project that could be seen from the figure 2.26. However, it could be understood from the figure that, wind speeds are low for WPP-6.

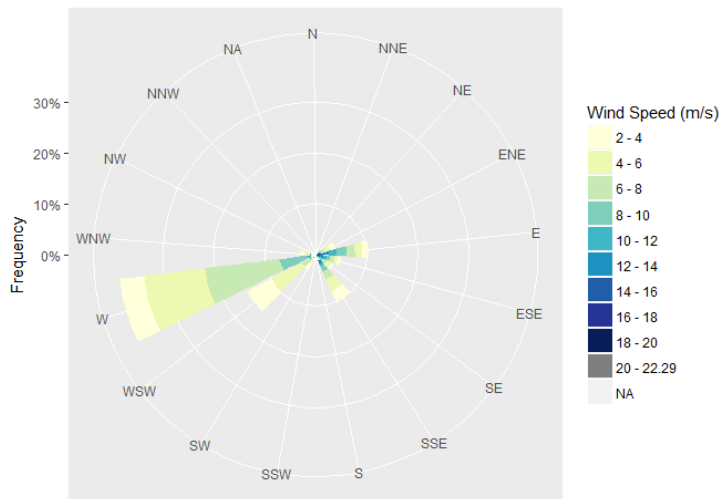


Figure 2.26 Wind Rose for WPP-6

Figure 2.27 shows that 4 ALADIN and 4 WRF grid locations that have been pointed on the map according to Observation Station and turbine locations. The location of observation station is 1021 m above the sea level. ALADIN 3 and WRF 1 grid points are the closer to the location of WOS. The terrain of the wind farm is surrounded by the maquis and valleys.

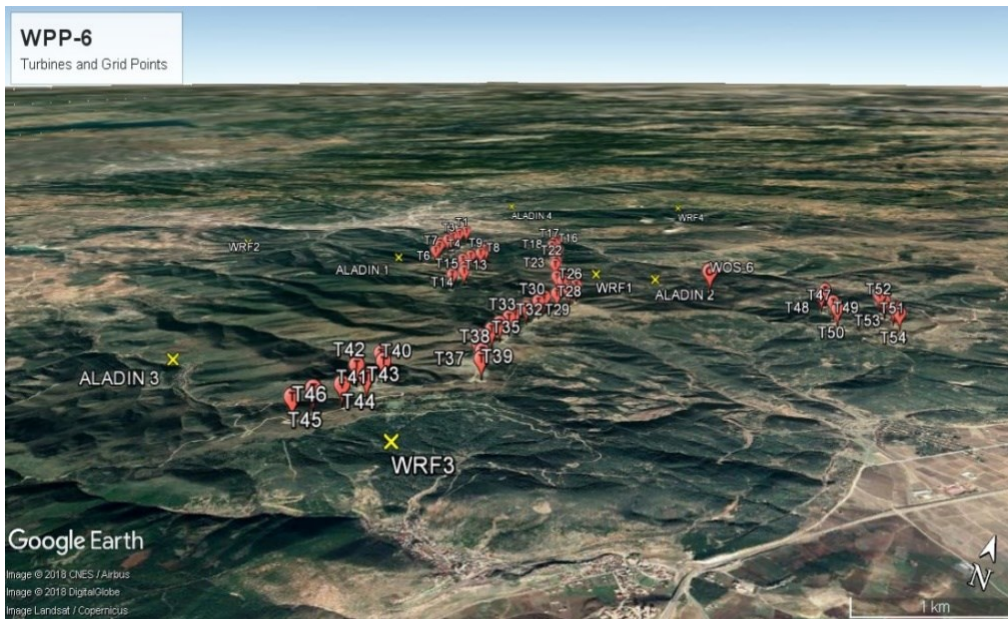


Figure 2.27 Location of WPP-6 turbines, Grid Points and WOS

CHAPTER 3

3. DATA ANALYSIS AND RESULTS

This chapter includes detailed analysis for wind speed predictions at different time scales for each WPP. First of all winds speed predictions are evaluated at monthly, daily, and hourly time scales. Statistical measures of RMSE, bias and correlation coefficient of predicted wind speed from each model have been calculated for each grid point. The most successful grid points have been determined according to lowest RMSE and mean bias and highest correlation. Diurnal analysis have been made for the selected best grid points. Energy predictions and error rates are also examined to find relationship between energy and wind speed.

Analyzing diurnal variation of wind speed and wind power is important for electricity markets. It is also required for planning issues on wind power plants. According to the amount of consumption, electricity tariffs are divided into 3 periods in Turkey as follows:

Puant Period: 17.00-22.00

Night Period: 22.00-06.00

Daytime Period: 06.00-17.00

The period with cheaper electricity for consumers and the more expensive period for producers is the night period (22:00-06:00), and the most expensive period for consumers is Puant Period (17:00-22:00). Therefore, error rates should be lower especially at puant periods for the producers to maximize their revenue [61].

3.1.WPP-1

The turbines of WPP-1 are laid down in southwest-northeast direction (Figure 2.3). The WOS data covers 27 months (between January 2013 and April 2015) because WOS station had been demolished in April 2015. Therefore, prediction and energy values have been arranged based on these data period.

3.1.1. Evaluation of Wind Speeds at Monthly, Daily, and Hourly Time Scales

Figure 3.1 shows the seasonal wind direction frequency of hourly data from observation (WOS). It shows that the wind speed has the highest values in summer and prevailing wind direction is NE and NNE for WPP 1. In spring and winter seasons wind speeds are lower than the other seasons. According to Table 2.5, rated wind speed is 13 m/s and cut in wind speed is 3 for WPP-1 turbines. Therefore it could be expected that the production of WPP-1 should be high in summer and fall. To understand this seasonal effect for production, WPP-1 monthly averages have been examined. Observation station has 3 wind speed sensors at different heights, v80 has been selected because the turbine hub height is also 80 m.

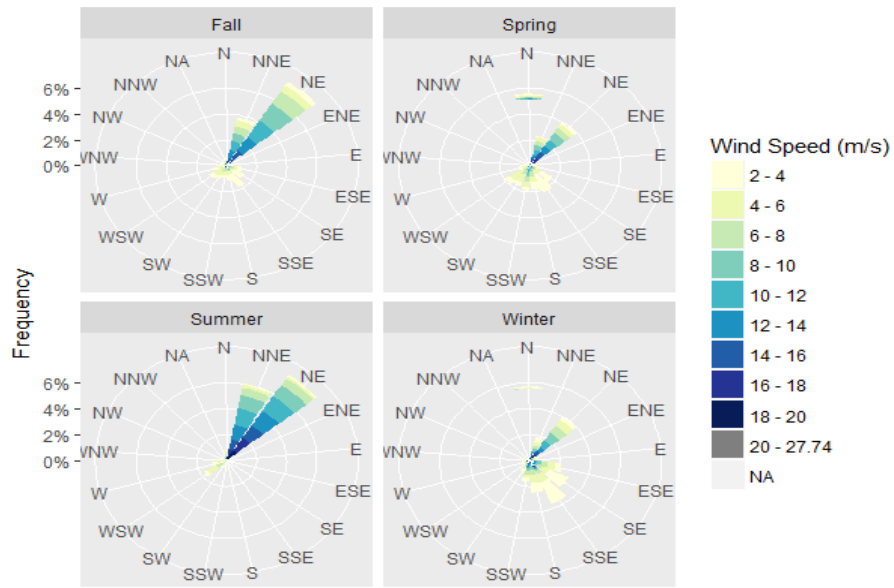


Figure 3.1 Seasonal Wind Rose from observed data (WPP-1)

Figure 3.2 shows the wind direction frequency at hourly time scale from observations and all models at four grid points. “vd78” and “vd48” are the WOS directions sensors with height (78 m.a.g.l or 48 m.a.g.l.) and they both show that the prevailing wind direction is approximately 45° (NE) with the frequencies of 40 to 70 percent. ALADIN prediction for Grid 1 and ECMWF predictions for all grid points show close match to observed direction and frequency range. GFS wind direction values are different for this wind farm. As it mentioned in Figure 2.6, WRF-1 (GFS and ECMWF Grid 1) and ALADIN 1 are the closest grid points to the WOS.

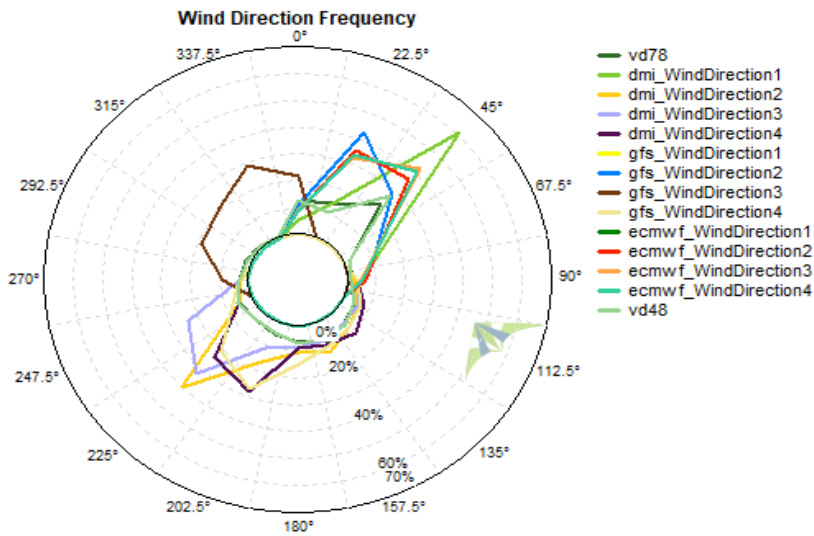


Figure 3.2 Wind Rose for all Grids (WPP-1)

Figure 3.3 shows the monthly mean wind speed calculated over 27 month of hourly data from observations (WS80, WS65, and WS50), ALADIN, GFS, and ECMWF at four grid points. WS80, WS65 and WS50 are the heights (m) of real measurement sensors. The dashed lines are the average values for 4 grids (ALADIN avg, GFS avg, ECMWF avg). Models unrealistically overestimate the monthly wind with reverse trend on January, February and March. All models follow a similar trend with observation during the rest of the months in the year. However, a significant underestimation behavior throughout the period exists. Among models ALADIN predictions, particularly for estimates from grid 4 show the best agreement with observation. The discrepancy between observations and models are greatly reduced with ALADIN model during summer months. GFS and ECMWF Grid 4 have the worst prediction performance. The locations of Grid 4 is 413 m.a.g.l. and the distance between Grid 4 and WOS is approximately 6 km which the outermost grid (see Table 2.2). The error should be reasoned this distance. Wind speeds reach the highest monthly mean values (up to 11 m/s) during summer months while they drop to 5-6 m/s during winter months.

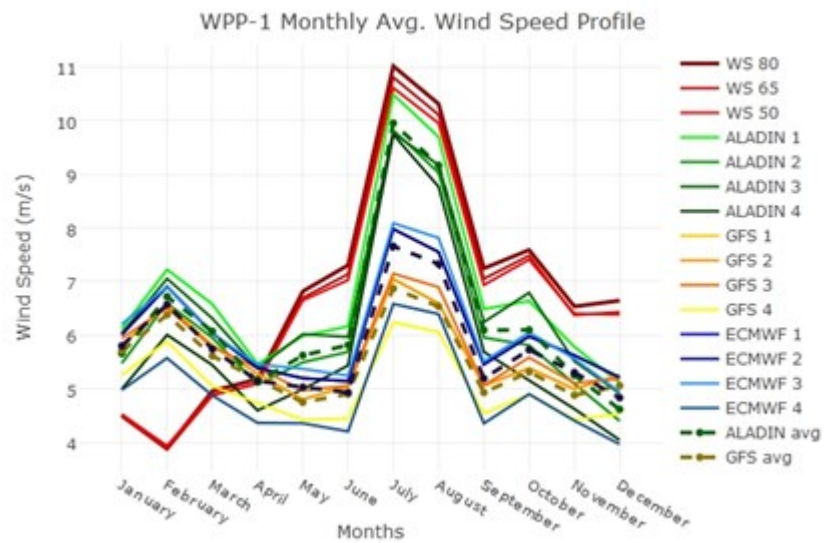


Figure 3.3 Monthly Wind Speed Profile (WPP-1)

Figure 3.4, 3.5, and 3.6 show scatter plots between observed and modeled daily averaged wind speed at each season for ALADIN, GFS, and ECMWF, respectively. Results from all grids points are shown in these figures. ALADIN model shows a similar performance from all grid points at each season. The overall underestimation feature for all range of wind values in fall, summer and spring is slightly improved with results from grid 1 (see Fig. 3.3). In winter, for wind speed higher than 7.5 m/s the model results show underestimation, while for wind speed less than 7.5 m/s they show overestimation.

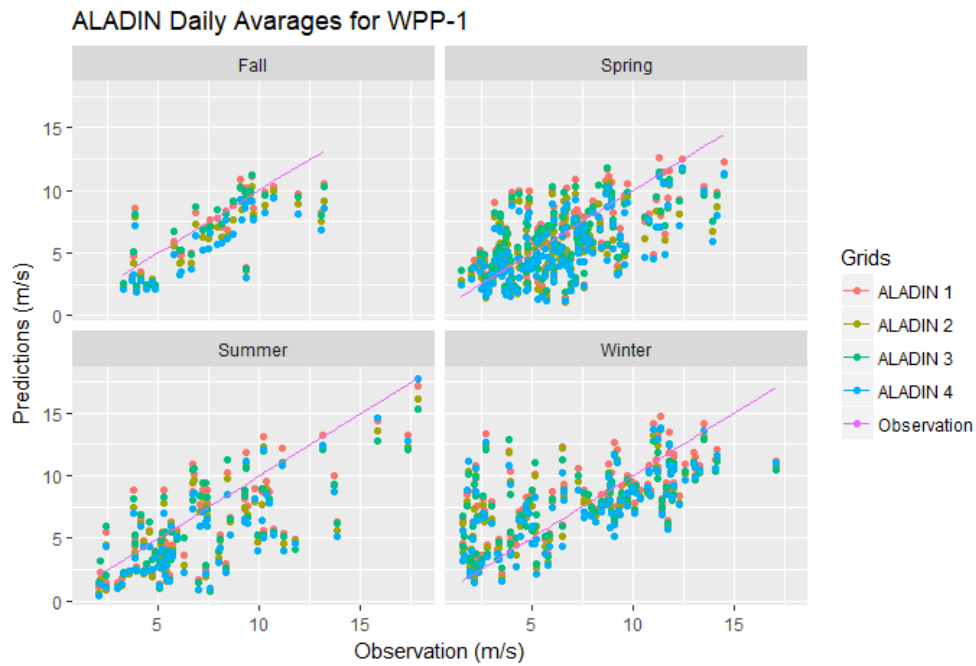


Figure 3.4 Daily Avg. Scatter Plot for ALADIN Predictions (WPP-1)

Throughout the range of daily wind speeds between 2.5 and 18 m/s GFS underestimates the wind in fall and summer (See Fig. 3.6). However, for low wind values up to 6 m/s in spring and up to 7.5 m/s in winter the GFS overestimates the wind. The level of underestimation increases largely toward higher wind speed values (see Fig 3.6). Among the grid points, GFS results from Grid 3 show slightly better performance in all seasons.

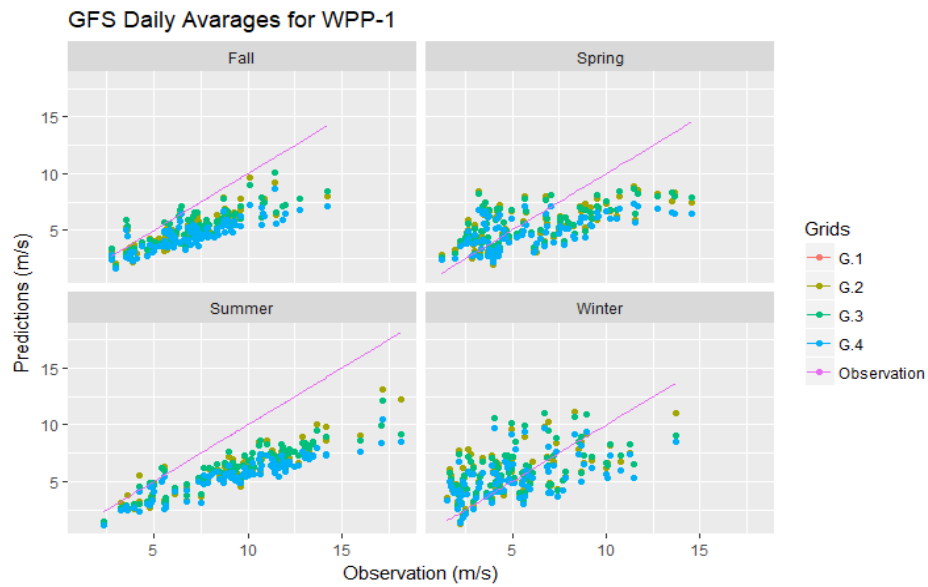


Figure 3.5 Daily Avg. Scatter Plot for GFS Predictions (WPP-1)

A similar prediction performance like in GFS seems to appear in ECMWF predictions at each season (Figure 3.6). The distribution is more scattered but the level of underestimation is more reduced with ECMWF results. The initial condition of WRF model is responsible for these changes. It seems that Grid 3 provides the best scatter distribution.

According to the analysis of averaged daily wind speed provided in these scatter plots (Fig 3.4, 3.5, and 3.6) the GFS model is less reliable for all seasons and other two models (ALADIN and ECMWF) depending on their seasonal performances are more preferable in wind power production.

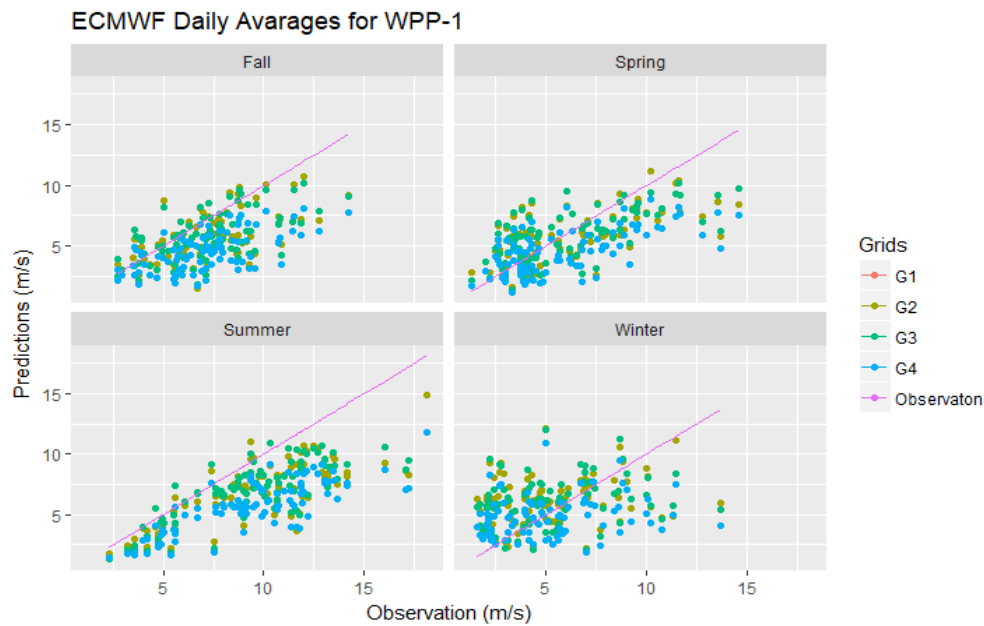


Figure 3.6 Daily Avg. Scatter Plot for ECMWF Predictions (WPP-1)

The time series of daily average wind speeds calculated from all data period from ALADIN, GFS and ECMWF for 4 grids are compared with observed wind speed in Figure 3.7. This figure shows that while GFS and ECMWF predictions are generally underestimated, ALADIN values are closer to observation values. This underestimation is more significant particularly for during summer and also towards fall season. WRF with ECMWF shows somewhat better skill than WRF with GFS. For winter and early spring all three models show slight overestimation.

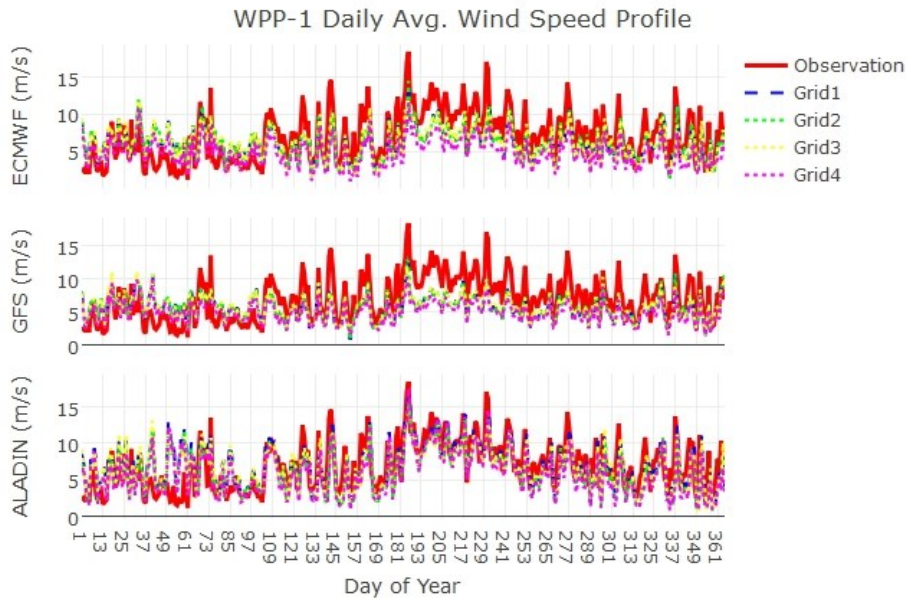


Figure 3.7 Daily Average Time Series of all NWP and Observation data (WPP-1)

Hourly statistics of bias, RMSE and Correlation Coefficients are calculated for each season and model grid points from ALADIN, GFS and ECMWF in Table 3.1. The table indicates that all three models show strong underestimation indicated with negative bias values for fall and summer and overestimation (positive bias) for winter. Winter correlations for all models are the lowest in the order of average 50% when it is compared with other seasons. ALADIN (grids 1 and 3) and ECMWF show overestimation for spring, GFS shows underestimation for this season. Based on the statistical measures available in this table, the most preferable grid that yields the lowest bias and RMSE and high correlation coefficient is selected with respect to each season and model as follows: ALADIN 1, GFS 3, and ECMWF 3 for fall, ALADIN 2, GFS 3, and ECMWF 2 for spring, ALADIN 1, GFS 3, and ECMWF 3 for summer, and ALADIN 3, GFS 3, and ECMWF 4 for winter. The evaluations provided in the following sub-sections are made according to these grids for each season. The optimum grid selection that provides the lowest bias and RMSE, and the highest

correlation coefficient for each model is highlighted and underlined in the table (blue for fall, yellow for spring, red for summer and purple for winter).

Table 3-1 Seasonal bias, RMSE and Correlation Coefficients for all models and grids from hourly data

Bias	SEASON	ALADIN-1	ALADIN -2	ALADIN -3	ALADIN -4	GFS-1	GFS-2	GFS-3	GFS-4	ECMWF-1	ECMWF-2	ECMWF-3	ECMWF-4
	Fall	-0,816	-1,500	-0,932	-1,965	-1,973	-1,973	-1,867	-2,497	-1,434	-1,434	-1,411	-2,563
	Spring	0,498	-0,003	0,379	-0,500	-0,074	-0,074	-0,013	-0,665	0,104	0,104	0,159	-0,923
	Summer	-0,700	-1,326	-1,231	-1,513	-3,508	-3,508	-3,346	-4,163	-2,746	-2,746	-2,577	-3,947
	Winter	1,329	0,673	1,184	0,188	1,027	1,027	1,036	0,382	1,206	1,206	1,204	0,013
RMSE	Fall	4,658	4,665	4,588	4,826	3,599	3,599	3,542	4,051	4,361	4,361	4,287	4,740
	Spring	4,835	4,719	4,783	4,744	4,706	4,706	4,654	4,770	4,626	4,626	4,659	4,693
	Summer	4,200	4,327	4,315	4,492	4,757	4,757	4,678	5,521	4,971	4,971	4,756	5,708
	Winter	6,668	6,469	6,513	6,494	5,441	5,441	5,395	5,187	5,934	5,934	5,945	5,529
CC	Fall	0,436	0,438	0,406	0,449	0,740	0,740	0,739	0,712	0,433	0,433	0,437	0,412
	Spring	0,453	0,447	0,433	0,450	0,377	0,377	0,384	0,329	0,402	0,402	0,392	0,373
	Summer	0,623	0,613	0,589	0,621	0,804	0,804	0,809	0,756	0,585	0,585	0,601	0,555
	Winter	0,063	0,047	0,083	0,017	0,232	0,232	0,246	0,215	0,058	0,058	0,058	0,047

In summary, these results show that all three models mostly underestimate wind speed at hourly, daily and monthly timescales for all seasons except winter at WPP-1. ALADIN 1 GFS 3, and ECMWF 3 provide better wind speed prediction performance generally.

ALADIN bias values is lower than ECMWF and GFS for fall season. ALADIN values show better distribution especially for summer and fall seasons than other predictions. ECMWF predictions are obviously insufficient for fall and summer seasons. Differences in WRF estimates depend on the accuracy of initial and boundary conditions from ECMWF and GFS. The higher resolution (11 km) of ECMWF products provides more representative initial condition during summer and fall seasons comparing to the coarse products (25 km) of GFS. However, ALADIN model better resolves the atmospheric physics in summer and fall for this study location. In wind power prediction variability in seasonal model performances is of critical importance.

3.1.2. Diurnal Variation

Diurnal variation of temperature, wind speed, and wind speed statistics (RMSE, bias and correlation coefficients) are prepared for each season at the assigned best grid location.

Figure 3.8 shows mean diurnal temperature profile from observation, ALADIN, GFS, and ECMWF at fall, spring, winter and summer. In a typical diurnal cycle of temperature the peak value occurs around 2 p.m. in the afternoon. All models except ECMWF shows this feature in all seasons. ECMWF shows 1-hr lag shift to earlier in the occurrence time of the peak. ECMWF and GFS show overestimation during daylight time and it is substantially high (3-4 °C) at peak time. Daylight performance of ALADIN in spring and summer is superior and it is also much better than ECMWF and GFS during fall and winter. However, temperature variation in nocturnal times is

better simulated by ECMWF and GFS in all seasons. ECMWF releases the highest amplitude in temperature variation between day and night in winter.

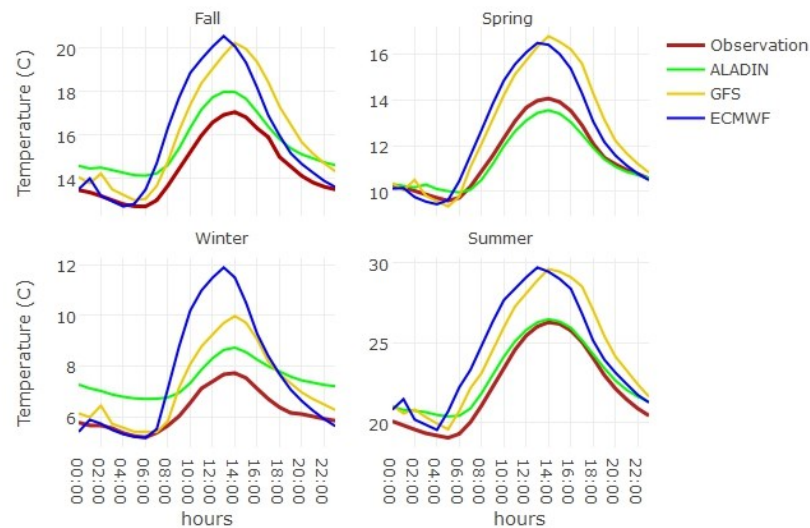


Figure 3.8 Diurnal Temperature by seasonally for the best grids (WPP-1)

Figure 3.9 indicates mean diurnal cycle of wind speed from observation and three models (ALADIN, GFS, and ECMWF) at fall, spring, winter and summer seasons. Observed wind speeds decrease from nighttime to midday and then starts to increase until evening hours (20:00) in fall season. ECMWF 3 shows a similar hourly oscillation with observed wind speed. GFS 3 is closer to them, however ALADIN 1 shows totally different hourly variations. All models show underestimation at each hour of the day in fall season. In spring season, all models except ALADIN 2 have almost same hourly oscillation with observed wind. Increasing trend shifted to earlier times (4 hours) in ALADIN 2 but its peak time is same with observation. Diurnal amplitude of ALADIN between day and night is the highest. Spring wind speed values are also lower than fall and summer. Winter predictions from all three models are worse than other seasons. Only GFS oscillations with smoother tendency are similar to observations. All three models except nocturnal hours of ECMWF show substantial

overestimation during the hours of day. Summer wind speeds are higher and ALADIN is closer to observed wind speeds. All models have same oscillation with earlier timing for minimum and maximum wind speed when they are compared with observed wind at summer. Significant underestimation feature from the models is also evident in this season. Among seasons the best model performances for diurnal cycles are obtained in spring. Maximum observed wind speed in the day occurs at 16-18 hours in winter and spring and at 20-22 hours in summer and fall seasons. All models hardly follow this feature in summer, fall, and winter and their occurrence time shifts to earlier.

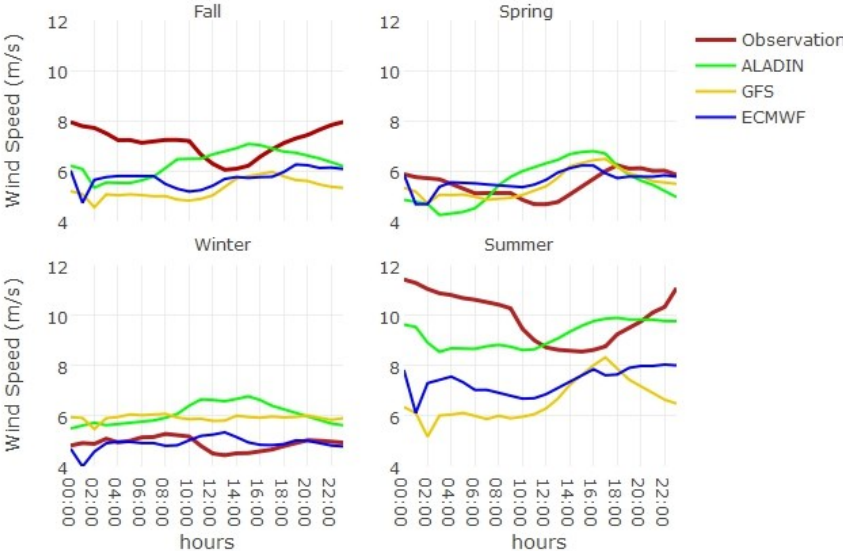


Figure 3.9 Diurnal Wind Speed by Seasonally for the best grids (WPP-1)

Figure 3.10, 3.11, and 3.12 show the diurnal variation of RMSE, Bias, and Correlation Coefficient for ALADIN, ECMWF and GFS at fall, spring, winter and summer seasons respectively. It is obvious that RMSE is higher at early times of day and it starts to decrease with the rising of the sun. After 17:00, RMSE starts to increase again for fall and winter. However, spring RMSE values are decreasing until 14:00 and start to increase until the sunset in opposite to temperature variation. GFS is obviously

successful for fall and winter and better than other models during the evening for summer.



Figure 3.10 Diurnal Cycles for RMSE of Wind Speed (WPP-1)

All range of diurnal bias values changes between + 2 and -6 m/s for all seasons (Fig. 3.11). ECMWF is better than other models for winter period. ECMWF and GFS have lower bias than ALADIN for spring. Spring bias values are also lower than other seasons. Generally, all models shows undereastimations during night and early morning periods but they showed overestimation at midday. ALADIN and GFS show positive bias (overestimation) during entire cycle in winter. In addition, ECMWF and GFS stay with negative bias (underestimation) during all hours of cycle in fall and summer. Crest region of ALADIN is always positively biased in all seasons. This is only the case with ECMWF and GFS in spring and winter. Summer season has the heighest negative bias, and ALADIN is better than other models.

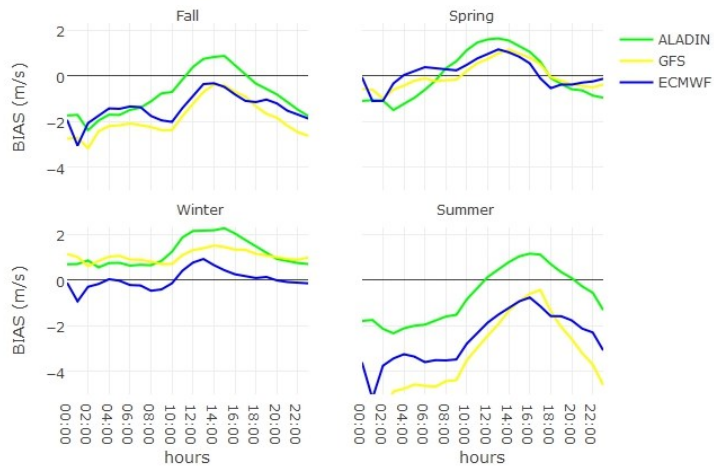


Figure 3.11 Diurnal Cycles for bias of Wind Speed (WPP-1)

It is obvious that GFS has the highest correlation for summer (0.8-0.9), fall (0.7-0.8) and winter (0.2-0.3) season (Fig. 3.12). In these seasons, correlation values are almost the same for all hours of the day. ECMWF and ALADIN show 30% decrease in correlation from these values for these seasons. Even though GFS produced higher RMSE and bias this model showed better diurnal trend. In spring, ALADIN has correlation values of 0.45-0.5 and they are better than the values released by GFS and ECMWF (0.3-0.4). Correlation coefficients during the day and night have not obvious oscillation like in RMSE and Bias plots.

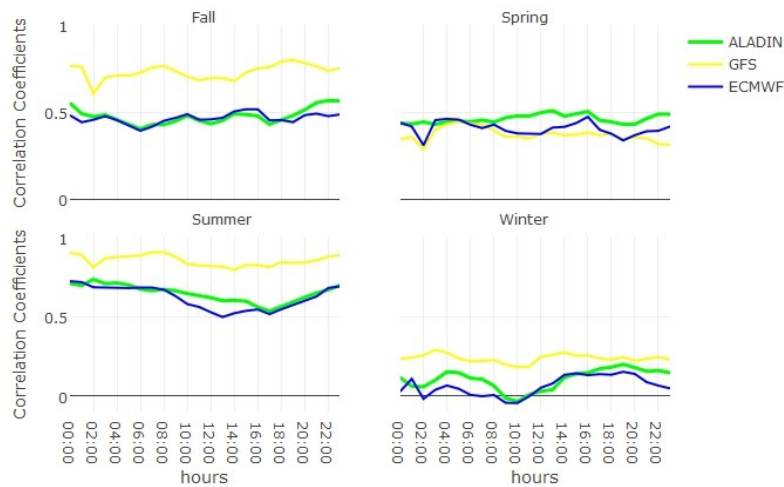


Figure 3.12 Diurnal Cycles for Correlation Coefficient of Wind Speed and Predictions (WPP-1)

3.1.3. Energy Comparison

Figure 3.13 shows the correlation between wind speed and power, and histograms of wind speed and power production values. The “Wind Speed Frequency” graph on the matrix shows the wind speed histogram. Wind speeds are getting intense between 3 and 8 m/s which means wind mostly blows within this range of wind values. The frequency of wind speeds also decreases until 20 m/s, which is fair enough for the producer. The scatter plot graph on the matrix shows the correlation between wind speed and power. It is similar to power curve (Figure 2.1). The “Power Frequency” graph shows the frequency of power values. The installed capacity of WPP-1 is 120 MW. However 0-5 MW productions are higher than others which means produced electricity is low for these wind farm. In fact, approximately % 33 percent of wind speed is smaller than the 3 m/s, this is the reason of lower produced power. The maximum produced power value for WPP-1 is approximately 89 MW which means the wind farm never produced full capacity electricity. The reason of this might be limitations on the grid in 2014, 2015 or the wind farm could be rise their capacity after those years. The pearson correlation coefficient between energy and wind speed is

0.87 which is indicated on the top right of the matrix. The 50% percent of the wind data corresponds to the wind values greater than 3-10 m/s. However, the mean wind speed is around 8.46 m/s.

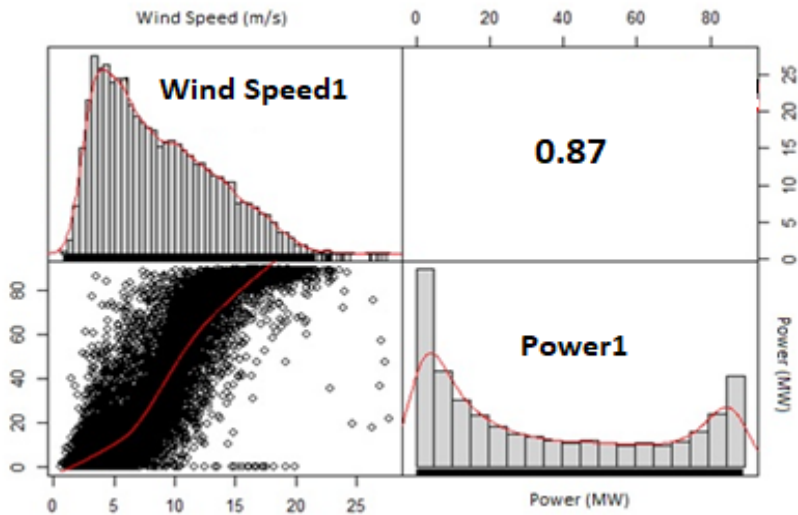


Figure 3.13 The Relationship between Observed Wind Speed and Produced Power (WPP-1)

Figure 3.14 shows the diurnal variation of predicted and observed energy and wind speed values at each season. Wind speed values are selected from the final step of RITM forecast system that combines all three NWP (ALADIN, ECMWF and GFS) model outputs. Final products from RITM system also include correction to predicted wind speeds. First row shows produced and predicted power values at each season and the bottom row shows the wind speed prediction and observed values for these seasons. Similar diurnal wind patterns shown in previous section also appear in these figures. Overall underestimation in fall and summer and overestimation in spring and winter seasons appears in these combined final wind product. With the modification performed in the system the weakness in models prediction performance is improved. However, the modification seems not affecting the winter performance. Wind energy production of WPP starts to decrease from 08:00 am to 12:00. It generally starts to

increase after the midday. Summer and spring energy predictions are closer to each other. However the difference between energy production and predictions are higher for fall and particularly for winter seasons depending on differences in wind speed prediction. Discrepancy in wind estimates also the cause for discrepancy in power estimates. Therefore, the accuracy of power estimates strongly depends on the reliability of wind predictions. It means quality of wind speed predictions directly affects energy predictions.

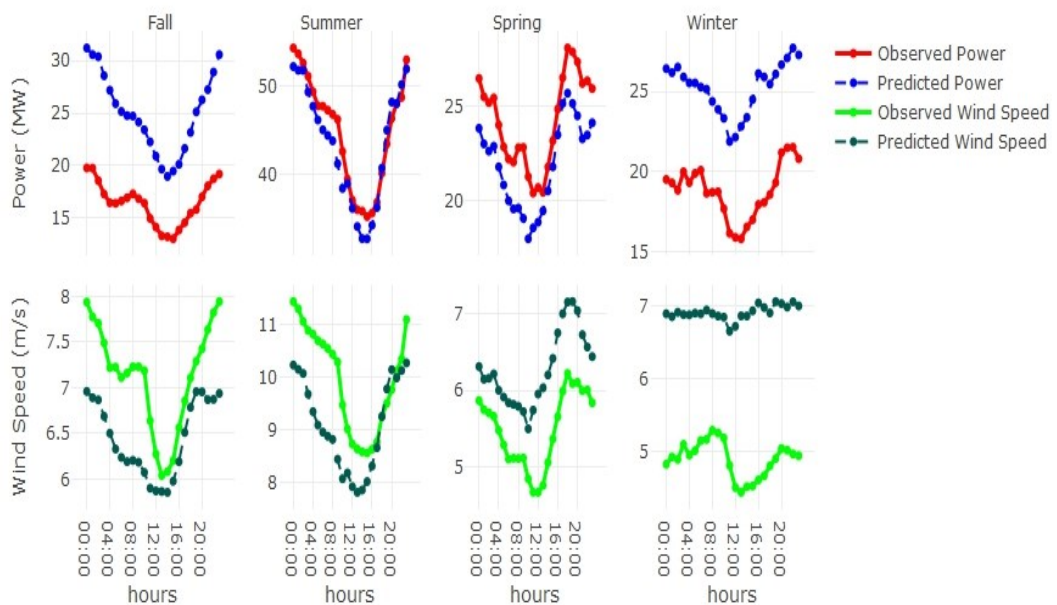


Figure 3.14 Diurnal Cycle for Energy and Wind Speed (WPP-1)

Figure 3.15 shows the monthly RMSE values according to final wind speed predictions and energy predictions for WPP-1. Wind speed RMSE values are higher at winter months and starts to decrease after April. Energy RMSE values are smaller than the wind speeds. They have an increasing trend after the September. This is also a strong indicator how the energy production depends on wind speed. The smaller the wind prediction error the more reliable forecast of energy production. Winter and fall seasons show the least reliable forecast of power production.

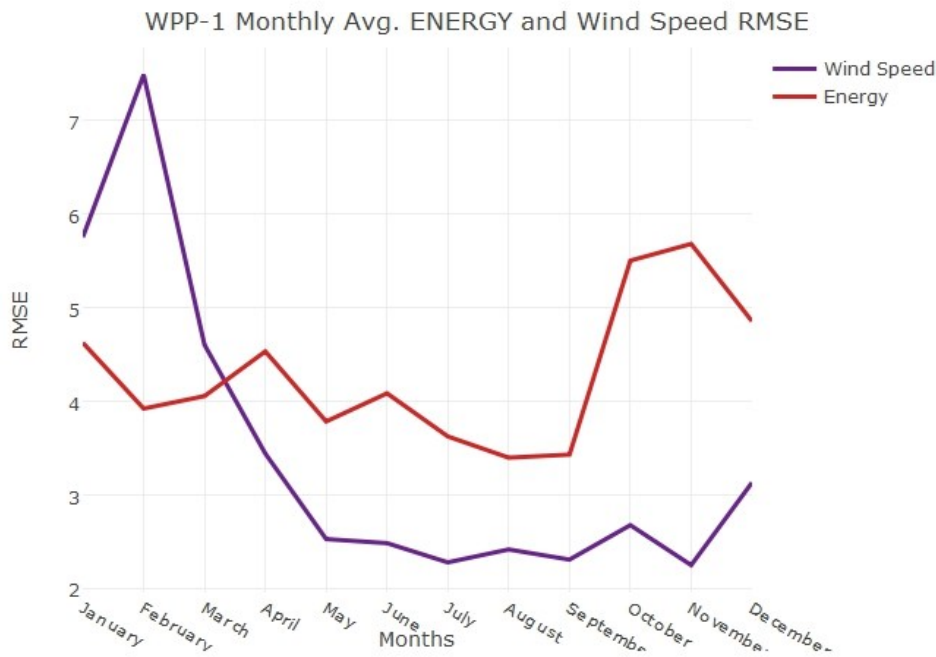


Figure 3.15 Monthly RMSE for Wind Speed Predictions (WPP-1)

3.2. WPP-2

The turbines of WPP-2 are laid down in southeast-northwest direction (Figure 2.7). The WOS data covers 4.1 years (between November 2012 and December 2016). Therefore, prediction and energy values have been arranged based on these data period. WPP-2 is located in more complex terrain than WPP-1.

3.2.1. Evaluation of Wind Speeds at Monthly, Daily, and Hourly Time Scales

Figure 3.16 shows the seasonal wind direction frequency of hourly data from WOS. It shows that the wind speeds reach the highest values in summer and prevailing wind direction is NNE for WPP 2. In spring and winter seasons wind speeds are lower than the other seasons. It could also be seen from the figure, there are two prevailing wind directions which are S and NNE for winter time. According to Table 2.5, rated wind

speed is 17 m/s and cut in wind speed is 3 m/s for WPP-2 turbines. Therefore it could be expected that the production of WPP-2 should be high in summer and fall. Observation station has 3 wind speed sensors at different heights (65, 50, 30 m), v65 has been selected because the turbine hub height is also 65 m.

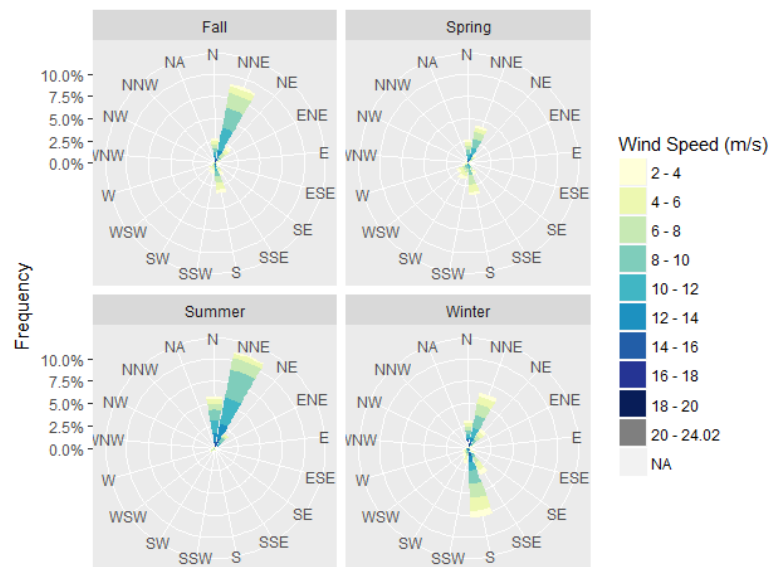


Figure 3.16 Seasonal Wind Rose (WPP-2)

Figure 3.17 shows the wind direction frequency at hourly time scale from observations and all models at four grid points. N is the prevailing wind direction for observation values, however, ALADIN grid 1, 2 are pointed to opposite directions, yet nearly all grid point predictions indicate NE.

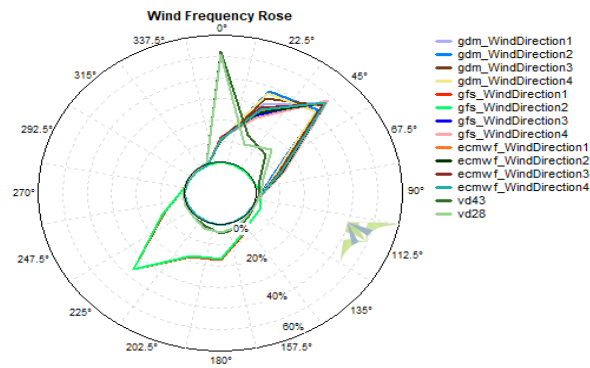


Figure 3.17 Wind Rose for all Grids (WPP-2)

Figure 3.18 shows the monthly mean wind speed calculated over 4.1 years of data from observations (WS65, WS50, and WS30), ALADIN, GFS, and ECMWF at four grid points. WS80, WS65 and WS50 are the heights (m) of real measurement sensors. The dashed lines are the average values for 4 grids (ALADIN avg, GFS avg, ECMWF avg).

It could be seen from the figure that monthly mean wind speed predictions for ALADIN are underestimated until June. ALADIN predictions are overestimated for summer months and underestimation occurs rest of the year. GFS and ECMWF grids are showed different fluctuation between each other. While GFS and ECMWF grid 2 is overestimated during November, December, January, February and March, the rest of GFS and ECMWF grids are underestimated for this months. All GFS and ECMWF grids are showed underestimation during April, May and June. However, overestimation occurs until the October for GFS. ECMWF Grid 2 is overestimated until the end of the year. ECMWF Grid 1 and 3 is underestimated for November, but underestimated for the rest of the year.

To brief, there isn't obvious better model for WPP-2 monthly averages. It should be stated that GFS predictions are closer to observation line during summer and fall months and the average line for ECMWF grids is closer to observations from January to April. Wind speeds have reached to the highest monthly mean values, particularly in summer times similar to WPP-1.

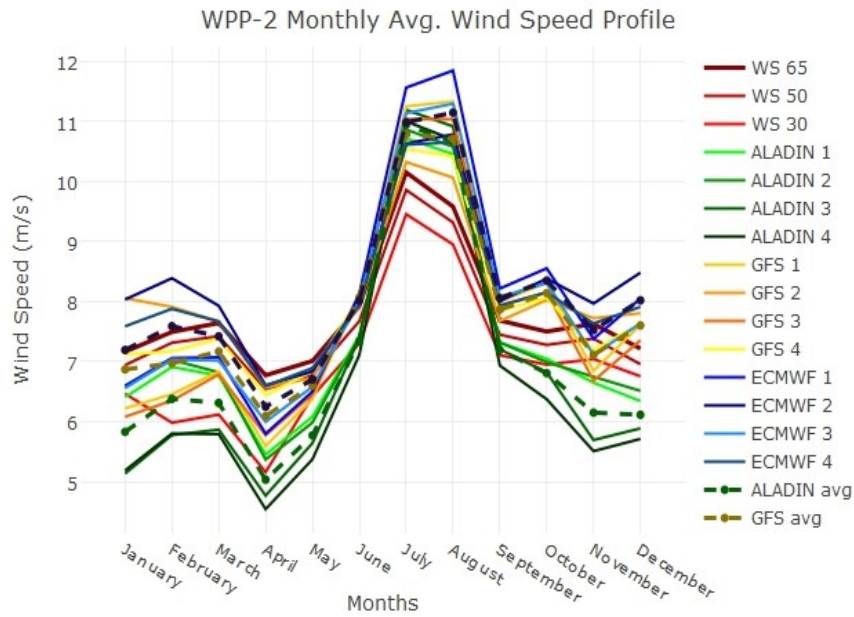


Figure 3.18 Monthly Average Wind Speed Profile (WPP-2)

Figure 3.19, 3.20, and 3.21 show scatter plots between observed and modeled daily averaged wind speed at each season for ALADIN, GFS, and ECMWF, respectively. Results from all grids points are shown in these figures. ALADIN model shows a similar performance from all grid points at each season. The overall underestimation feature for all range of wind values in fall, spring and summer (see Fig. 3.19). In winter, for wind speed higher than 8 m/s the model results show overestimation while for wind speed less than 8 m/s they show underestimation.

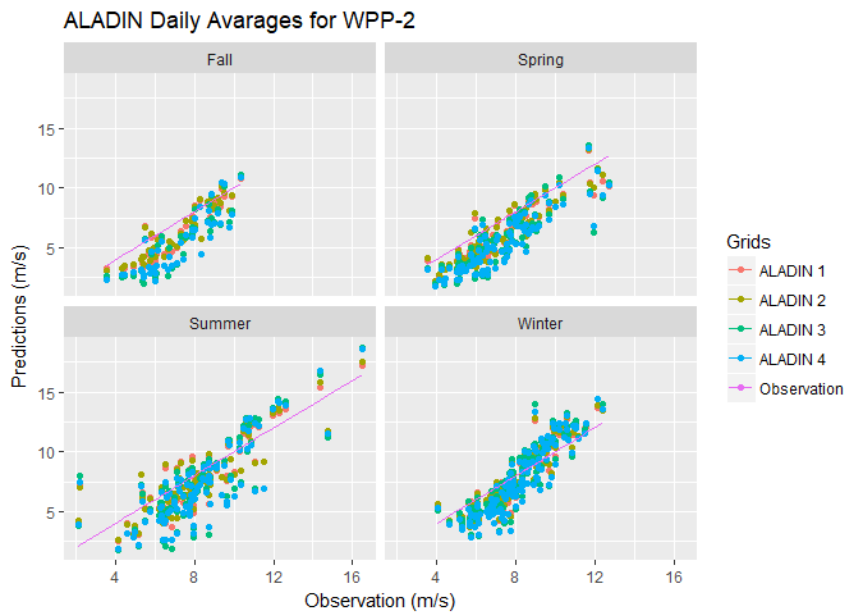


Figure 3.19 Daily Avg. Scatter Plot for ALADIN Predictions (WPP-2)

Throughout the range of daily wind speeds between 4 and 10 m/s GFS mostly have been distributed equally the wind in fall and summer (See Fig. 3.20). In spring and winter the range of daily wind speeds between 4 and 12 m/s. However, for low wind values up to 9 m/s in GFS underestimates the wind for spring. In winter, GFS overestimates the wind particularly the range of daily wind speeds between 7 and 11 m/s. Summer wind speed predictions for GFS distributed equally and summer wind speeds are higher than all seasons (4-16 m/s).

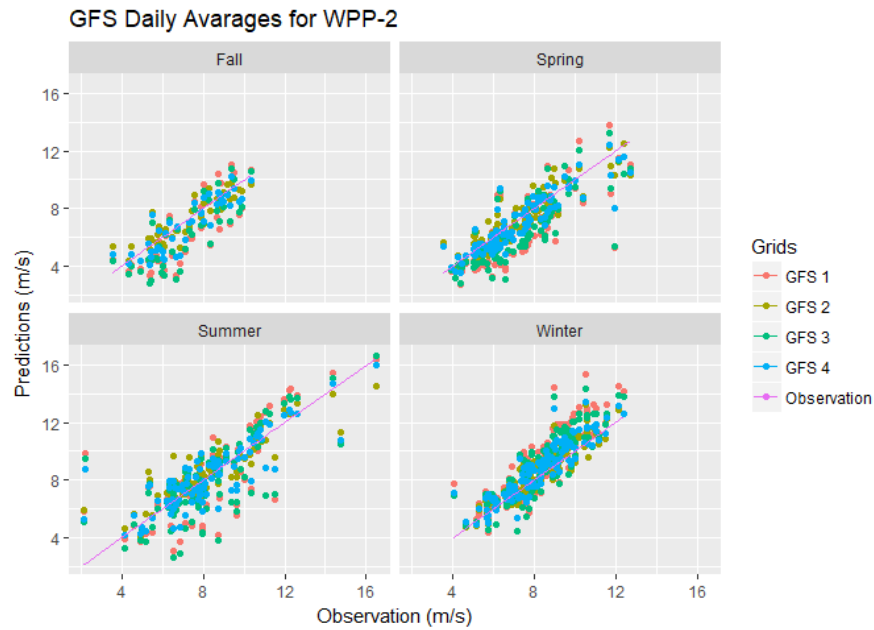


Figure 3.20 Daily Avg. Scatter Plot for GFS Predictions (WPP-2)

A similar prediction performance like in GFS seems to appear in ECMWF predictions at each season (Figure 3.21). Only, winter predictions for ECMWF are obviously overestimated.

According to the analysis of averaged daily wind speed provided in these scatter plots (Fig 3.3, 3.4, and 3.5) the ALADIN model is less reliable for all seasons and other two models (GFS and ECMWF) depending on their seasonal performances are more preferable in wind power production.

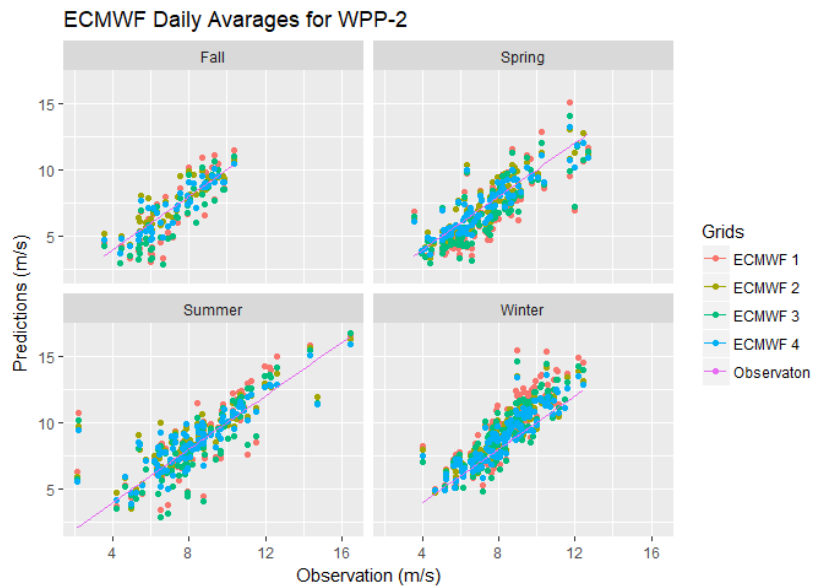


Figure 3.21 Daily Avg. Scatter Plot for ECMWF Predictions (WPP-2)

The time series of daily average wind speeds calculated from all data period from ALADIN, GFS and ECMWF for 4 grids are compared with observed wind speed in Figure 3.22. This figure shows that while GFS and ALADIN predictions are generally underestimated, ECMWF values are closer to observation values until the summer months. However, ECMWF and GFS are closer to observations than ALADIN rest of the year. WRF with ECMWF and GFS shows somewhat better skill than ALADIN.

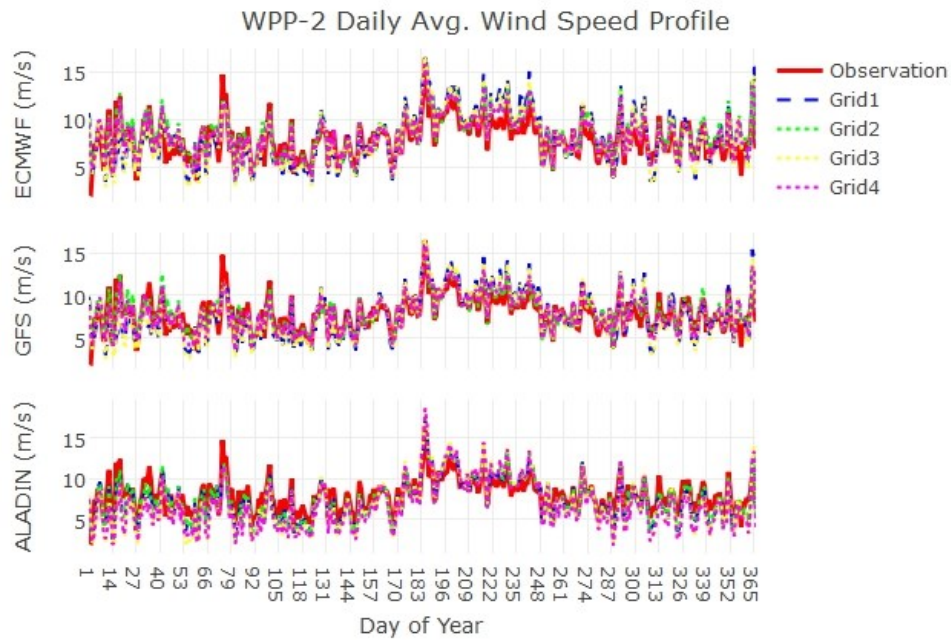


Figure 3.22 Daily Average Time Series of all NWP and Observation data (WPP-2)

Hourly statistics of bias, RMSE and Correlation Coefficients are calculated for each season and model grid points from ALADIN, GFS and ECMWF in Table 3.2. The table shows that ALADIN shows strong underestimation indicated with negative bias values for fall, spring and winter and overestimation (positive bias) for summer. GFS and ECMWF show overestimation for fall, summer and winter and underestimation for spring. Winter has high RMSE and lowest correlation compared with other seasons among all models.

Based on the statistical measures available in this table, the most preferable grid that yields lowest bias and RMSE and high correlation coefficient is selected with respect to each season and model as follows: ALADIN 2, GFS 2, and ECMWF 4 for fall, ALADIN 1, GFS 2, and ECMWF 4 for spring, ALADIN 1, GFS 4, and ECMWF 4 for summer, and ALADIN 2, GFS 2, and ECMWF 4 for winter. The evaluations provided in the following sub-sections are made according to these grids for each season. The optimum grid selection that provides lowest bias and RMSE, and highest correlation

coefficient for each model is highlighted and best value for each season underlined in the table (blue for fall, yellow for spring, red for summer and purple for winter).

Table 3-2 Seasonal bias, RMSE and Correlation Coefficients for all models and grids from hourly data

Bias	SEAS ON	ALADIN- 1	ALADIN - 2	ALADIN - 3	ALADIN - 4	GFS- 1	GFS- 2	GFS- 3	GFS- 4	ECMWF- 1	ECMWF- 2	ECMWF- 3	ECMWF- 4
	Fall	-0,650	-0,631	-1,123	-1,412	0,024	0,176	-0,113	0,028	0,362	0,464	0,134	0,246
	Spring	-1,046	-1,078	-1,728	-1,906	-0,876	-0,154	-0,823	-0,275	-0,690	-0,015	-0,631	-0,106
	Summer	0,308	0,389	0,603	0,369	1,016	0,222	0,835	0,452	1,278	0,576	0,917	0,512
	Winter	-0,755	-0,596	-1,655	-1,703	-0,424	0,634	-0,602	0,068	0,040	1,037	-0,147	0,523
RMSE	Fall	5,946	5,921	9,966	10,189	11,470	4,703	9,759	5,407	11,364	4,894	9,156	4,533
	Spring	6,788	6,937	11,280	11,491	10,591	5,078	9,388	5,362	10,080	4,806	8,607	4,580
	Summer	4,520	5,038	7,151	7,837	9,757	4,347	6,955	4,126	10,266	4,629	6,869	3,877
	Winter	14,682	14,206	22,928	21,595	23,493	11,753	21,915	13,424	22,867	12,593	20,624	12,338
CC	Fall	0,851	0,853	0,786	0,796	0,703	0,827	0,718	0,805	0,731	0,842	0,747	0,843
	Spring	0,824	0,822	0,768	0,770	0,707	0,811	0,726	0,802	0,719	0,827	0,738	0,826
	Summer	0,867	0,862	0,849	0,839	0,807	0,844	0,829	0,857	0,811	0,854	0,831	0,868
	Winter	0,667	0,675	0,559	0,578	0,454	0,666	0,480	0,612	0,487	0,686	0,521	0,662

3.2.2. Diurnal Variation

Figure 3.23 indicates to diurnal temperature profile seasonally. The graph roughly appropriate for general diurnal variation of temperature. The difference between day and night temperatures is quite low for spring and winter and high for summer. ECMWF and GFS temperature predictions are mostly overestimated for fall, spring and summer during the day. In night time all predictions nearly show underestimation. ALADIN have different oscillation than other for each season particularly in winter. It should be stated that ALADIN is worse than all models.

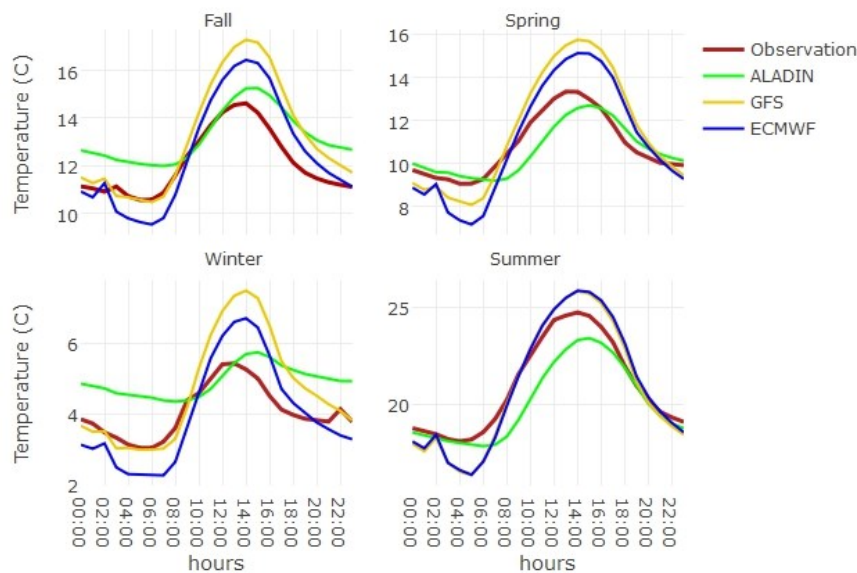


Figure 3.23 Diurnal Temperature by seasonally for the best grids (WPP-2)

Figure 3.24 indicates mean diurnal cycle of wind speed from observation and three models (ALADIN, GFS, and ECMWF) at fall, spring, winter and summer seasons.

Observed wind speeds are almost constant during the night and starts to decrease until the 14:00. ECMWF and GFS predictions are similar to each other. ALADIN is totally different from them. Summer and fall oscillations are better than winter and spring. Winter predictions are worse than other seasons. Summer wind speeds are higher than

other seasons similar to previous graphics. All wind speed predictions has suddenly decreased at 02:00 am. Spring wind speed values are also lower than fall and summer. Wind speeds reaches maximum value at 18:00 for each season.

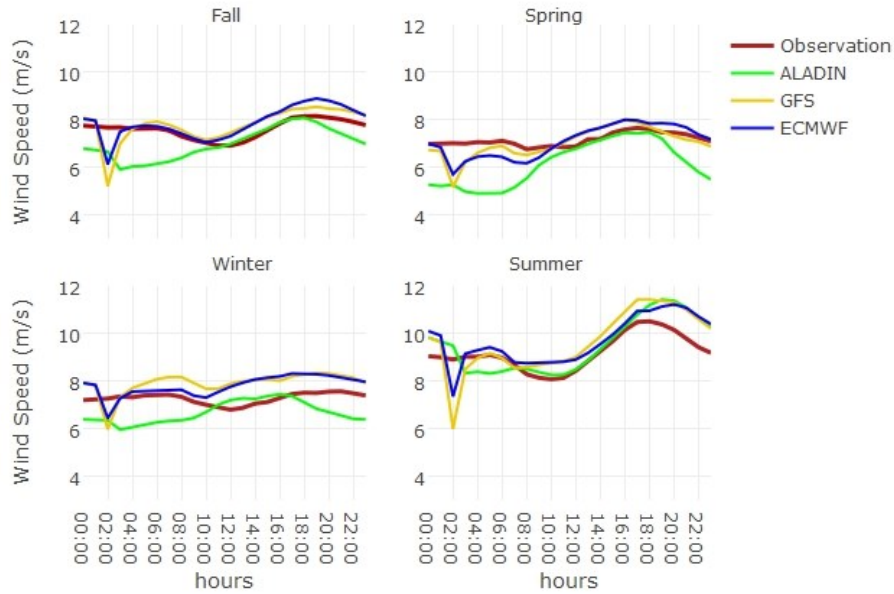


Figure 3.24 Diurnal Wind Speed by Seasonally for the best grids (WPP-2)

Figure 3.25 indicates mean diurnal cycle of RMSE for three models (ALADIN, GFS, and ECMWF) at fall, spring, winter and summer seasons. It is obvious that RMSE is higher at early times of day and it starts to decrease with the. After 14:00, RMSE starts to increase again. GFS and ECMWF is better than ALADIN for all seasons. Winter RMSE values are higher than other seasons. GFS is better than other models for winter. Summer RMSE values are also lower than other seasons. ALADIN is better during the midday for summer. RMSE values are generally higher for all seasons at puant and night period which means revenue of wind farm should be low for this hours.



Figure 3.25 Diurnal Cycles for RMSE of Wind Speed (WPP-2)

Figure 3.26 indicates mean diurnal cycle of bias for three models (ALADIN, GFS, and ECMWF) at fall, spring, winter and summer seasons similar to the diurnal RMSE graphics. Diurnal bias values change between + 1 and -2 m/s for fall and spring season. GFS and ECMWF error rates are smaller than the ALADIN, except from summer. ALADIN shows underestimation for fall and winter during the night. ECMWF 4 is better than other for fall and winter. ECMWF and GFS have lower bias than ALADIN for spring. Summer bias values are also lower than other seasons.

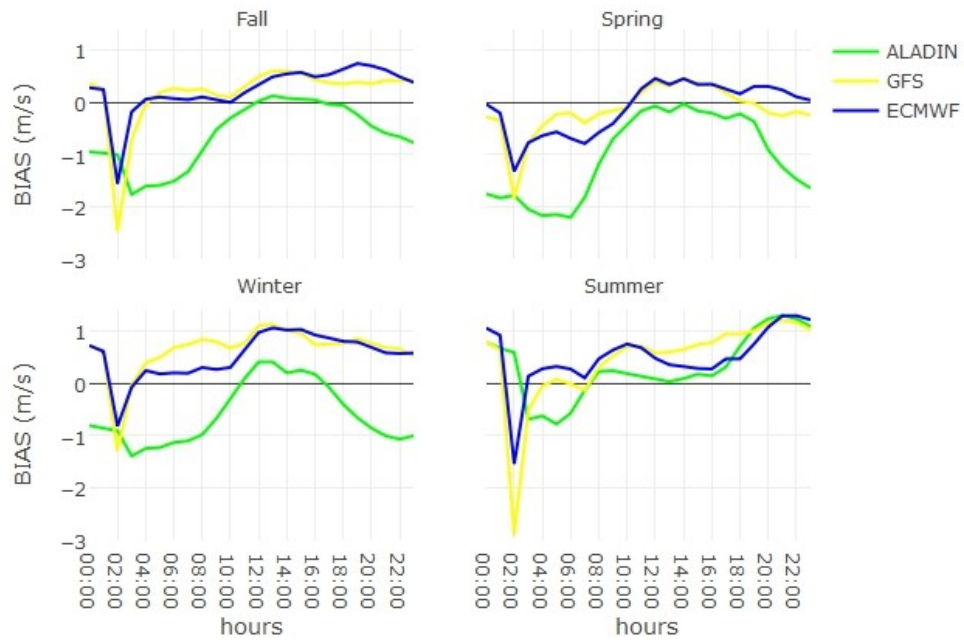


Figure 3.26 Diurnal Cycles for bias of Wind Speed (WPP-2)

Figure 3.27 indicates diurnal cycle of correlation coefficients between wind speed and three models (ALADIN, GFS, and ECMWF) at fall, spring, winter and summer seasons. In fall ALADIN has higher correlation than others, however ECMWF and GFS have been reached the highest values at midday. Fall, spring and summer correlations are higher than other seasons for all models (0.8-0.9). The lowest correlations are seen at winter (0.6, 0.75). ECMWF has better correlation than others for winter at midday and ALADIN better than other for early morning hours. There is a decreasing trend during the night and increasing trend during the day until the sunset.

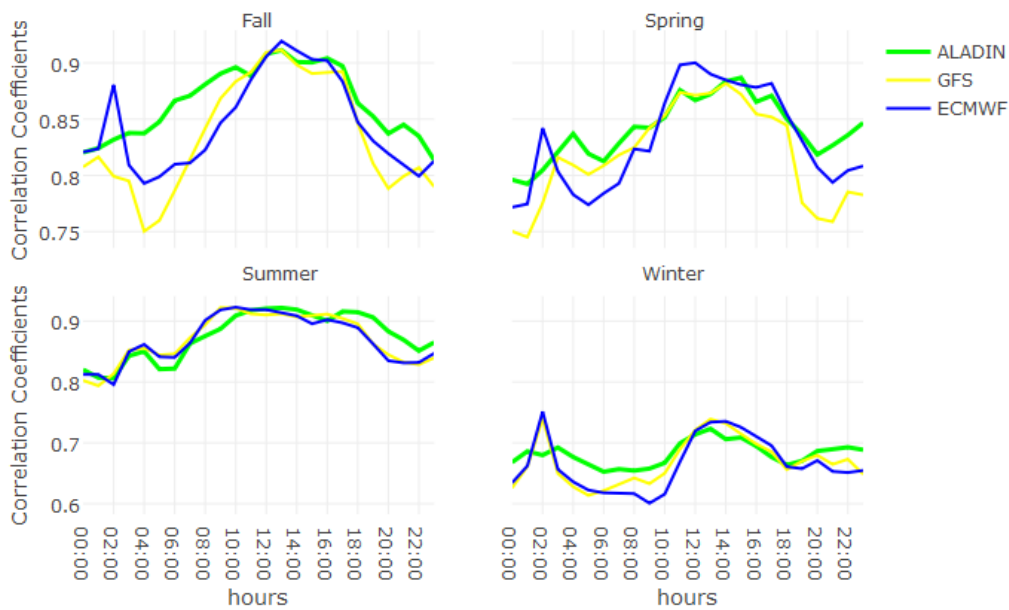


Figure 3.27 Diurnal Cycles for Correlation Coefficient of Wind Speed and Predictions (WPP-2)

3.2.3. Energy Comparison

Figure 3.28 shows the correlation between wind speed and power, and histograms of wind speed and power production values. The “Wind Speed2” graph on the matrix shows the wind speed histogram. Wind speeds are getting intense between 3 and 15 m/s which means wind mostly blows within this range of wind values. The frequency of wind speeds also decreases between 15 and 20 m/s, which is enough for the producer. The scatter plot graph on the matrix (the graph on the left bottom) shows the correlation between wind speed and power. It is similar to power curve (Figure 2.1). The “Power2” graph shows the frequency of power values. The installed capacity of WPP 2 is 240 MW. However the 50 % percent of energy values are greater than 20-50 MW. The maximum produced power value for WPP-2 is also around 240 MW. The pearson correlation coefficient between energy and wind speed is 0.83 which is indicated on the top right of the matrix.

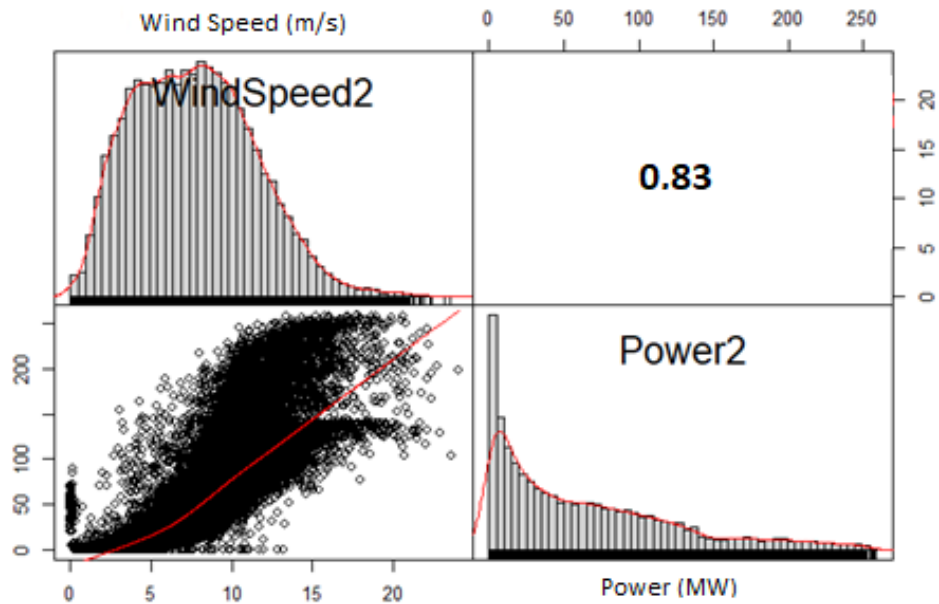


Figure 3.28 Relationship between Observed Wind Speed and Produced Power (WPP-2)

Figure 3.29 shows the diurnal variation of Energy and Wind Speed values by seasonally. Predicted values are combination of all methods in the RITM forecast system for both energy and wind speeds. First row shows to produced and predicted power values by seasonally and the bottom row shows the wind speed prediction and observed values. All seasons same diurnal variations are performed both power and wind speed. The diurnal variation of observed wind speed are same with the produced power for all seasons. As it is expected prediction values of wind speed and energy have same trend during the day. Production drops at midday hours for fall summer and winter by depending on the wind speeds. In spring, there is 2 hours lag shift to earlier in the occurrence time of the peak between predicted and observed values. Although energy and wind speed predictions dramatically decrease from early morning to midday, observed values shows reverse trend. Underestimation in wind speed predictions during all seasons are reflected to the energy predictions except from

summer. Power predictions are well regulated by RITM combining methods for this season.

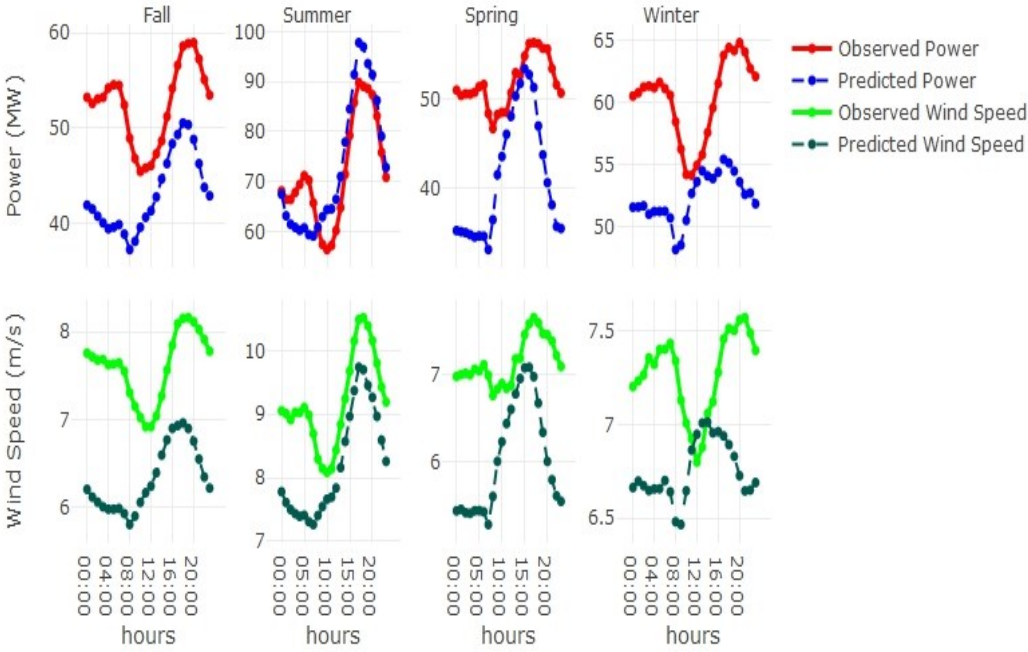


Figure 3.29 Diurnal Cycle for Energy and Wind Speed (WPP-2)

Figure 3.30 shows the monthly RMSE values according to final wind speed predictions and energy predictions for WPP-2. Energy RMSE values are higher at winter months and starts to decrease after March. Energy RMSE values are higher than the wind speeds. There is an increasing trend after the September. Wind speed RMSE values seems nearly constant during the entire year and smaller than the energy RMSE.

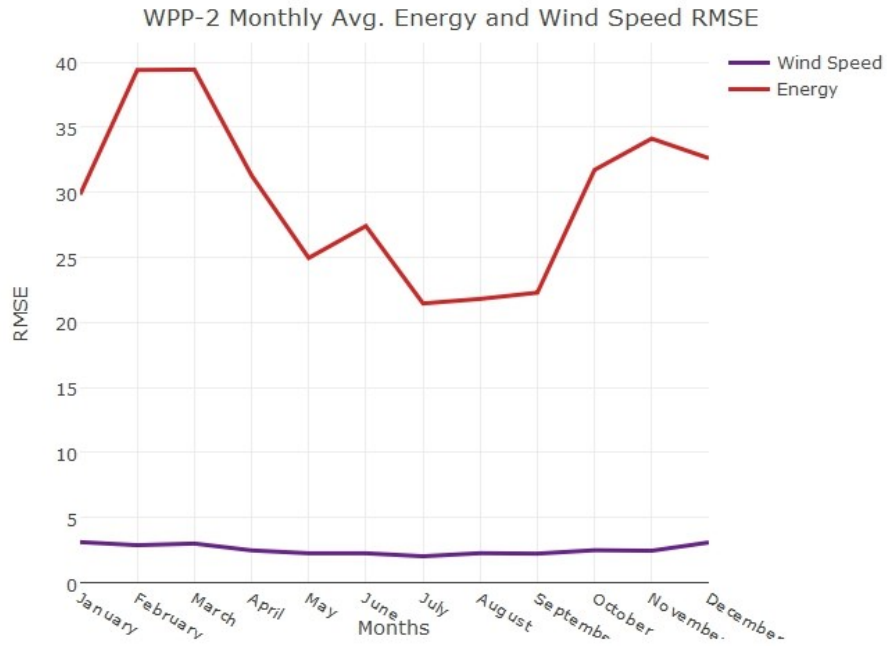


Figure 3.30 Monthly RMSE for Wind Speed Predictions (WPP-2)

3.3. WPP-3

WPP-3 is the most flat terrain in this study. The turbines of WPP-3 located in 0-30 m.a.s.l and laid down in northwest-southeast direction (see figure 2.13). The grid points of WPP-3 are located in sea which means sea-atmosphere and land-sea interactions should be taken into account for this models. The observation station of WPP-3 has 2 wind speed sensors at different heights (45 and 30 m), v45 has been selected because the turbine hub height is 46 m.

3.3.1. Evaluation of Wind Speeds at Monthly, Daily, and Hourly Time Scales

Figure 3.31 shows the prevailing wind direction seasonally. The figure shows that prevailing wind direction is the North for all seasons. However, wind speed values are low particularly in spring and winter. The highest wind speed values occur in summer season. Fall has better wind speeds than spring and winter. According to Table 2.5, rated wind speed is 13 m/s and cut in wind speed is 3 m/s for WPP-3 turbines. Therefore it could be expected that the production of WPP-3 should be high at summer season.

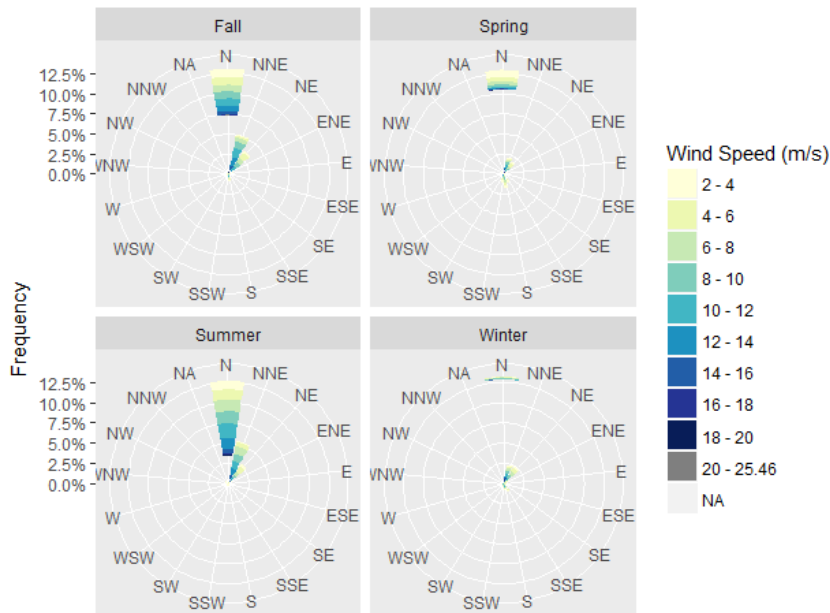


Figure 3.31 Seasonal Wind Rose (WPP-3)

Figure 3.32 shows the wind direction frequency at hourly time scale from observations and all models at four grid points. “vd43” and “vd28” are the WOS directions sensors with height (43 m.a.g.l or 28 m.a.g.l.) and they both show that the prevailing wind direction is approximately 45° (N) with the frequencies of 60 percent. GFS prediction for Grid 1 and 2 indicates to opposite direction of other models and grid points which

are the closest points of wind farm. Other models shows the NE prevailing wind direction. ALADIN Grid 1 is located in land which also shows NE. The differences between models and observation are originated from land-sea differences.

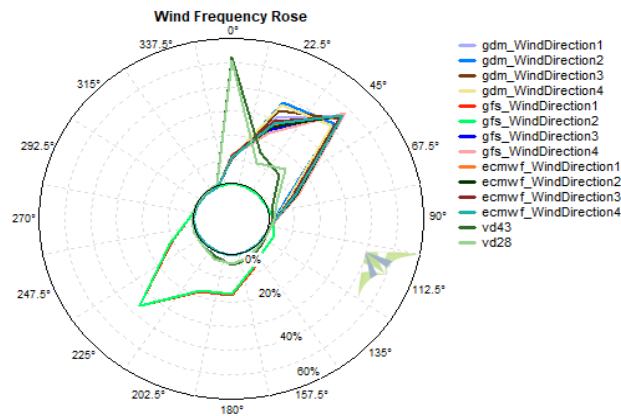


Figure 3.32 Wind Rose for All Grids (WPP-3)

Figure 3.33 shows the monthly mean wind speed calculated over 4 year of data from observations (WS45, and WS30), ALADIN, GFS, and ECMWF at four grid points. WS45 and WS30 are the heights (m) of real measurement sensors. The dashed lines are the average values for 4 grids (ALADIN avg, GFS avg, ECMWF avg). Models unrealistically overestimate the monthly wind for all months. Wind speeds reach to the highest monthly mean values, particularly in February. The sensor at 30 m is closer to prediction values and their monthly variation. The difference between models and observation sensors is quite high until at June. However, ALADIN is closer than other predictions between May and August.

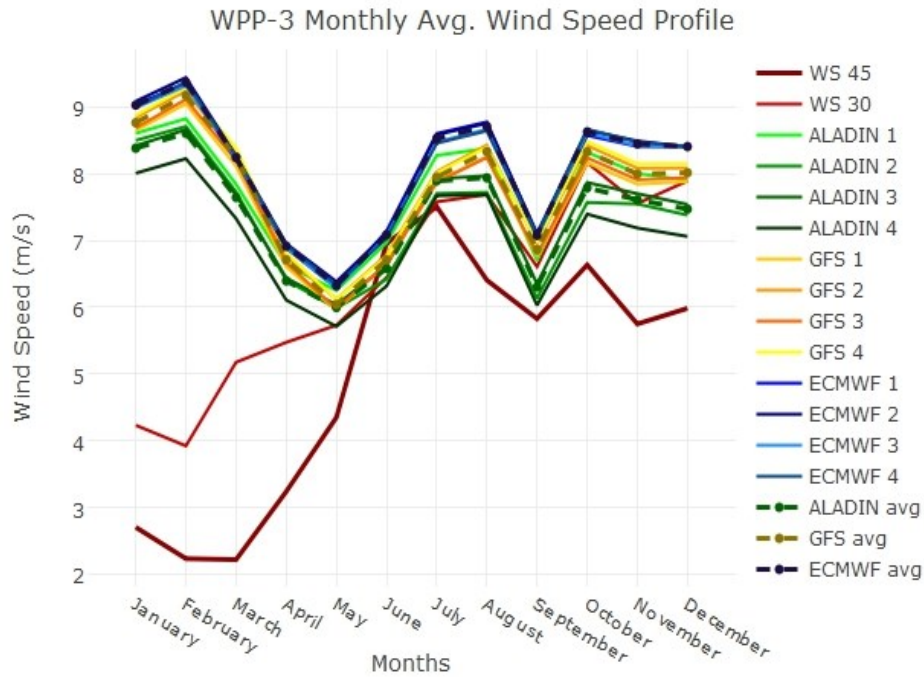


Figure 3.33 Monthly Average Wind Speed Values (WPP-3)

Figure 3.34, 3.35 and 3.36 indicates scatter plots between observed and modeled daily averaged wind speed at each season for ALADIN, GFS, and ECMWF, respectively. Results from all grids points are shown in these figures. ALADIN fall and summer predictions show overestimation and also spring and winter values closer to observation line. (see figure 3.34). Fall values are smaller than 10 m/s and overestimation is obvious. In summer for wind speed higher than 10 m/s models shows underestimation.

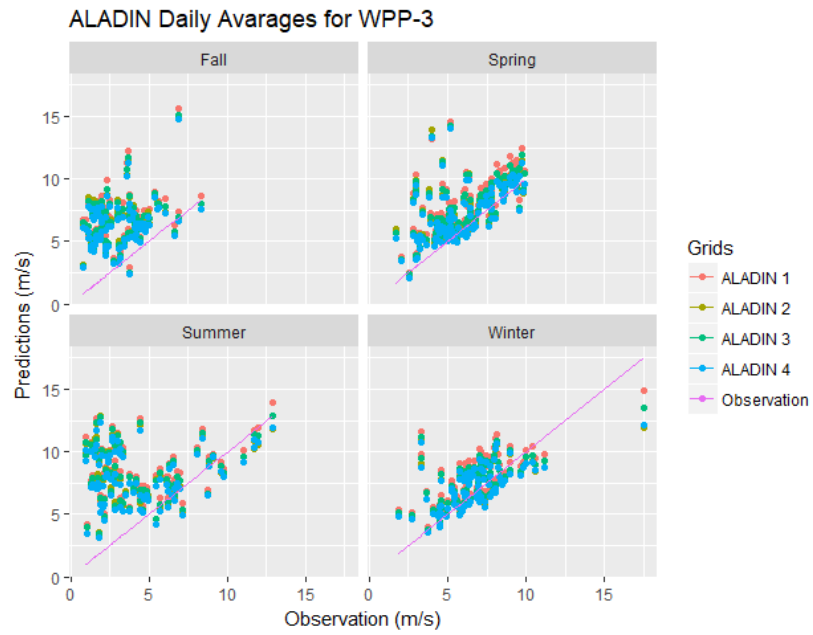


Figure 3.34 Daily Avg. Scatter Plot for ALADIN Predictions (WPP-3)

GFS values could be seen from the Figure 3.35. All grid points for GFS predictions are overestimated. Only winter time seems better like ALADIN. Wind speed values are the same interval with the ALADIN.

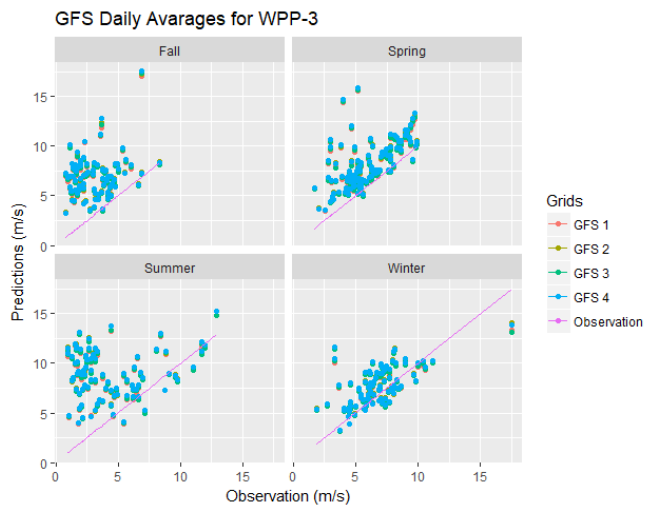


Figure 3.35 Daily Avg. Scatter Plot for GFS Predictions (WPP-3)

Figure 3.36 shows the ECMWF predictions likewise for GFS and ALADIN. All seasons even winter and all grid points show overestimation for ECMWF.

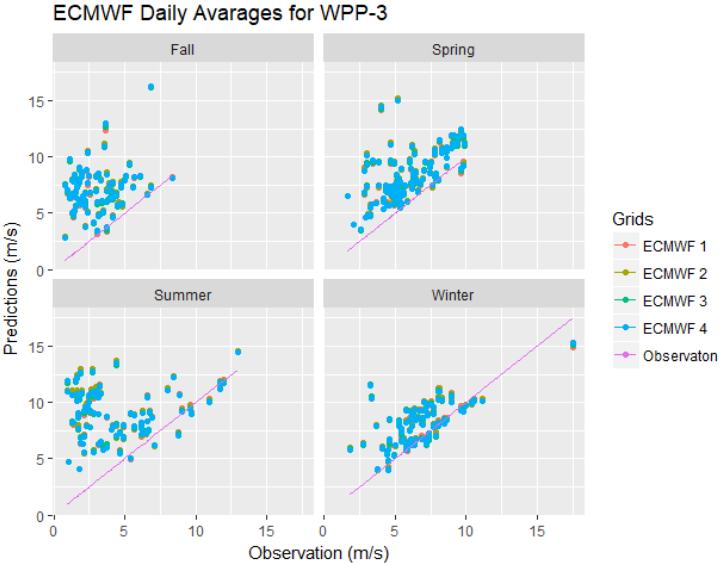


Figure 3.36 Daily Avg. Scatter Plot for ECMWF Predictions (WPP-3)

To sum up, these results show that the ALADIN, GFS and ECMWF initial data predictions are mostly overestimated. Winter time ALADIN predictions are better than other seasons and predictions. Monthly average observed wind speeds are lower in winter, however, predicted wind speeds are higher. There is also big difference between predicted and observed values. Observed wind speeds are higher for summer time and lower winter time. Monthly averages are not higher than 9 m/s. One can understand that the models are not good enough to predict lower wind speeds. But other results have to be examined as well.

The time series of daily average wind speeds calculated from all data period from ALADIN, GFS and ECMWF for 4 grids are compared with observed wind speed in Figure 3.37. This figure shows the overestimation at first quarter of the year which is similar to monthly averages (see figure 3.34). However daily average wind speeds are

higher than monthly averages. All models are better at second half of the year and wind speed values changes between approximately 5 to 12 m/s.

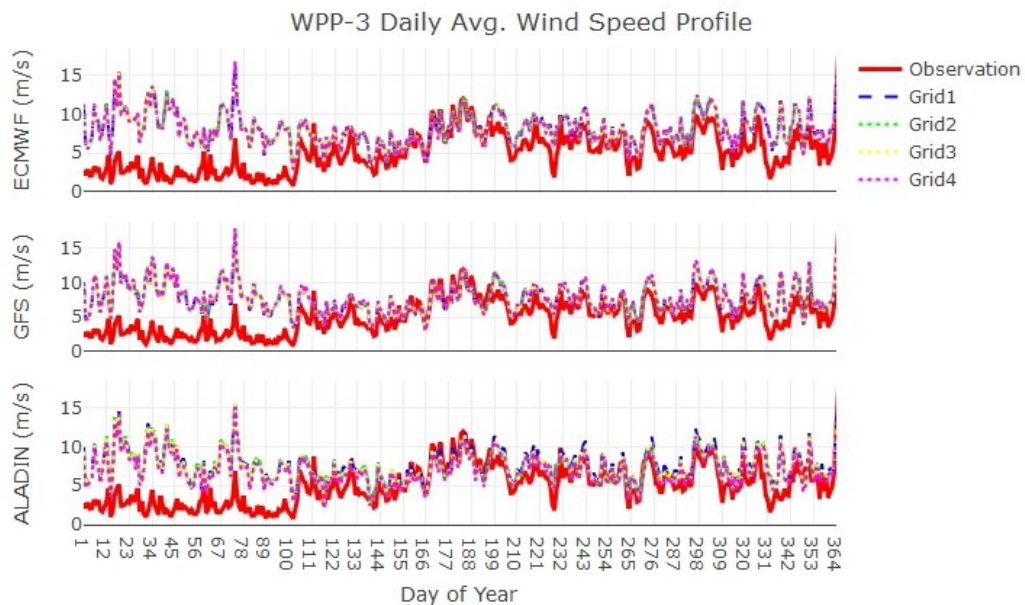


Figure 3.37 Time Series of all NWP and Observation data (WPP-3)

Hourly statistics of bias, RMSE and correlation coefficients are calculated for each season and model grid points from ALADIN, GFS and ECMWF in Table 3.3. The table indicates that all three models show strong overestimation indicated with positive bias values for all seasons. Winter and spring correlations for all models are the lowest in the order of average 25% when it is compared with other seasons. RMSE values are higher in winter. Based on the statistical measures available in this table, the most preferable grid that yields lowest bias and RMSE and high correlation coefficient is selected with respect to each season and model as follows: ALADIN 4, GFS 1, and ECMWF 1 for fall, ALADIN 4, GFS 1, and ECMWF 3 for spring, ALADIN 2, GFS 3, and ECMWF 4 for summer, and ALADIN 4, GFS 1, and ECMWF 3 for winter. The evaluations provided in the following sub-sections are made according to these grids

for each season. The optimum grid selection that provides lowest bias and RMSE, and the highest correlation coefficient for each model is highlighted and underlined in the table (blue for fall, yellow for spring, red for summer and purple for winter).

Table 3-3 Seasonal bias, RMSE and Correlation Coefficients for all models and grids from hourly data

Bias	SEASON	ALADIN-1	ALADIN -2	ALADIN -3	ALADIN -4	GFS-1	GFS-2	GFS-3	GFS-4	ECMWF-1	ECMWF-2	ECMWF-3	ECMWF-4
	Fall	1,582	0,978	1,207	0,772	1,486	1,715	1,540	1,763	1,918	1,979	1,922	1,965
	Spring	3,583	3,374	3,390	3,053	3,547	3,712	3,602	3,755	3,791	3,857	3,794	3,831
	Summer	0,969	0,375	0,601	0,319	0,706	0,858	0,697	0,830	1,272	1,247	1,166	1,141
	Winter	4,797	4,545	4,558	4,115	4,882	5,079	4,936	5,129	5,288	5,331	5,263	5,284
RMSE	Fall	4,434	4,424	4,412	4,332	4,399	4,493	4,432	4,530	4,515	4,564	4,522	4,549
	Spring	5,973	5,878	5,847	5,624	6,092	6,214	6,160	6,277	6,117	6,174	6,110	6,145
	Summer	4,148	4,079	4,128	4,125	4,097	4,146	4,101	4,156	4,158	4,129	4,076	4,054
	Winter	7,747	7,594	7,600	7,282	7,841	7,984	7,879	8,014	7,960	8,023	7,920	7,952
CC	Fall	0,640	0,596	0,615	0,607	0,638	0,639	0,636	0,637	0,646	0,643	0,645	0,644
	Spring	0,313	0,284	0,302	0,297	0,259	0,266	0,255	0,261	0,288	0,288	0,290	0,289
	Summer	0,576	0,546	0,552	0,540	0,564	0,566	0,563	0,562	0,584	0,590	0,594	0,598
	Winter	0,238	0,219	0,229	0,233	0,248	0,252	0,247	0,253	0,256	0,252	0,254	0,252

In brief, these results show that all three models strongly overestimate at hourly, daily and monthly time scales for all seasons. Winter season has the worst results for at all time scales and it has the highest RMSE, lowest correlation and highest bias. It could be stated that, the initial conditions of NWP models have to be arranged for land-sea interactions at terrains near the sea. It seems the models are more successful at lands.

3.3.2. Diurnal Variation

Figure 3.38 indicates to diurnal temperature profile seasonally. The temperature sensor height is 7 m.a.g.l. The diurnal variation of temperature is appropriate for general temperature variation. However overestimation occurs similar to the wind speed predictions. ALADIN is the closest to observed temperatures at winter. The temperature differences between day and night are smaller for all seasons due to the location of wind farm. The biggest difference between models and observation are seen at summer season.

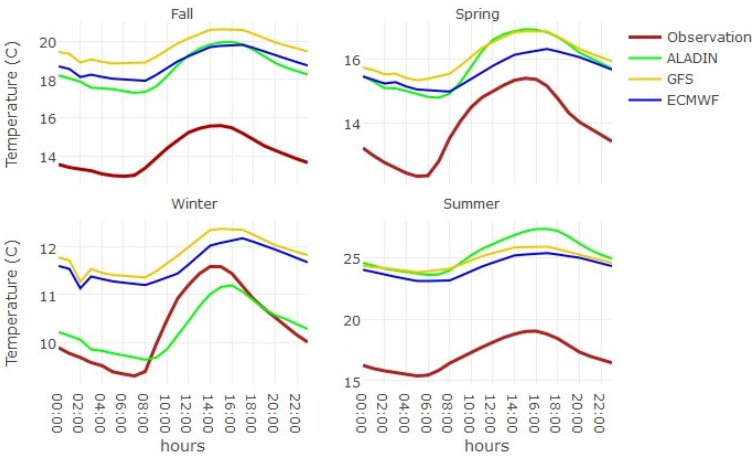


Figure 3.38 Diurnal Temperature by seasonally for the best grids (WPP-3)

Figure 3.39 indicates mean diurnal cycle of wind speed from observation and three models (ALADIN, GFS, and ECMWF) at fall, spring, winter and summer seasons. The figure shows that observed wind speed is nearly constant during the day and night except from summer. The predictions are closer to observations at this seasons and diurnal variation of wind speed is similar to diurnal variation of temperature. Spring and winter predictions are worse than other seasons. Observed wind speeds are always higher at 14:00 am except from winter. ALADIN predictions seems better distribution than other models for all seasons.

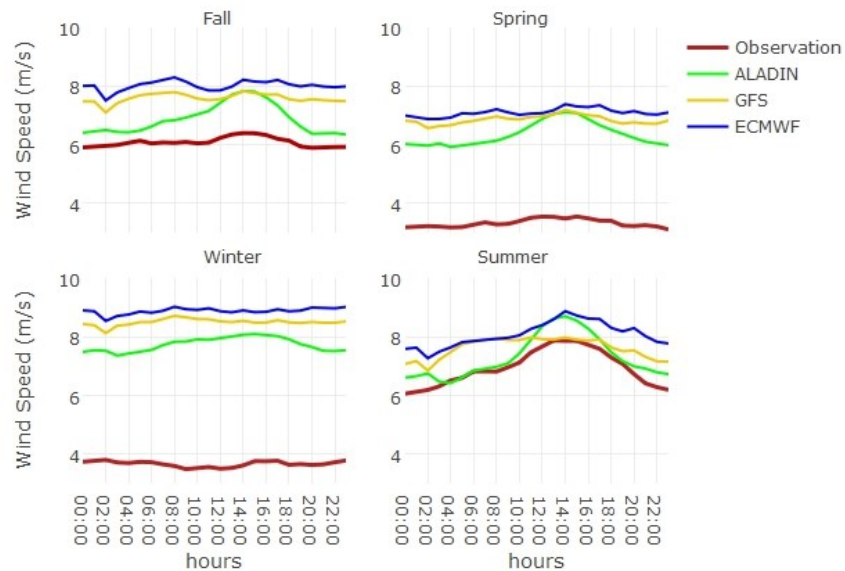


Figure 3.39 Diurnal Wind Speed by Seasonally for the best grids (WPP-3)

Figure 3.40 indicates mean diurnal cycle of RMSE for three models (ALADIN, GFS, and ECMWF) at fall, spring, winter and summer seasons. ALADIN has the lowest RMSE for fall. Spring RMSE values for GFS and ECMWF is similar to fall. However, ALADIN has different fluctuation. ALADIN RMSE values reach the highest values at 14:00 am. In winter, ALADIN again has the lowest RMSE and the biggest errors

also occurs for this season. Summer season has the lowest RMSE values and the variation is similar to wind speed and temperature variations. It means that, when the temperature and wind speed increase, errors are also increase during day for fall and spring. Winter and spring has the highest RMSE values.

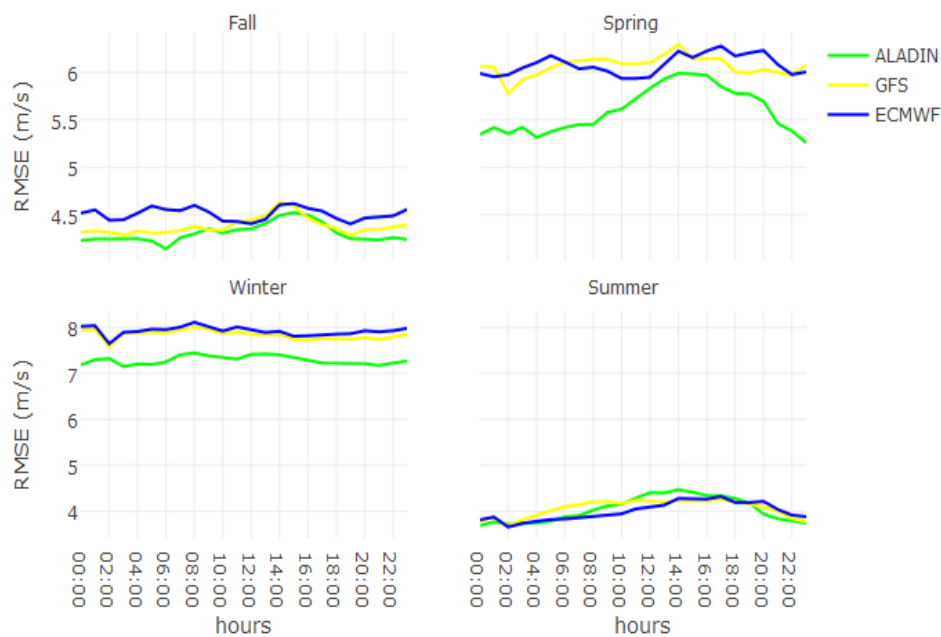


Figure 3.40 Diurnal Cycles for RMSE of Wind Speed (WPP-3)

Figure 3.41 indicates mean diurnal cycle of bias for three models (ALADIN, GFS, and ECMWF) at fall, spring, winter and summer seasons similar to the diurnal RMSE graphics. Diurnal bias values change between + 0.5 and + 2 m/s for fall season. GFS and ECMWF error rates are bigger than the ALADIN. Winter bias values are bigger than other seasons for all models. (changes between + 4 and + 5.5 m/s). ALADIN has negative bias between 04:00 and 06:00 for summer season. ALADIN has lower bias

at sun rise and sunset times for all seasons. GFS has lower bias than ECMWF for all seasons.

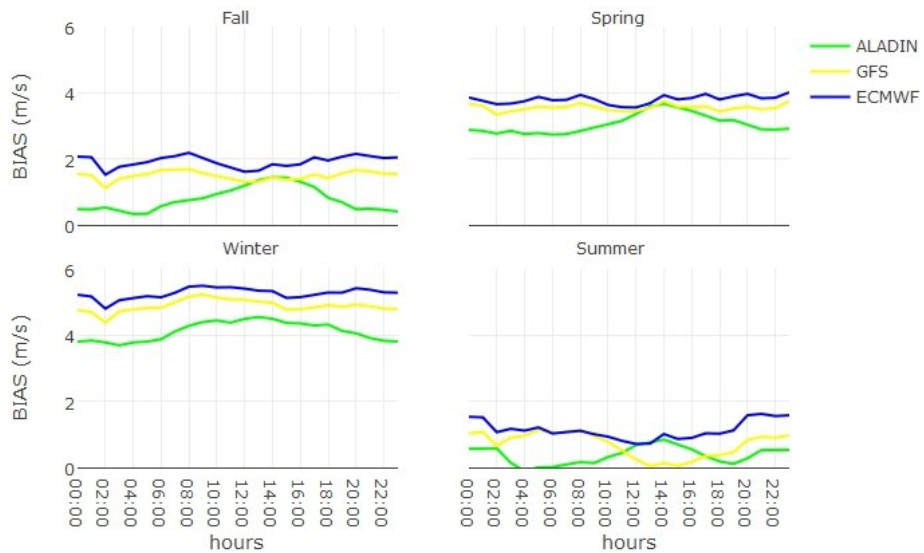


Figure 3.41 Diurnal Cycles for Bias of Wind Speed (WPP-3)

Figure 3.42 indicates diurnal cycle of correlation coefficients between wind speed and three models (ALADIN, GFS, and ECMWF) at fall, spring, winter and summer seasons. It is obvious that ECMWF has the highest correlation for summer and fall. In fall, summer and winter ECMWF predictions is better than others. The lowest correlations are seen at winter and spring. There is an increasing trend for ALADIN at midday hours for fall and spring. The sunset and sunrise correlations are lower than other hours for spring season. GFS has lowest correlations during the spring. Winter correlations for GFS is better than other models from 06:00 to 14:00.

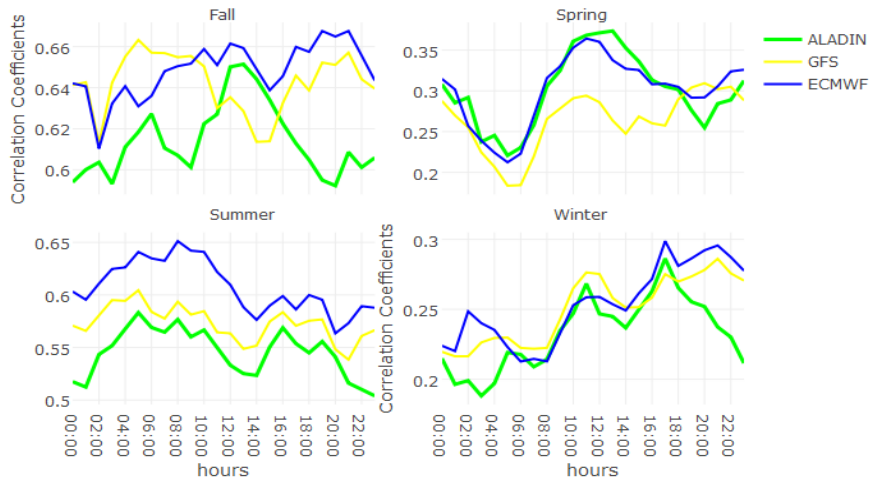


Figure 3.42 Diurnal Cycles for Correlation Coefficient of Wind Speed and Predictions (WPP-3)

3.3.3. Energy Comparison

Figure 3.43 shows the correlation between wind speed and power, and histograms of wind speed and power production values. The “Wind Speed3” graph on the matrix shows the wind speed histogram. Wind speeds are intense in between 3 to 15 m/s and power production starts to increase this wind speeds. The relationship between wind speed and power is nearly linear. The “Power3” graph shows the frequency of power values. The installed capacity of WPP-3 is 10.2 MW. However 0-5 MW production frequencies are higher than others. The maximum produced power value for WPP-3 is 10 MW which means the wind farm rarely produced full capacity electricity. The scatter plot graph on the left bottom of the matrix shows the correlation between wind speed and power. It is similar to power curve (Figure 2.1). The relationship between wind speed and power is nearly linear. The frequency of wind speeds are also high until 15 m/s, which is fair enough for the producer. The pearson correlation coefficient between energy and wind speed is 0.82 which is indicated on the top right of the

matrix. The mean wind speed of entire data is 7.53 m/s and mean produced energy is approximately 3.6 MW.

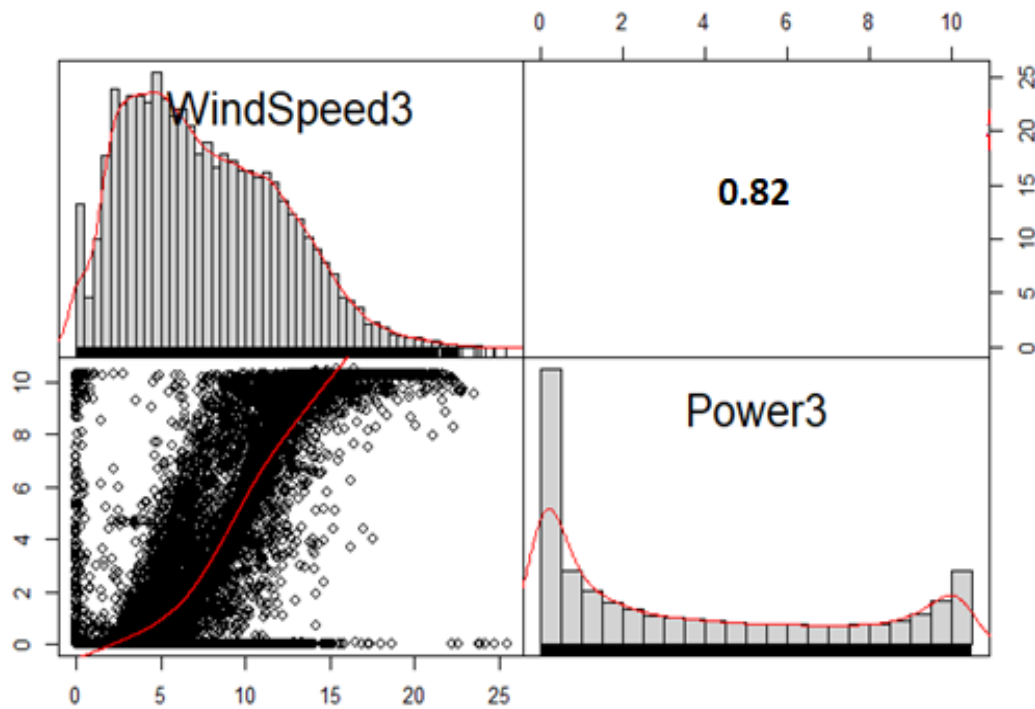


Figure 3.43 The Relationship between Observed Wind Speed and Produced Power (WPP-3)

Figure 3.44 shows the diurnal variation of Energy and Wind Speed values by seasonally. Wind speed values are selected from the final step of RITM forecast system which means a combination of all NWP model outputs. First row shows to produced and predicted power values by seasonally and the bottom row shows the wind speed prediction and observed values. All seasons same diurnal variations are performed both power and wind speed. The difference between production and predictions are always high for all seasons except from summer. Spring and winter wind speed prediction differences are bigger than other seasons. It is not possible to say the

relationship between wind speed predictions and energy predictions are similar to each other for spring season. It means combining all models could not be work for all regions. The reason of this might be NWP grid points on the sea. Although the biggest errors occur in winter predictions. Wind speed and energy predictions have a similar trend. In fall energy predictions starts to increase from midnight to midday. Even if the difference between observed and predicted wind speeds is higher the variation of energy and wind speed are similar to each other during the fall season. All models have the best performance during the summer.

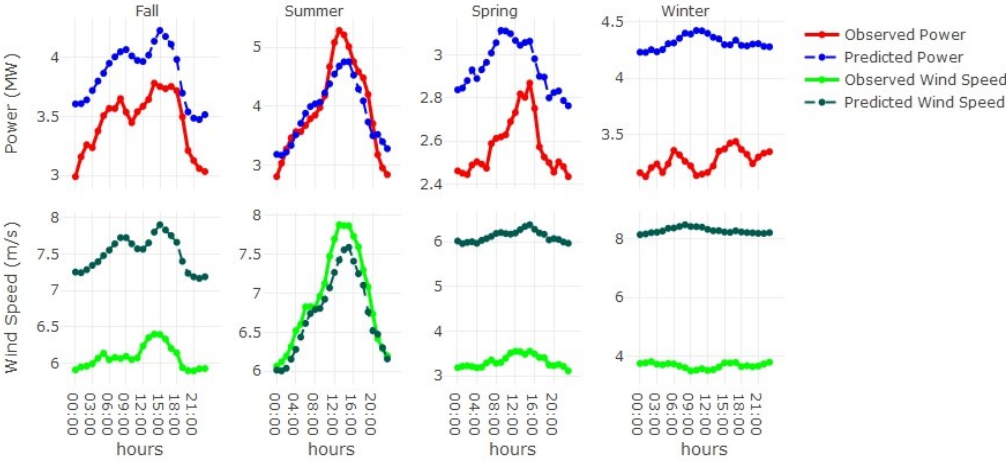


Figure 3.44 Diurnal Cycle for Energy and Wind Speed (WPP-3)

Figure 3.45 shows the monthly RMSE values according to final wind speed predictions and energy predictions for WPP-3. Wind speed RMSE values are higher at winter months. Energy RMSE values are smaller than the wind speeds. They have an increasing trend after the September.

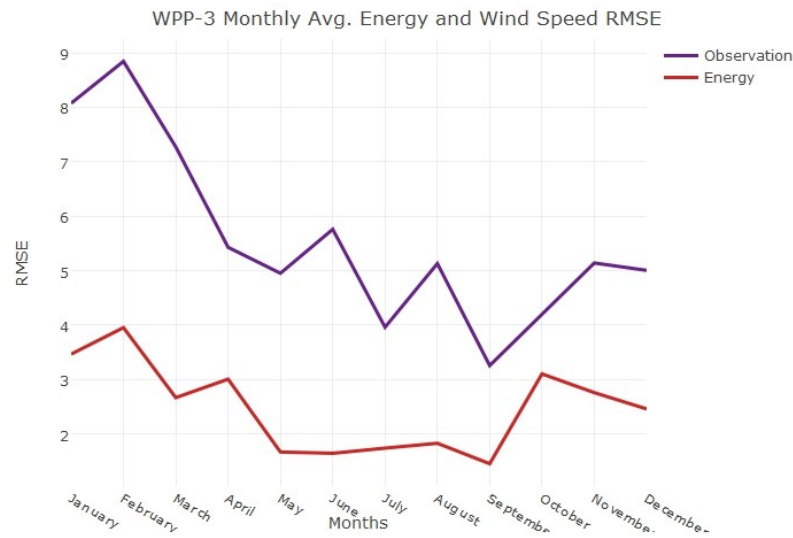


Figure 3.45 Monthly RMSE for Wind Speed and Energy Predictions (WPP-3)

3.4. WPP-4

WPP-4 is located in a land which is effected by the sea from two different direction (NE and NW). ALADIN-1 is the nearest grid for the wind farm. GFS and ECMWF Grid 4 are located over the sea.

3.4.1. Evaluation of Wind Speeds at Monthly, Daily, and Hourly Time Scales

Figure 3.46 shows the seasonal wind direction frequency of hourly data from WOS. The figure shows that prevailing wind direction is NE for fall and summer seasons. However, wind speed values are low particularly in spring and winter. Prevailing wind direction is NW for those seasons. The highest wind speed values occur in the summer season. Fall has better wind speeds than spring and winter seasons but they aren't that much bigger than summer wind speeds. The geographical location of wind farm could

be responsible for two different wind direction. According to Table 2.5 rated wind speed is 15 m/s and cut in wind speed is 4 m/s for WPP-4 turbines. Therefore it could be expected that the production of WPP-4 should be high at summer season.

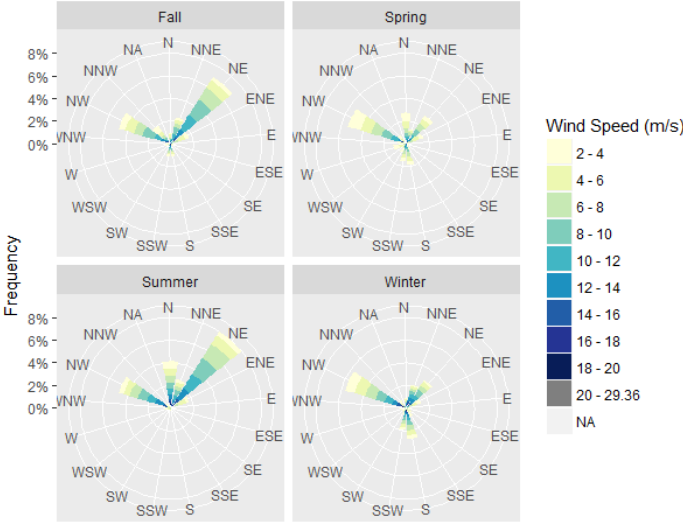


Figure 3.46 Seasonal Wind Rose (WPP-4)

Figure 3.47 shows the wind direction frequency at hourly time scale from observations and all models at four grid points. “vd78” is the WOS direction sensors with height (78 m.a.g.l). NE is the prevailing wind direction for observation values, however, nearly all grids are pointed to opposite direction except from ALADIN 2, GFS 4. ALADIN 2 is located northwestern side of the wind farm which is near by the sea (see figure 2.18). GFS 4 is also indicates to NE prevailing wind direction which is located at the sea.

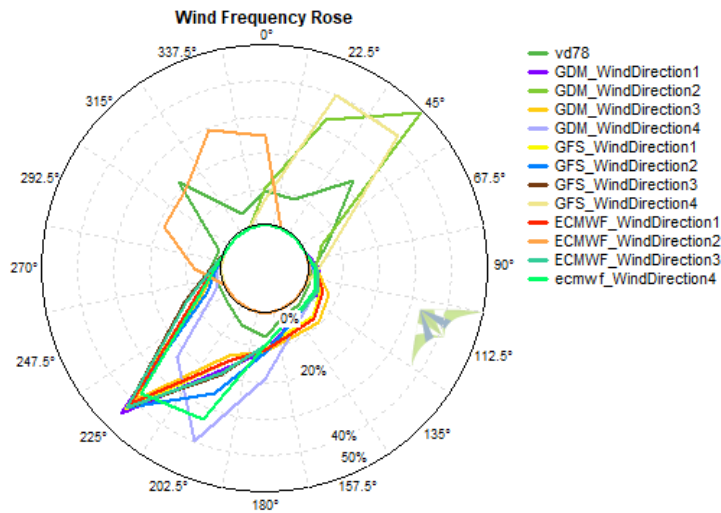


Figure 3.47 Wind Rose for All Grids (WPP-4)

Figure 3.48 shows the monthly mean wind speed calculated over 4.7 year of data from observations (WS80, WS65, and WS50), ALADIN, GFS, and ECMWF at four grid points. WS80, WS65 and WS50 are the heights (m) of real measurement sensors. The figure shows that all models show underestimation and ECMWF predictions are closer to observations. February and August values are bigger than other seasons. ALADIN has worse predictions than others. The spring months are lower than other months.

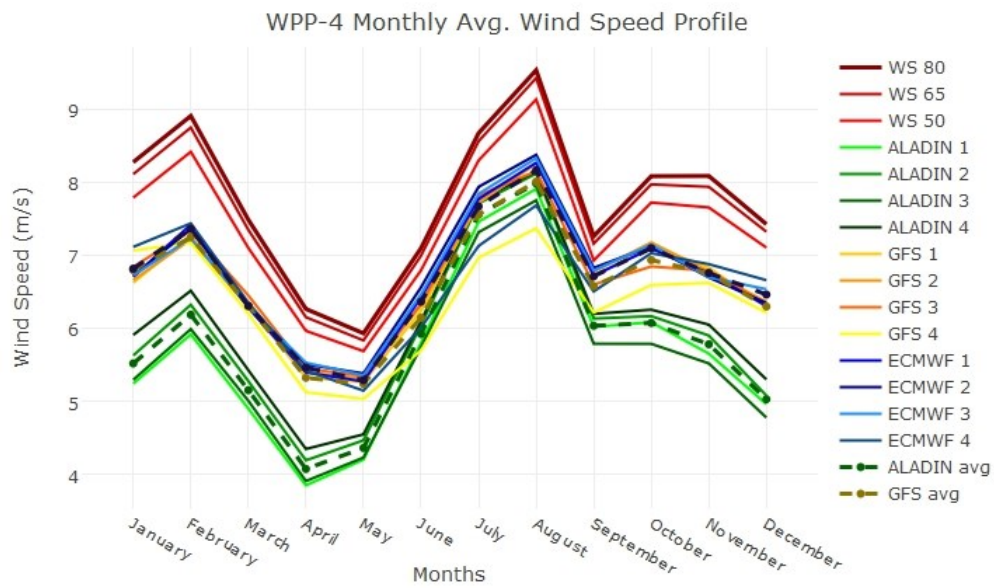


Figure 3.48 Monthly Average Wind Speeds (WPP-4)

Figure 3.49, 3.50, and 3.51 show scatter plots between observed and modeled daily averaged wind speed at each season for ALADIN, GFS, and ECMWF, respectively. Results from all grids points are shown in these figures. ALADIN model shows a similar performance from all grid points at each season. The model results show underestimation for all seasons. It shows that ALADIN values for all seasons nearly for all grids are underestimated. In fall times wind speeds are not higher than 12 m/s and all values underestimated. In spring and summer wind speeds changes between 5 m/s and 12.5 m/s. However, in winter times, daily averages have reached to 15 m/s but again underestimation exists.

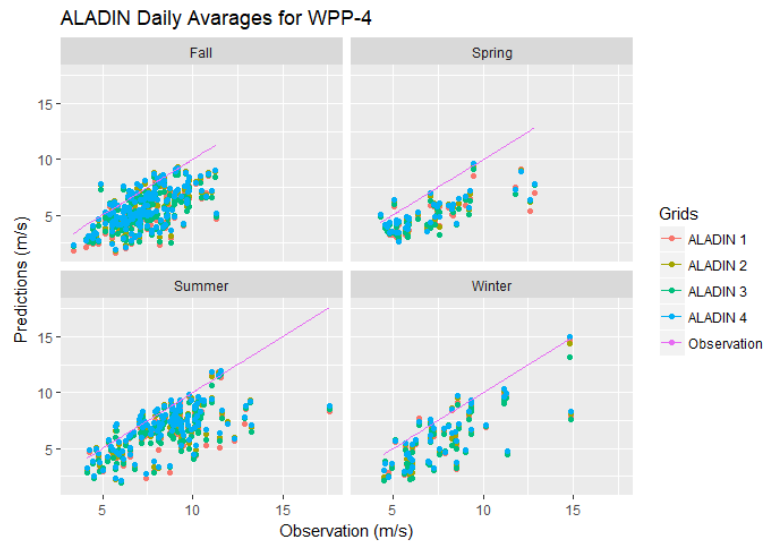


Figure 3.49 Daily Avg. Scatter Plot for ALADIN Predictions (WPP-4)

GFS predictions are similar to ALADIN for all seasons (Fig.3.50). However they are closer than ALADIN to observation line.

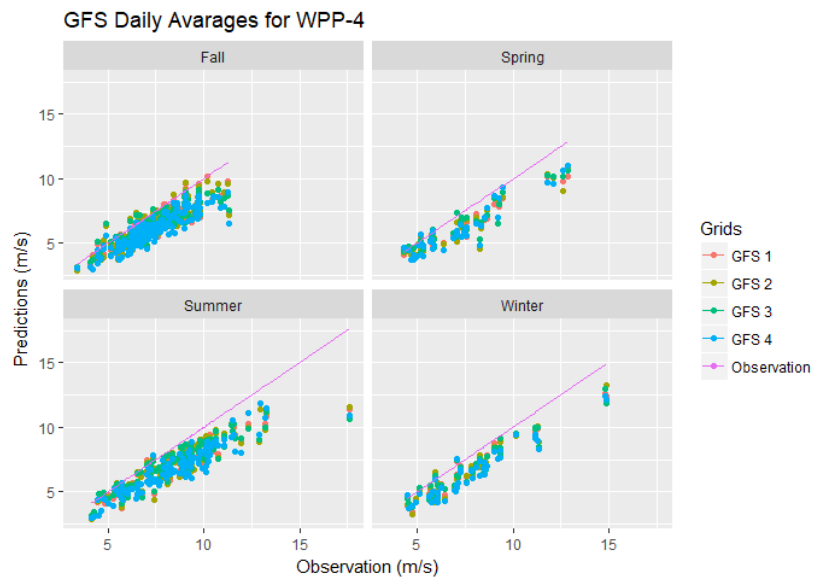


Figure 3.50 Daily Avg. Scatter Plot for GFS Predictions (WPP-4)

A similar prediction performance like in GFS seems to appear in ECMWF predictions at each season (Figure 3.51). The distribution is same with the GFS.

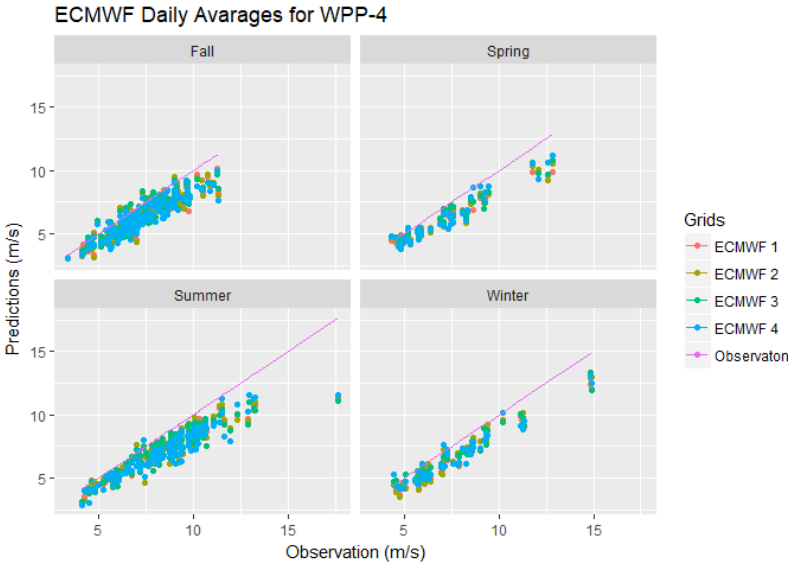


Figure 3.51 Daily Avg. Scatter Plot for ECMWF Predictions (WPP-4)

According to the analysis of averaged daily wind speed provided in these scatter plots (Fig 3.49, 3.50 and 3.51) the ALADIN model is less reliable for all seasons and other two models (GFS and ECMWF) depending on their seasonal performances are more preferable in wind power production.

The time series of daily average wind speeds calculated from all data period from ALADIN, GFS and ECMWF for 4 grids are compared with observed wind speed in Figure 3.52. This figure shows that while ALADIN predictions are generally underestimated, GFS and ECMWF values are closer to observation values. This underestimation is more significant particularly for during summer and also towards winter season. However all models generally show underestimation.

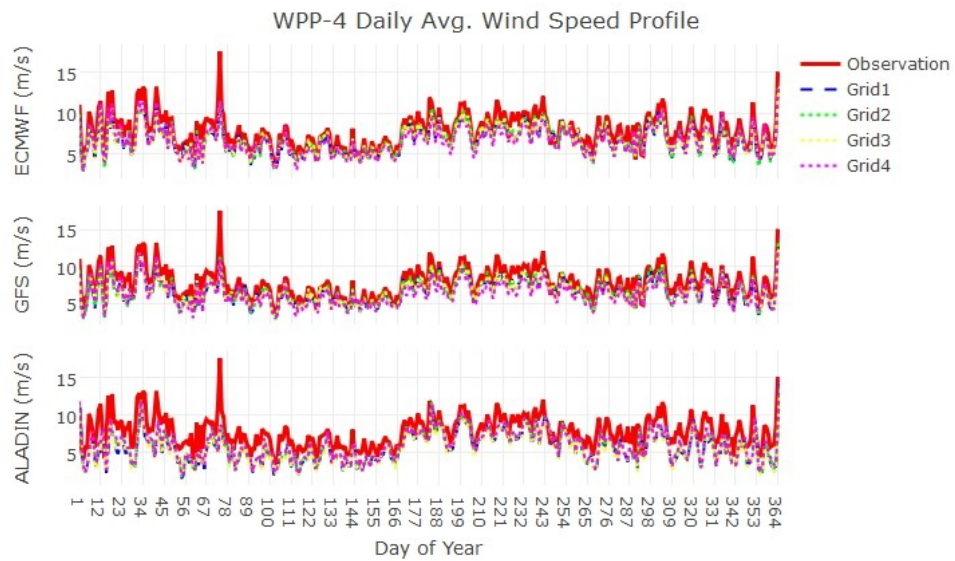


Figure 3.52 Time Series of all NWP and Observation data (WPP-4)

Hourly statistics of bias, RMSE and correlation coefficients are calculated for each season and model grid points from ALADIN, GFS and ECMWF in Table 3.4. The table indicates that all three models show strong underestimation indicated with negative bias values for all seasons. ALADIN correlations are lower for all seasons than other models and RMSE values of ALADIN has also the highest for all seasons. The most successful season for ALADIN is summer, however other models are again better than the ALADIN. ECMWF has better than other models for all seasons. Based on the statistical measures available in this table, the most preferable grid that yields lowest bias and RMSE and high correlation coefficient is selected with respect to each season and model as follows: ALADIN 4, GFS 1, and ECMWF 4 for fall, ALADIN 4, GFS 3, and ECMWF 1 for spring, ALADIN 4, GFS 3, and ECMWF 3 for summer, and ALADIN 4, GFS 1, and ECMWF 4 for winter. The evaluations provided in the following sub-sections are made according to these grids for each season. The optimum grid selection that provides the lowest bias and RMSE, and highest

correlation coefficient for each model is highlighted and underlined in the table (blue for fall, yellow for spring, red for summer and purple for winter).

Table 3-4 Seasonal bias, RMSE and Correlation Coefficients for all models and grids from hourly data

Bias	SEASON	ALADIN-1	ALADIN-2	ALADIN-3	ALADIN-4	GFS-1	GFS-2	GFS-3	GFS-4	ECMWF-1	ECMWF-2	ECMWF-3	ECMWF-4
	Fall	-1,917	-1,772	-2,127	-1,677	-0,929	-0,901	-1,057	-1,312	-0,976	-0,946	-0,931	-0,967
	Spring	-2,168	-1,845	-2,100	-1,727	-0,872	-0,841	-0,765	-1,068	-0,858	-0,784	-0,782	-0,890
	Summer	-1,280	-1,039	-1,390	-0,997	-0,917	-0,895	-0,905	-1,646	-0,823	-0,687	-0,758	-1,345
	Winter	-2,801	-2,522	-2,843	-2,289	-1,464	-1,432	-1,358	-1,382	-1,382	-1,379	-1,334	-1,106
RMSE	Fall	4,72635 4994	4,672724 292	4,772118 498	4,620149 327	2,367624 466	2,484570 209	2,391757 139	2,574722 216	2,389780 095	2,493284 001	2,307763 347	2,307462 619
	Spring	4,45348 4988	4,300929 352	4,409882 853	4,238863 442	2,494942 376	2,565749 83	2,414434 712	2,592228 157	2,394273 488	2,469137 315	2,366186 885	2,406260 037
	Summer	3,44507 1107	3,364164 849	3,515432 593	3,335947 77	2,271664 931	2,327889 703	2,201097 46	2,643283 436	2,147191 693	2,139501 64	2,009979 027	2,335225 919
	Winter	5,68500 0805	5,535648 303	5,580132 958	5,488385 946	2,865264 264	2,964790 033	2,918514 913	2,912361 001	2,767631 097	2,861008 853	2,794653 919	2,732901 334
CC	Fall	0,407	0,413	0,411	0,415	0,840	0,821	0,844	0,832	0,840	0,824	0,849	0,851
	Spring	0,399	0,404	0,391	0,408	0,779	0,763	0,787	0,772	0,799	0,780	0,799	0,798
	Summer	0,685	0,683	0,679	0,679	0,861	0,850	0,871	0,866	0,874	0,867	0,890	0,888
	Winter	0,428	0,441	0,447	0,432	0,859	0,842	0,844	0,846	0,867	0,854	0,862	0,854

3.4.2. Diurnal Variation

Figure 3.53 indicates to diurnal temperature profile seasonally. The temperature sensor height is 9 m.a.g.l. The diurnal variation of temperature is appropriate general temperature variation. However overestimation occurs in contrast to wind speed predictions. ECMWF and GFS have same variation for all seasons. ALADIN is different from them. The difference between day and night temperatures are not high for observations, but high for models except from ALADIN.

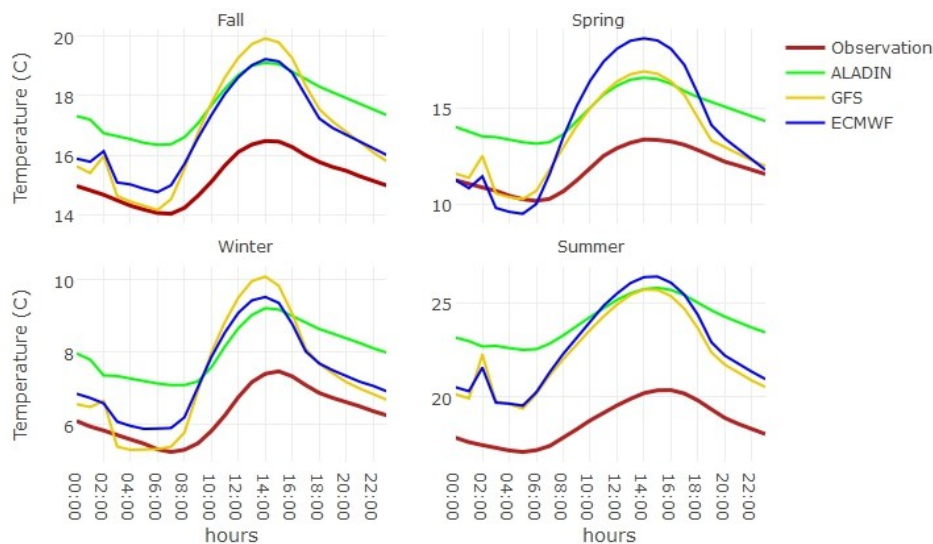


Figure 3.53 Diurnal Temperature by seasonally for the best grids (WPP-4)

Figure 3.54 indicates mean diurnal cycle of wind speed from observation and three models (ALADIN, GFS, and ECMWF) at fall, spring, winter and summer seasons. All models are showed underestimation. In fall, ECMWF variation with time is almost same with the observed wind speed except from 02:00 am to entire day. All models are suddenly decreased at this hour. In winter, observed wind speeds are higher at mornings and getting decreased until the sunset. The fluctuation of models and observed wind is different from each other for this season. In spring, only

ECMWF is closer to observation line and all models have different fluctuation. However, GFS has same variation with observed wind speeds from midnight to morning. In summer, all models seem better than other seasons. Wind speeds are nearly constant during the night and starts to increase after midday.

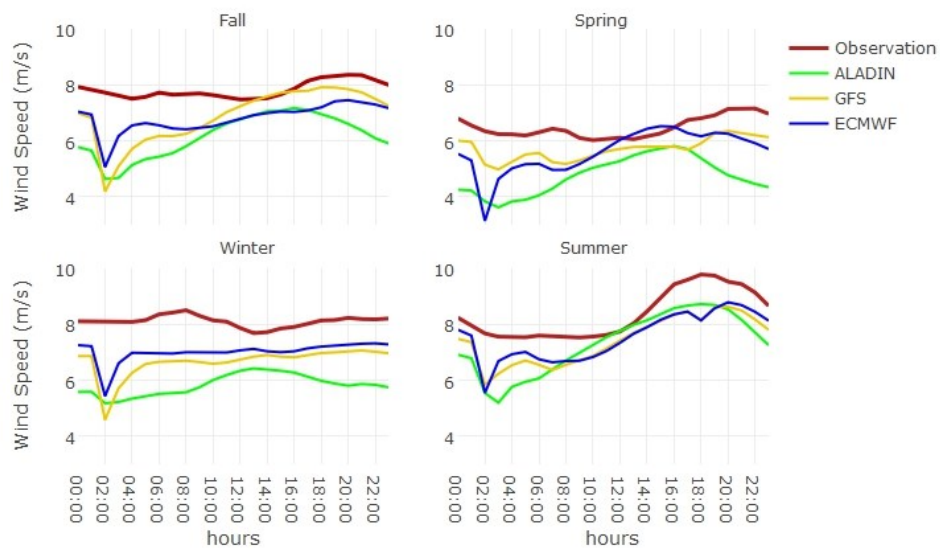


Figure 3.54 Diurnal Wind Speed by Seasonally for the best grids (WPP-4)

Figure 3.55 indicates mean diurnal cycle of RMSE for three models (ALADIN, GFS, and ECMWF) at fall, spring, winter and summer seasons. The figure shows that ALADIN has the highest RMSE for all seasons and grids. GFS and ECMWF have same fluctuation similar to wind speeds. ECMWF has lowest RMSE for all seasons. RMSE is also nearly constant during the day except from 02:00 am. Summer RMSE values are smaller than other seasons.

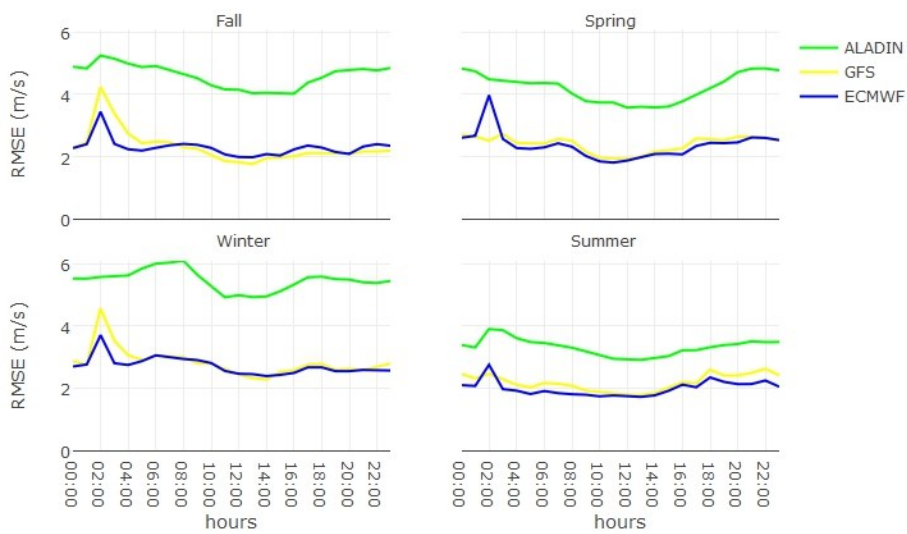


Figure 3.55 Diurnal Cycles for RMSE of Wind Speed (WPP-4)

Figure 3.56 indicates mean diurnal cycle of bias for three models (ALADIN, GFS, and ECMWF) at fall, spring, winter and summer seasons similar to the diurnal RMSE graphics. Diurnal bias values change between -3 and 0 m/s for fall season. GFS and ECMWF error rates are smaller than the ALADIN, except from midday hours of summer. ECMWF is better during the night and GFS is better during the day for fall season. ECMWF is better for winter at all hours. In spring, GFS bias values are smaller than other models during the night. However, when the sun rises ECMWF grid 1 are showed better bias values than GFS until 20:00. Summer bias values for GFS and ECMWF is similar to other figures, however ALADIN bias values are smaller than these two model during the day.

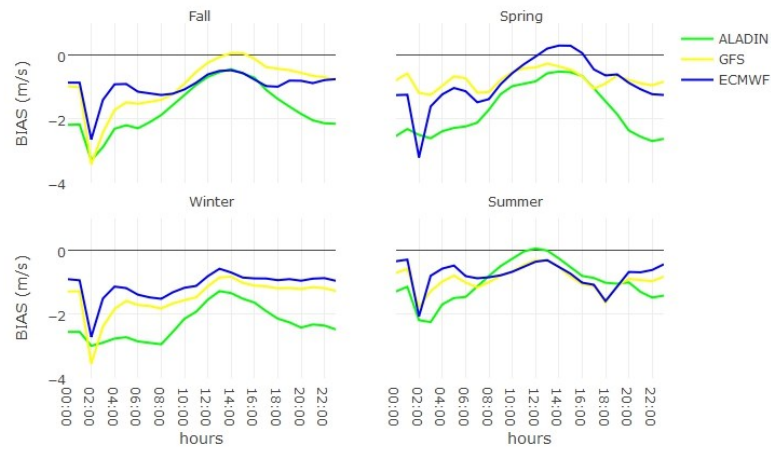


Figure 3.56 Diurnal Cycles for bias of Wind Speed (WPP-4)

Figure 3.57 shows the diurnal cycle for correlation coefficients between wind speed predictions and observations. ALADIN correlation coefficients are the lowest as it is expected for all seasons. GFS and ECMWF have better and similar variation. The highest correlation between wind speed and predictions occurs at summer time. However, summer night correlations are lower when compared to day values. ECMWF is better at summer and spring. GFS for winter and fall have better correlation during the day hours. ECMWF is better during the midnight hours for these seasons.

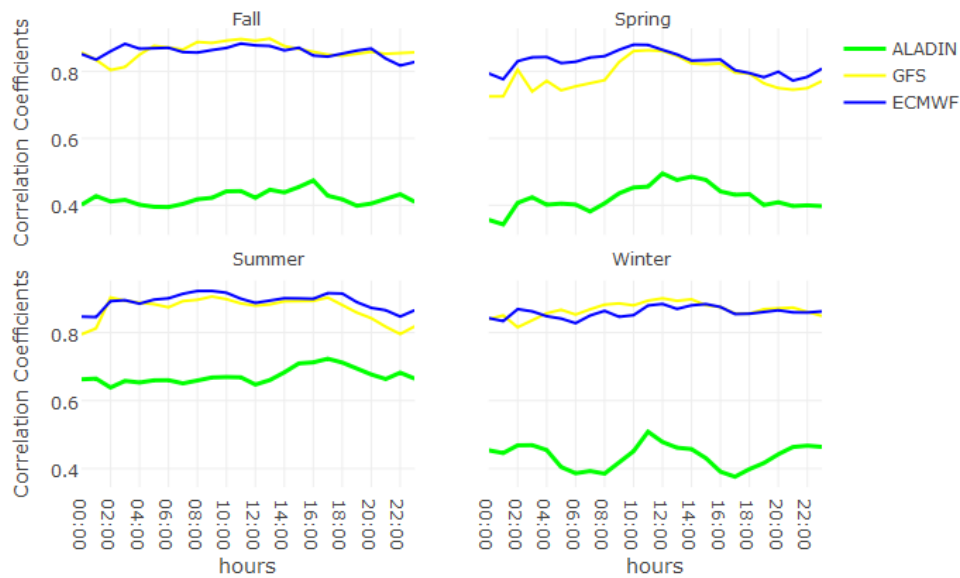


Figure 3.57 Diurnal Cycles for Correlation Coefficient of Wind Speed and Predictions (WPP-4)

3.4.3. Energy Comparison

Figure 3.58 shows the correlation between wind speed and power, and histograms of wind speed and power production values. The “Wind Speed4” graph on the matrix shows the wind speed histogram. Wind speeds are intense in between 3 to 13 m/s and power production starts to increase this wind speeds. The “Power4” graph shows the frequency of power values. The installed capacity of WPP-4 is 15 MW. However 0-5 MW productions are higher than others. The maximum produced power value for WPP-4 is 15 MW which means the wind farm rarely produced full capacity electricity. The scatter plot graph on the left bottom of the matrix shows the correlation between wind speed and power. It is similar to power curve (Figure 2.1). The relationship between wind speed and power is nearly linear. The frequency of wind speeds are also high until 15 m/s, which is fair enough for the producer. The pearson correlation coefficient between energy and wind speed is 0.88 which is indicated on the top right

of the matrix. The mean wind speed of entire data is 7.08 m/s and mean produced energy is approximately 5 MW.

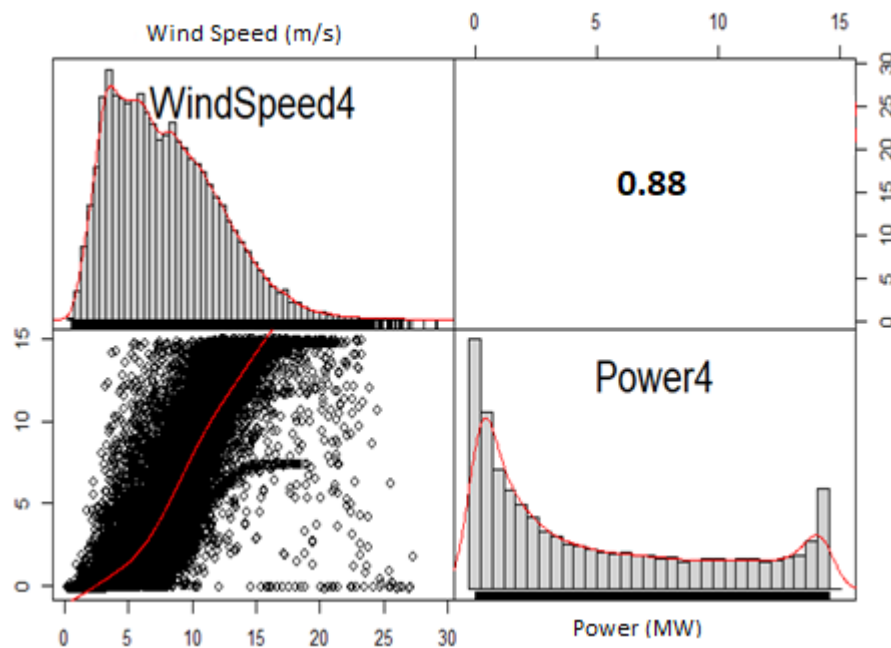


Figure 3.58 The Relationship between Observed Wind Speed and Produced Power (WPP-4)

Figure 3.59 shows the diurnal variation of energy and wind speed values by seasonally. Wind speed values are selected from the final step of RITM forecast system which means a combination of all NWP model outputs. First row shows to produced and predicted power values by seasonally and the bottom row shows the wind speed prediction and observed values. All seasons same diurnal variations are performed both power and wind speed. The difference between observed and predicted wind speed are responsible for the differences in energy predictions during the fall seasons. Summer predictions better for both energy and wind speeds. In spring and winter time, there is a decreasing trend from midnight to midday for observed data, however models predict to decreasing trend until the sunrise. There is an increasing trend from sunrise

to 15:00 for predicted data during winter and spring. NWP and energy oscillations are similar to each other again.

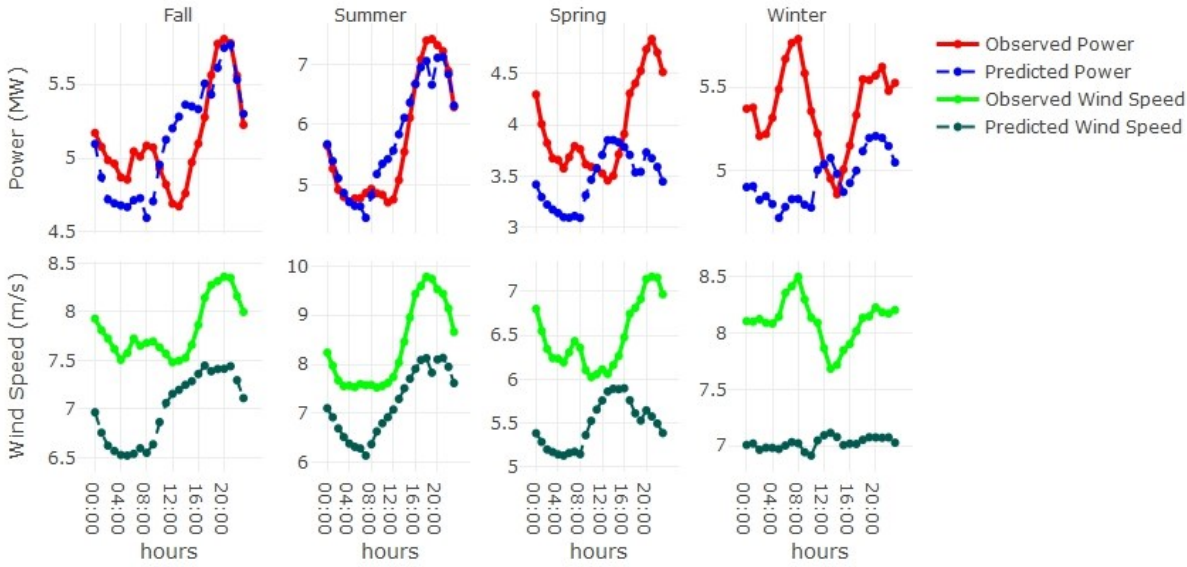


Figure 3.59 Diurnal Cycle for Energy and Wind Speed (WPP-4)

Figure 3.60 demonstrates the monthly RMSE values according to final wind speed predictions and energy predictions for WPP-4. Wind speed RMSE values are lower than energy RMSE values during winter and summer months and starts to increase after April.

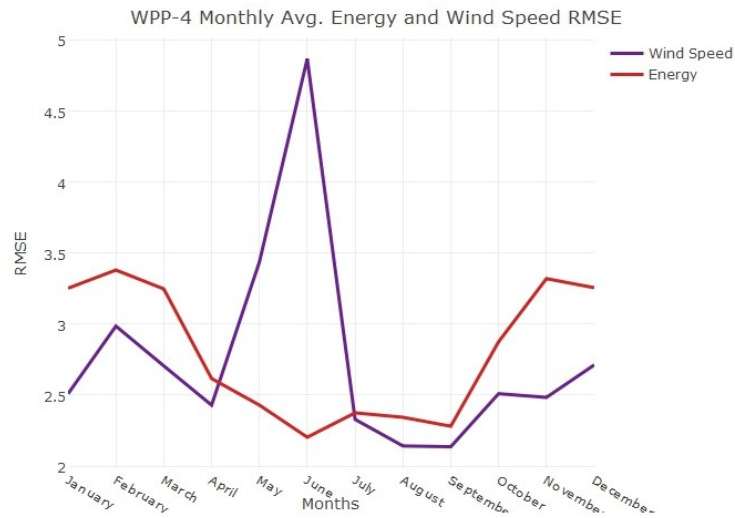


Figure 3.60 Monthly RMSE for Wind Speed and Energy Predictions (WPP-4)

3.5. WPP-5

The turbines of WPP-5 are laid down in northwest-southeast direction. The wind farm is surrounded by two hills from west and southeast that are approximately over 1400 m above the sea level (Figure 2.3). The WOS data covers 4 year. WPP-5 is located in one of the most complex terrain in this study. The height of the wind farm is 646 m.a.s.l. and all grids are over the 500 m.a.s.l.

3.5.1. Evaluation of Wind Speeds at Monthly, Daily, and Hourly Time Scales

Figure 3.61 shows the seasonal wind direction frequency of hourly data from WOS. It shows that the wind speeds reach the highest values in summer and prevailing wind direction is NW for WPP 5. In spring and winter seasons wind speeds are lower than the other seasons. According to Table 2.5, rated wind speed is 17 m/s and cut in wind

speed is 4 for WPP-5 turbines. Therefore it could be expected that the production of WPP-5 should be high in summer and fall.

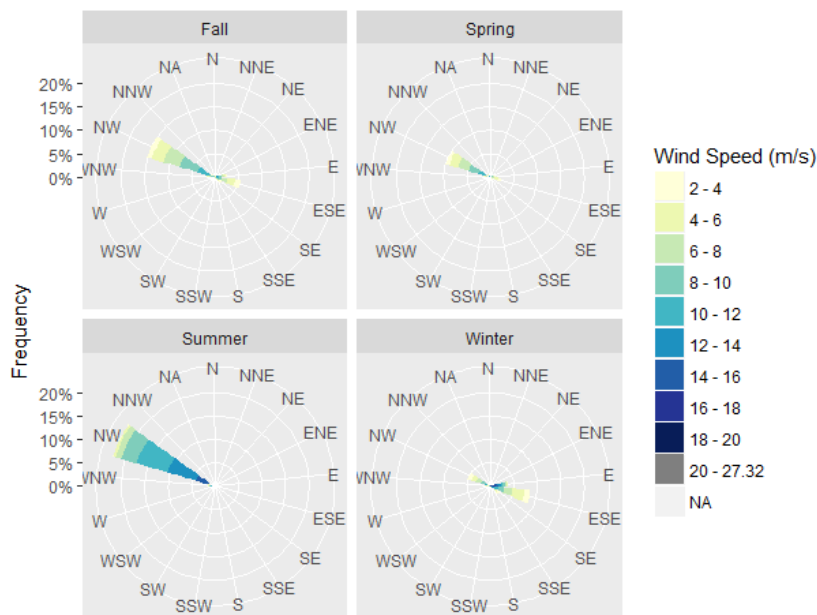


Figure 3.61 Seasonal Wind Rose (WPP-5)

Figure 3.62 shows the wind direction frequency at hourly time scale from observations and all models at four grid points. “vd78” and “vd48” are the WOS directions sensors with height (78 m.a.g.l or 48 m.a.g.l.) and they both show that the prevailing wind direction is approximately 315° (NW) with the frequencies of 40 to 70 percent. ECMWF Grid 3 shows the same prevailing wind direction with observations. However, GFS and ECMWF Grid 4 shows the 112.5° (SEE), ECMWF Grid 1 shows 90° (E) and GFS Grid 2 shows 67.5° (NEE) which are different from prevailing wind direction. Other models and grid points are also indicate to opposite wind direction (SE). According to Table 2-2 ECMWF and GFS Grid 4 is located in 327 m.a.s.l. and WOS located in 626 m.a.s.l. The height differences between all grid points may be responsible for this differences.

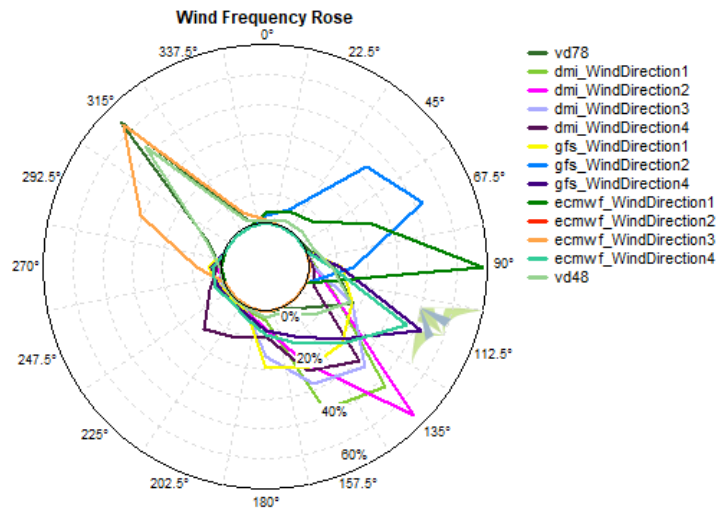


Figure 3.62 Wind Rose for All Grids (WPP-5)

Figure 3.63 shows monthly mean wind speeds calculated over 4-year data from observations (WS80, WS65, and WS50), ALADIN, GFS, and ECMWF at four grid points. WS80, WS65 and WS50 are the heights (m) of real measurement sensors. The dashed lines are the average values for 4 grids (ALADIN avg, GFS avg, ECMWF avg). Models underestimate the monthly wind except from GFS grids 2 and 3 and ECMWF grids 2 and 3. All models follow a similar trend with observation during the rest of the months in the year except from ALADIN grid 4.

Among models ALADIN predictions strongly underestimates particularly from grid 4. The discrepancy between observation and models is greatly reduced with ECMWF and GFS model during summer months. GFS grid 2 and 3 have same wind speed data. ECMWF grid 2 and 3 also have same problem. This problem would be reasoned from same coordinate records for both grids on RITM system.

Wind speeds reach the highest monthly mean values (up to 13 m/s) during summer months while they drop to 6-7 m/s during winter months.

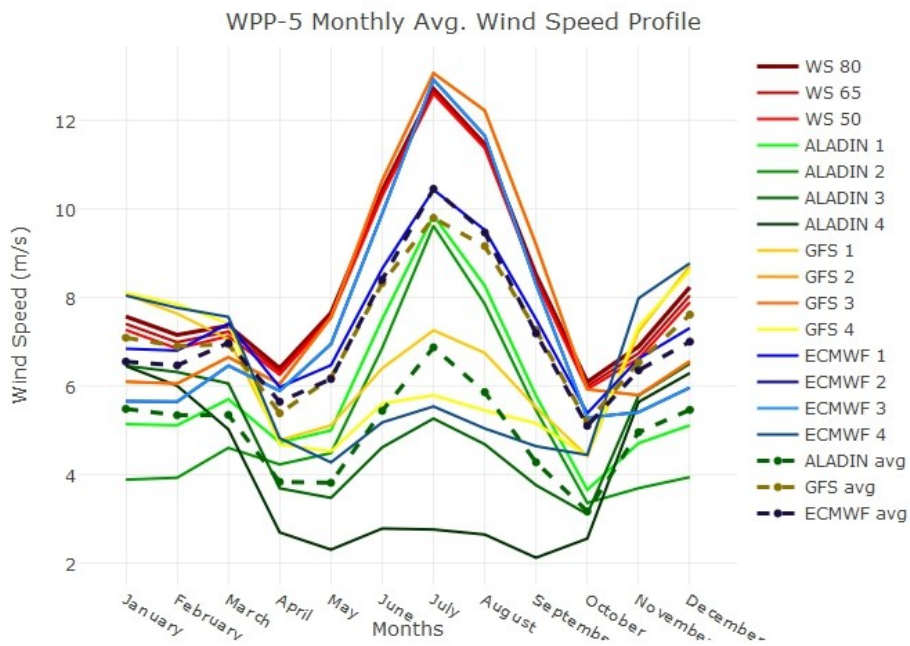


Figure 3.63 Monthly Average Wind Speed Values (WPP-5)

Figure 3.64, 3.65, and 3.66 show scatter plots between observed and modeled daily averaged wind speed at each season for ALADIN, GFS, and ECMWF, respectively. Results from all grids points are shown in these figures. The scatter plot graphs of WPP-5 are different from other 4 wind farms due to the obvious grid scattering. It means the discrepancy of each grid point is obvious for WPP-5.

ALADIN model is obviously showed underestimation for spring and winter seasons. ALADIN grid 1 is showed better distribution than other grids for spring and winter. Wind speed ranges for these seasons are approximately 3-13 m/s for observations. ALADIN grid 4 has the lowest wind speed predictions for winter season. Fall and summer predictions are better than other seasons. However, all grid points are showed underestimation, except from ALADIN grid 4 which is closer to observation line.

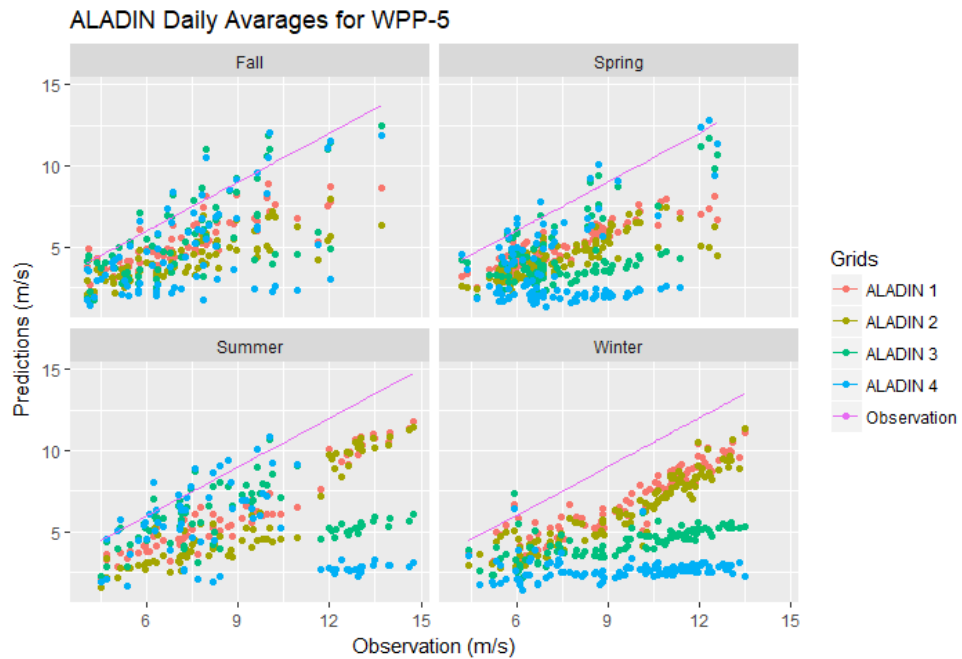


Figure 3.64 Daily Avg. Scatter Plot for ALADIN Predictions (WPP-5)

Throughout the range of daily wind speeds between 3 and 12.5 m/s GFS grid 1 and 4 underestimate the wind in winter and spring (See Fig. 3.65). The range of daily wind speeds between 3 and 10 m/s GFS predictions are better than ALADIN in summer and fall. GFS 1 and 4 are mostly showed underestimation at the range of daily wind speeds between 3 and 10 m/s in spring. Fall predictions of GFS are better than other seasons.

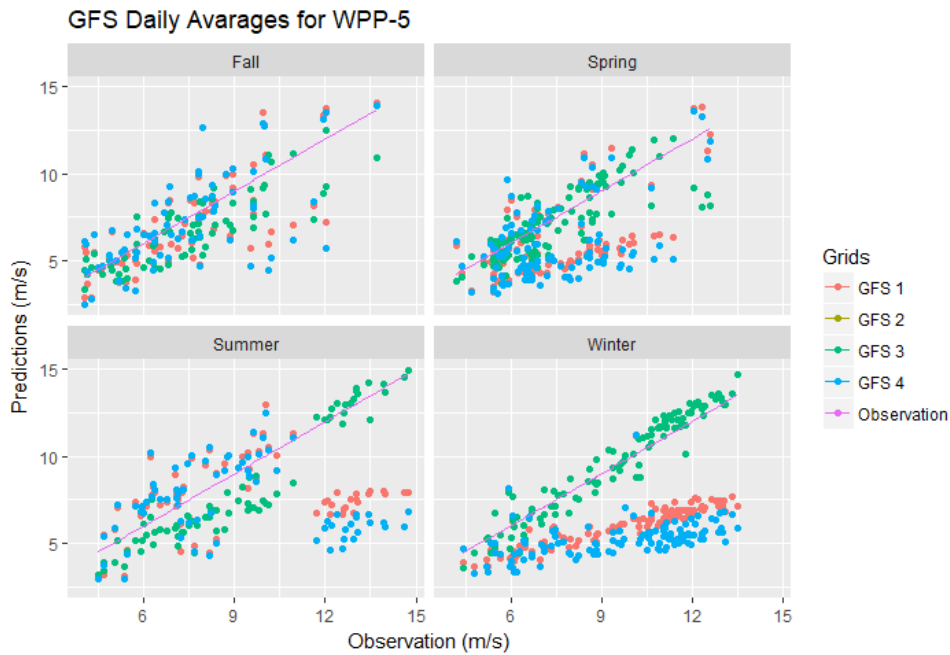


Figure 3.65 Daily Avg. Scatter Plot for GFS Predictions (WPP-5)

Figure 3.66 shows the ECMWF predictions likewise for GFS. The distribution is more scattered but the level of underestimation is more reduced with ECMWF results. The initial condition of WRF model is responsible for these changes. It seems that Grid 3 provides the best scatter distribution for winter. ECMWF Grid 1 has better performance up to 10 m/s wind speeds in fall and summer. In spring, not only grid 1 but also grid 3 has better performance up to 9 m/s.

According to the analysis of averaged daily wind speed provided in these scatter plots (Fig 3.64, 3.65, and 3.66) the ALADIN model is less reliable for all seasons and other two models (GFS and ECMWF) depending on their seasonal performances are more preferable in wind power production.

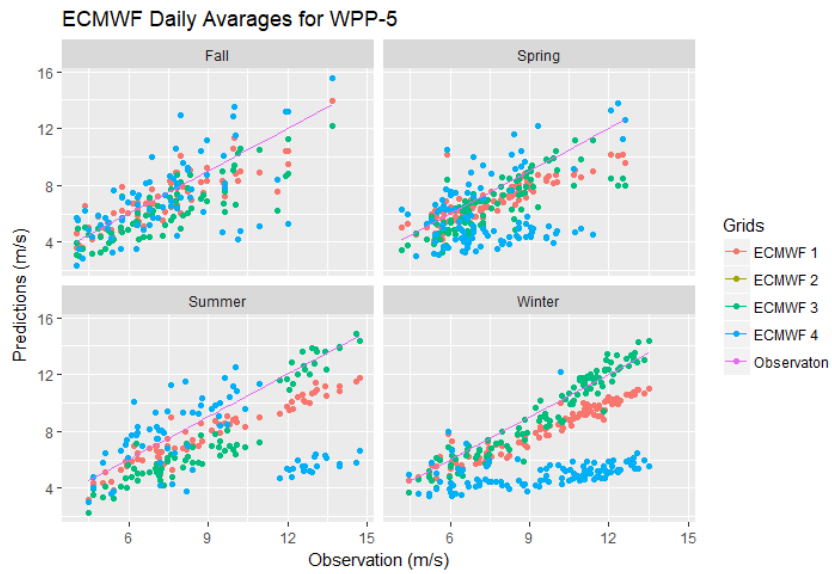


Figure 3.66 Daily Avg. Scatter Plot for ECMWF Predictions (WPP-5)

The time series of daily average wind speeds calculated from all data period from ALADIN, GFS and ECMWF for 4 grids are compared with observed wind speed in Figure 3.67. This figure shows that while ALADIN predictions are generally underestimated, GFS and ECMWF values are closer to observation values particularly in summer and fall months. ECMWF and GFS Grid 3 shows somewhat better skill than other grids. For winter and early spring all three models show better distribution.

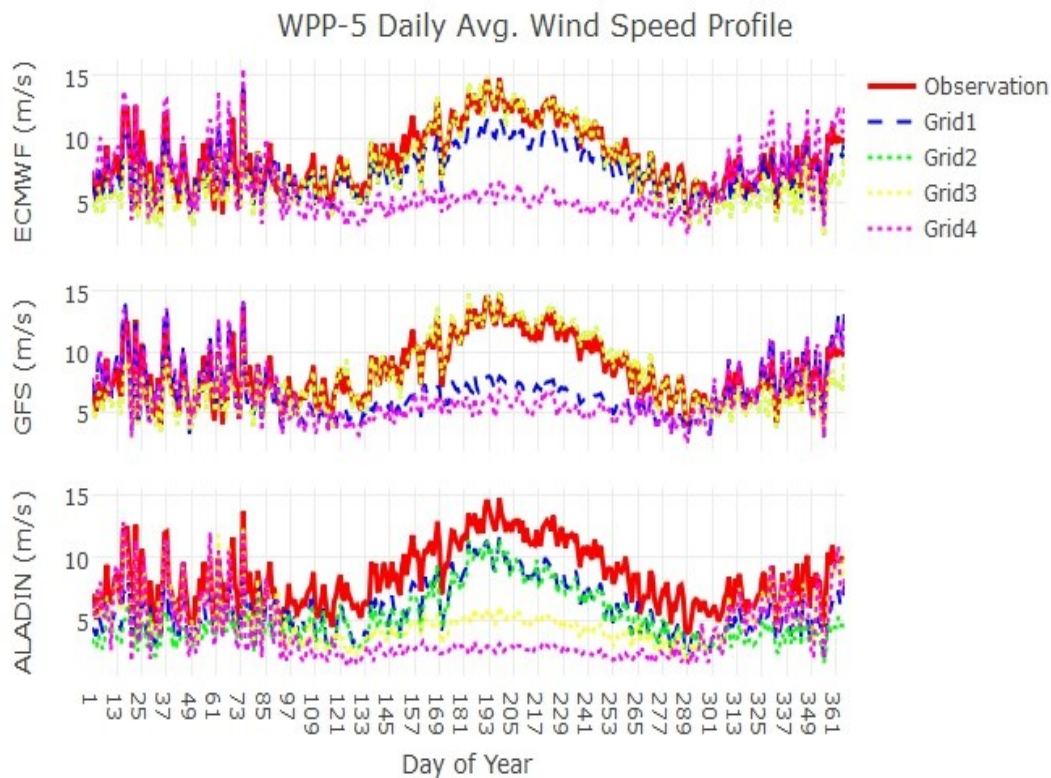


Figure 3.67 Time Series of all NWP and Observation data (WPP-5)

Hourly statistics of bias, RMSE and correlation coefficients are calculated for each season and model grid points from ALADIN, GFS and ECMWF in Table 3.5. The table indicates that all three models show strong underestimation indicated with negative bias values for all seasons. ALADIN bias and RMSE values are obviously bigger than GFS and ECMWF. Based on the statistical measures available in this table, the most preferable grid that yields lowest bias and RMSE and high correlation coefficient is selected with respect to each season and model as follows: ALADIN 1, GFS 2 and 3, and ECMWF 1 for fall and spring, ALADIN 1, GFS 2 and 3, and ECMWF 2 and 3 for summer, and ALADIN 3, GFS 2 and 3, and ECMWF 1 for winter. The evaluations provided in the following sub-sections are made according to these grids for each season. The optimum grid selection that provides the lowest bias and

RMSE, and highest correlation coefficient for each model is highlighted and underlined in the table (blue for fall, yellow for spring, red for summer and purple for winter).

Table 3-5 Seasonal bias, RMSE and Correlation Coefficients for all models and grids from hourly data

Bias	SEAS ON	ALADIN- 1	ALADIN - 2	ALADIN - 3	ALADIN - 4	GFS- 1	GFS- 2	GFS- 3	GFS- 4	ECMWF- 1	ECMWF- 2	ECMWF- 3	ECMWF- 4
	Fall	-2,449	-2,996	-2,946	-3,725	-1,444	-0,193	-0,193	-1,520	-0,661	-0,832	-0,832	-1,476
	Spring	-2,192	-2,826	-3,148	-4,259	-1,732	-0,396	-0,396	-1,907	-0,616	-0,690	-0,690	-1,886
	Summ er	-3,009	-3,437	-6,685	-8,803	-4,728	0,475	0,475	-5,927	-1,990	-0,020	-0,020	-6,292
	Winter	-2,566	-3,775	-1,226	-1,393	0,558	-1,359	-1,359	0,595	-0,641	-1,856	-1,856	0,585
RMSE	Fall	3,271	3,787	4,227	5,443	3,367	2,762	2,762	3,655	2,283	2,750	2,750	4,045
	Spring	3,217	3,780	4,273	5,530	3,298	2,918	2,918	3,834	2,604	2,885	2,885	4,040
	Summ er	3,592	4,130	7,104	9,320	5,269	2,908	2,908	6,518	2,896	2,836	2,836	6,847
	Winter	3,741	4,945	3,359	4,403	3,390	3,144	3,144	3,456	2,645	3,396	3,396	3,499
CC	Fall	0,728	0,680	0,480	0,220	0,559	0,687	0,687	0,485	0,745	0,706	0,706	0,415
	Spring	0,723	0,673	0,548	0,313	0,602	0,664	0,664	0,459	0,693	0,679	0,679	0,416
	Summ er	0,758	0,708	0,506	0,051	0,551	0,611	0,611	0,370	0,675	0,626	0,626	0,359
	Winter	0,809	0,732	0,766	0,642	0,780	0,781	0,781	0,757	0,823	0,777	0,777	0,757

3.5.2. Diurnal Variation

Figure 3.68 indicates to diurnal temperature profile seasonally. The figure shows that although, temperature differences between day and night are smaller for observed values, models shows to opposite. In contrast to wind speed predictions, ALADIN temperature predictions are better than GFS and ECMWF. These two model are showed overestimation for all seasons. Winter average temperatures for observed values are not higher than 7 °C.

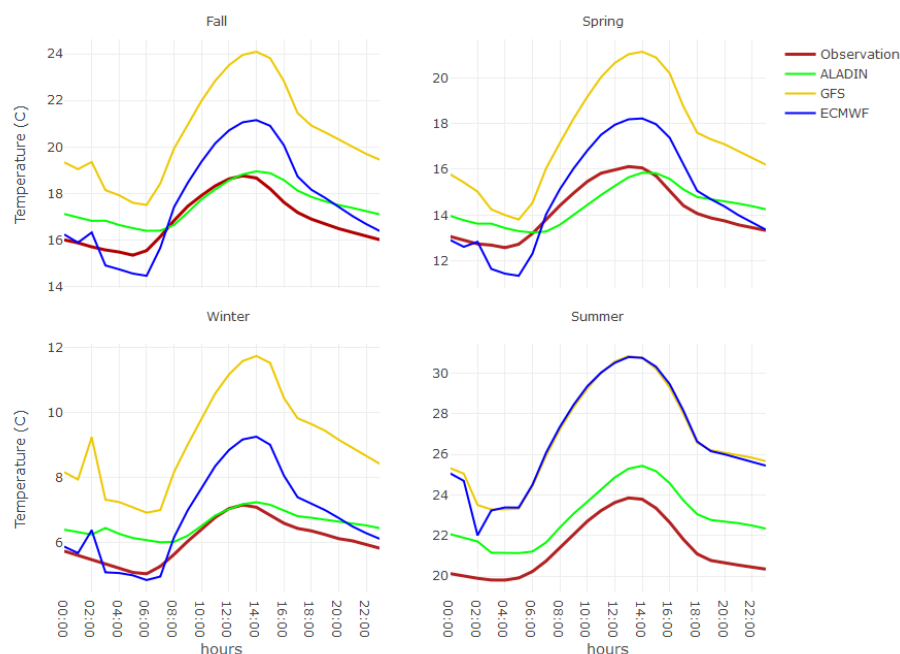


Figure 3.68 Diurnal Temperature by seasonally for the best grids (WPP-5)

Figure 3.69 indicates mean diurnal cycle of wind speed from observation and three models (ALADIN, GFS, and ECMWF) at fall, spring, winter and summer seasons. Observed wind speeds decrease from nighttime to midday and then starts to increase until evening hours (20:00) in fall, spring and summer season. ECMWF shows a similar hourly oscillation with observed wind speed in fall and spring. GFS is closer to them, however ALADIN shows strong underestimation during these seasons.

However the diurnal fluctuation of ALADIN is almost similar to observed values for all seasons. Yet, there is a big wind speed difference between ALADIN and observations. Winter predictions seems better than other seasons for all three models, however the variation of wind speed at hours of day aren't occur for this season. All models and observations are almost constant during the day, except from ECMWF at 02:00 am. All models show underestimation at each hour of the day. However, GFS shows overestimation in between 18:00 and 23:00 in fall and spring and summer. ECMWF and GFS has sharp decrease at 02:00 am for all seasons. Maximum observed wind speed in the day occurs at 16-18 hours in summer and spring and at 20-22 hours in fall season.

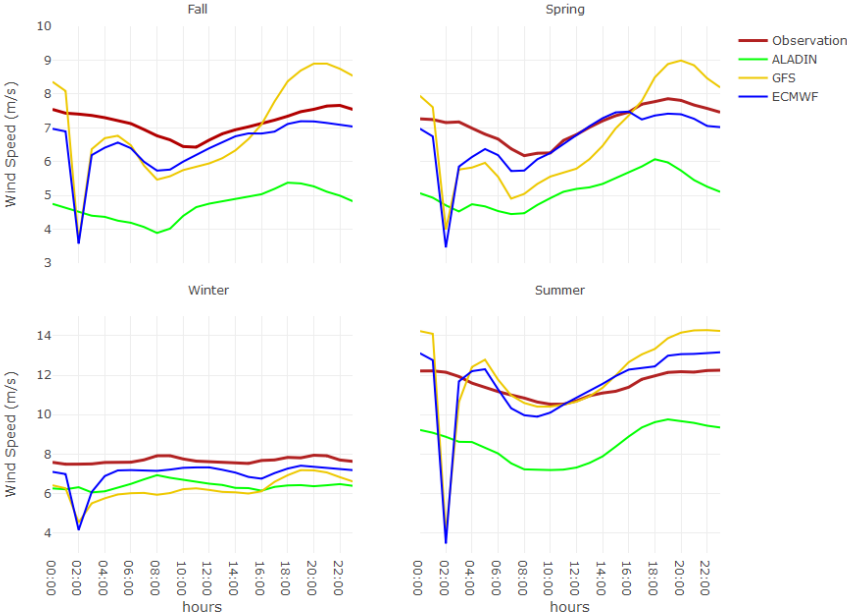


Figure 3.69 Diurnal Wind Speed by Seasonally for the best grids (WPP-5)

Figure 3.70, 3.71, and 3.72 show the diurnal variation of RMSE, bias, and correlation coefficient for ALADIN, ECMWF and GFS at fall, spring, winter and summer

seasons. It is obvious that RMSE is higher for ALADIN at all all times of day and seasons. The sharp increasing of GFS and ECMWF at 02:00 am are reasoned from sharp decreasing of wind speed at this hours (see figure 3.69). Summer, spring and fall RMSE values are lower at midday. Winter RMSE is almost constant like wind speeds. ECMWF has lowest RMSE for all seasons.

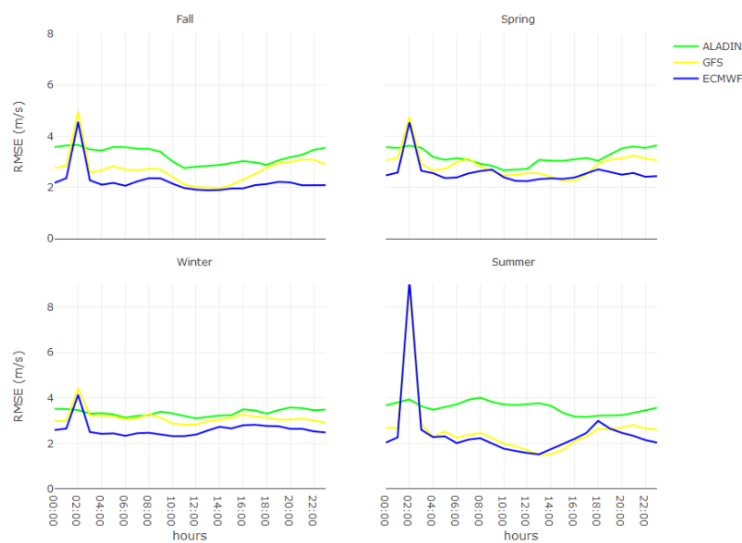


Figure 3.70 Diurnal Cycles for RMSE of Wind Speed (WPP-5)

All range of diurnal bias values changes between + 1 and -4 m/s for fall and spring (Fig. 3.71). Strong underestimation occurs in winter season. Winter bias values changes between 0.5 to 3 m/s. All models show underestimation occurs at early morning and midday hours of summer season except from ALADIN. ECMWF is better than other models for all seasons. ALADIN show negative and highest bias (underestimation) during entire cycle of all seasons. GFS has positive bias throughout the range of 18:00 and 23:00.

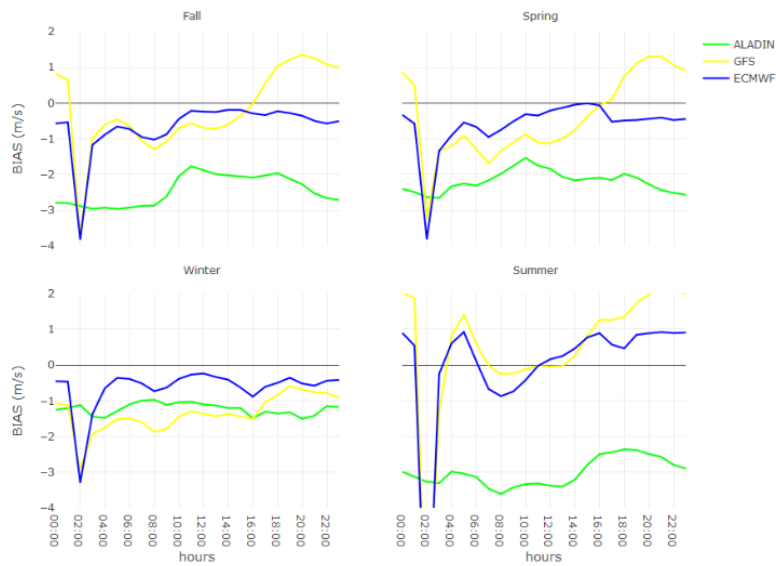


Figure 3.71 Diurnal Cycles for bias of Wind Speed (WPP-5)

ECMWF has obviously the highest correlation for fall (0.8-0.9) and winter (0.8-0.9) (Figure 3.72). For these seasons, correlation values are almost the same for all hours of the day. In spring season ALADIN has highest correlations. Even though ALADIN produced higher RMSE and bias, the model showed better diurnal trend in spring for the range of 04:00 to 16:00 hours (0.7-0.8). ECMWF has better prediction performance in summer during the daytime up to 18:00. A sharp decrease is occurred at 02:00 and 18:00 hours for this season. ALADIN has better performance for this hours.

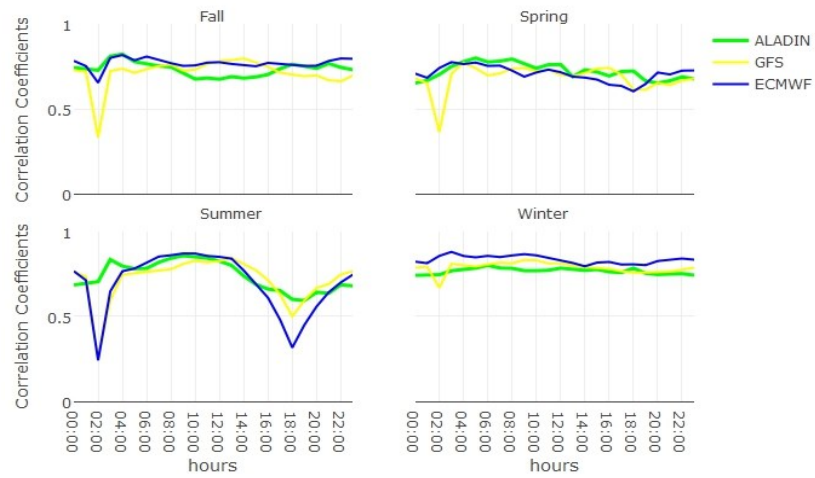


Figure 3.72 Diurnal Cycles for Correlation Coefficient of Wind Speed and Predictions (WPP-5)

3.5.3. Energy Comparison

Figure 3.73 shows the correlation between wind speed and power, and histograms of wind speed and power production values. The “Wind Speed5” graph on the matrix shows the wind speed histogram. Wind speeds are intense in between 3 to 15 m/s and power production starts to increase this wind speeds. Power value reaches to 40 MW + by depending on the wind speeds. The relationship between wind speed and power is nearly linear. The frequency of wind speeds also decreases until 18 m/s, which is fair enough for the producer. The scatter plot graph on the left bottom of the matrix shows the correlation between wind speed and power. It is similar to power curve (Figure 2.1). The “Power5” graph shows the frequency of power values. The installed capacity of WPP 5 is 48 MW. However 0-10 MW productions are higher than others. The maximum produced power value for WPP-5 is approximately 48 MW which means the wind farm rarely produced full capacity electricity. The correlation coefficient between energy and wind speed is 0.92 which is indicated on the top right

of the matrix. The mean wind speed of entire data is 8.4 m/s and mean produced energy is approximately 15 m/s.

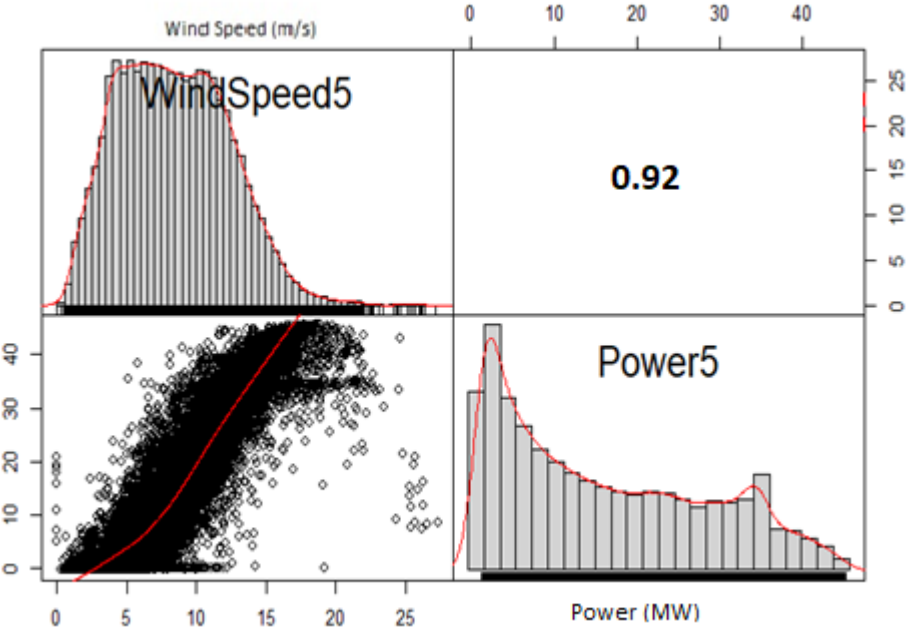


Figure 3.73 The relationship between Observed Wind Speed and Produced Power (WPP-5)

Figure 3.74 demonstrates the diurnal variation of predicted and observed energy and wind speed values at each season. Wind speed values are selected from the final step of RITM forecast system that combines all three NWP (ALADIN, ECMWF and GFS) model outputs. Final products from RITM system also include correction to predicted wind speeds. First row shows produced and predicted power values at each season and the bottom row shows the wind speed prediction and observed values for these seasons. Overall underestimation in all seasons appears in these combined final wind product. With the modification performed in the system the weakness in models prediction performance is improved. However, the modification seems not affecting the winter performance. Wind energy production of WPP starts to decrease from night to

morning. It generally starts to increase after 09:00 am. Summer and fall energy predictions are closer to each other. However the difference between energy production and predictions are higher for spring and particularly for winter seasons depending on differences in wind speed prediction. The relationship between wind speeds and predictions are quite different from each other during the winter for entire day. This results are reflected to the power values as it is expected. This results proves to significance of better NWP would result reliable wind power forecasts.

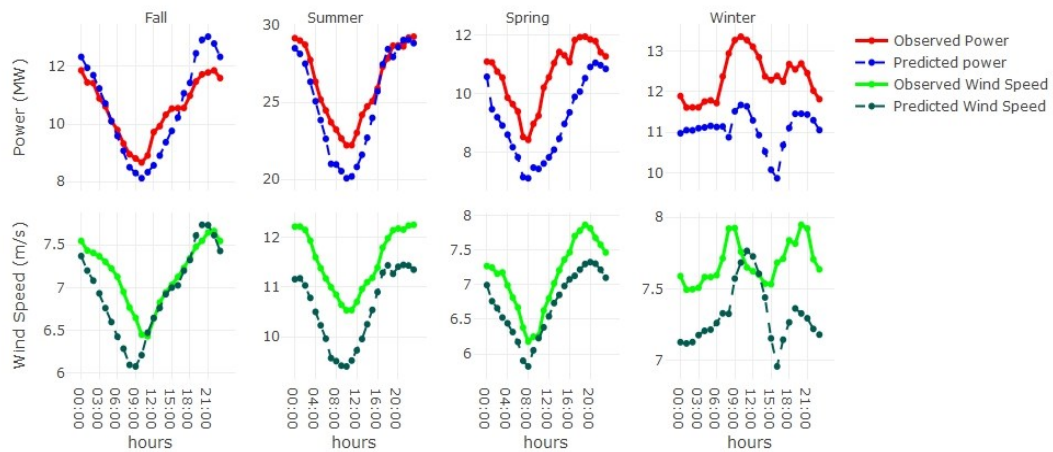


Figure 3.74 Diurnal Cycle for Energy and Wind Speed (WPP-5)

Monthly RMSE values according to final wind speed predictions and energy predictions for WPP-5 are illustrated in figure 3.75. Wind speed RMSE values are higher from November to January. Wind speed RMSE values are smaller than the energy values. Energy RMSE values have a decreasing trend from June to October. Wind speed trends are also similar to energy values. This is a strong indicator how the energy production depends on wind speed. The smaller the wind prediction error the more reliable forecast of energy production.

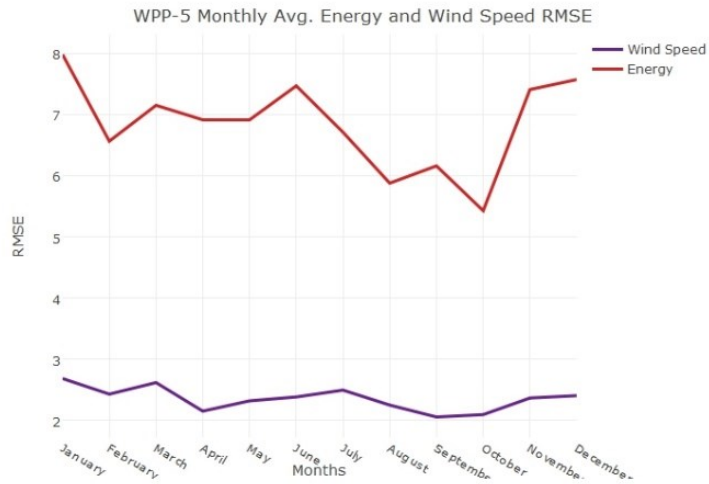


Figure 3.75 Monthly RMSE for Wind Speed and Energy Predictions (WPP-5)

3.6. WPP-6

WPP-6 is located in a mountainous area in southern part of Turkey. The wind farm has the highest roughness and elevation m.a.s.l which means the most complex terrain in this study. As it mentioned in Chapter 2, there is also a high hill which has the height over the 1600 m.a.s.l. located in the north-eastern part of the wind farm.

3.6.1. Evaluation of Wind Speeds at Monthly, Daily, and Hourly Time Scales

Figure 3.76 is about the prevailing wind direction frequency of hourly data from WOS for each season. The figure shows that prevailing wind direction is NW for all seasons except from winter (ESE). However, wind speed values are low in particularly for spring and winter. The wind speeds reach the highest values in summer.

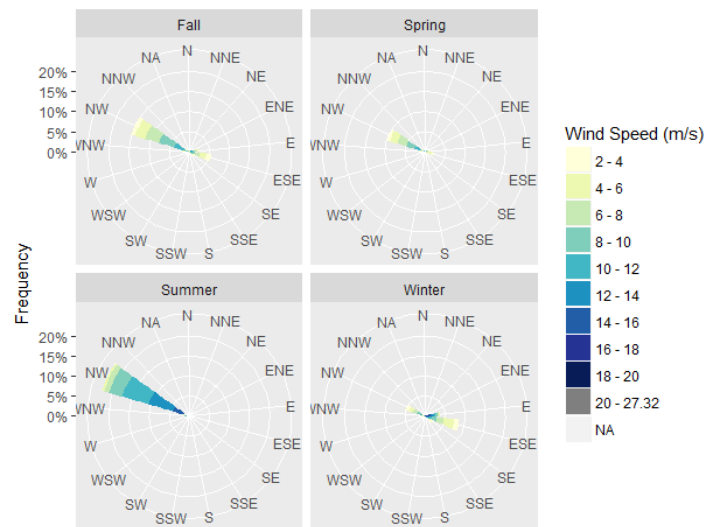


Figure 3.76 Seasonal Wind Rose (WPP-6)

According to Table 2.5, rated wind speed is 13.5 m/s and cut in wind speed is 3.5 m/s for WPP-6 turbines. Therefore it could be expected that the production of WPP-6 should be higher at summer season.

Figure 3.77 demonstrates the wind direction frequency at hourly time scale from observations and all models at four grid points. “WD78” and “WD48” are the WOS directions sensors with height (78 m.a.g.l or 48 m.a.g.l.) and they both show that the prevailing wind direction is approximately 45° (W) with the frequencies of 40 to 20 % respectively. NW is the prevailing wind direction for most of prediction values.

However, three of GFS direction predictions have indicated different directions except from GFS grid 2.

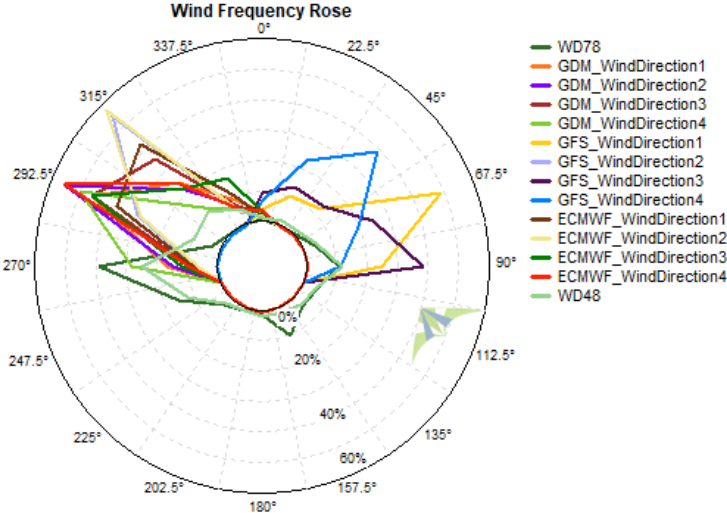


Figure 3.77 Wind Rose for All Grids (WPP-6)

Figure 3.78 shows the monthly mean wind speed calculated over 3.6 year of data from observations (WS80, WS65, and WS50), ALADIN, GFS, and ECMWF at four grid points. WS80, WS65 and WS50 are the heights (m) of real measurement sensors. The dashed lines are the average values for 4 grids (ALADIN avg, GFS avg, ECMWF avg). As it mentioned Chapter 3, turbine hub height of WPP-6 is 80 m, so only 80 m sensor will be taken into account for this wind farm. Following parts of this chapter will discuss which grid or prediction is better for WPP-6. The line graph illustrates that while ALADIN wind speed predictions are showed underestimation, GFS and ECMWF has overestimation during the year except from winter and early spring months. ECMWF and GFS predictions at these months are closer to WOS values. Observed monthly averages are gradually changes during the entire year (5-7 m/s). During the first half of the year, there is an upward trend in ECMWF and GFS predictions and downward trend occurs the rest of the year for these models. In summer, wind speeds are peaked for both observed and predicted wind speeds.

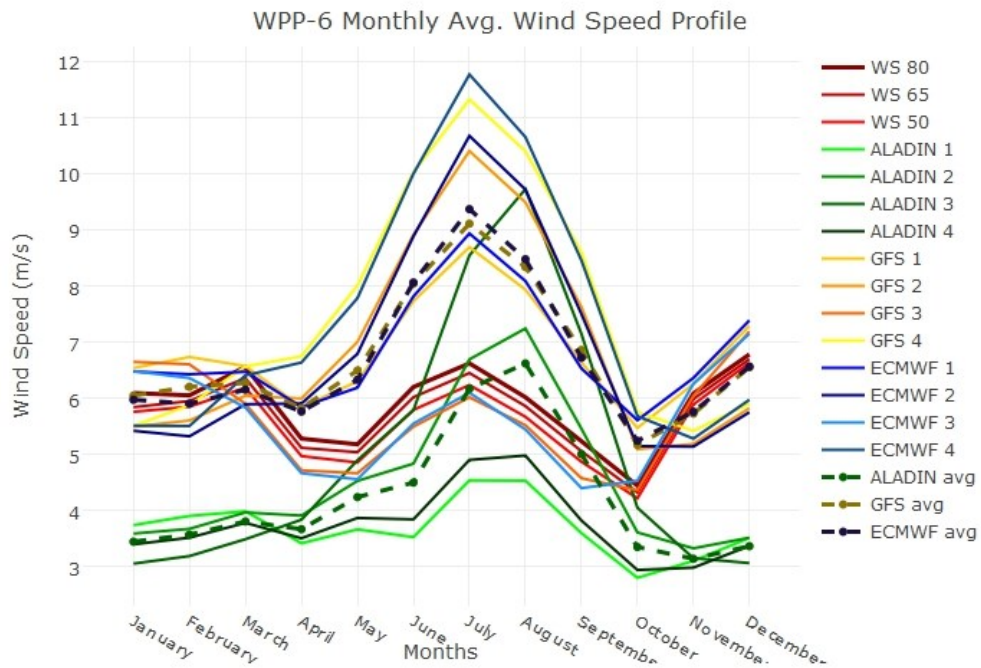


Figure 3.78 Monthly Average Wind Speed Values (WPP-6)

Figure 3.79, 3.80, and 3.81 show scatter plots between observed and modeled daily averaged wind speed at each season for ALADIN, GFS, and ECMWF, respectively. Results from all grids points are shown in these figures.

ALADIN values are showed underestimation for grid 1 and 4, and overestimation for grid 2 and 3 throughout the range of wind speed 3 and 7 m/s in fall and summer (see fig. 3.79). ALADIN grid 2 and 3 are also showed better distribution for these range and seasons. In spring, clear underestimation occurs. Winter daily average of observed values mostly change between 5-8 m/s and underestimated by grid 1 and 4 and overestimated by grid 2 and 3. The predictions and observed values of spring and winter seasons are intense around the 5 m/s and 10 m/s for spring.

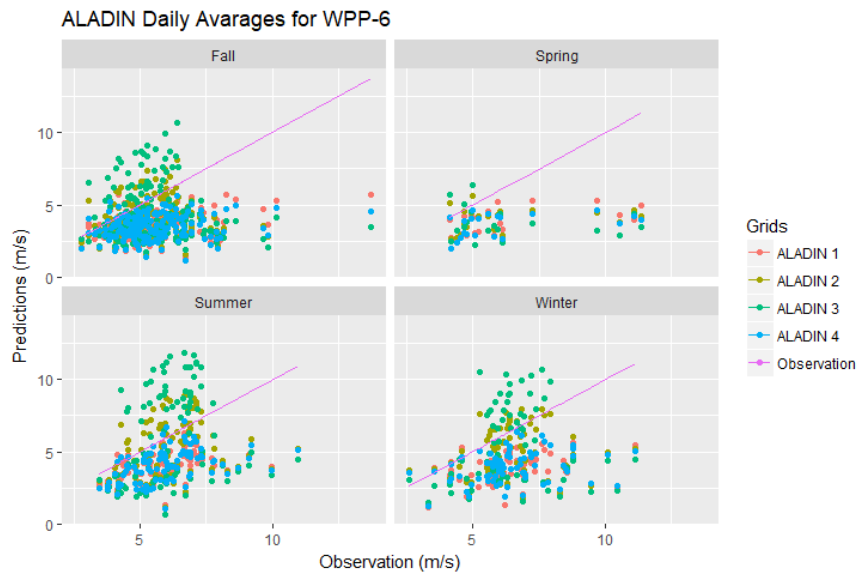


Figure 3.79 Daily Avg. Scatter Plot for ALADIN Predictions (WPP-6)

A similar graph to ALADIN are illustrated for GFS in figure 3.80. Throughout the range of daily wind speeds between 2.5 and 7.5 m/s GFS grid 1, 2 and 4 overestimates the wind in fall and summer. Spring predictions of GFS are same with the ALADIN. In winter GFS grid 1, 2 and 4 are showed underestimation the range of daily wind speeds 6 and 8 m/s.

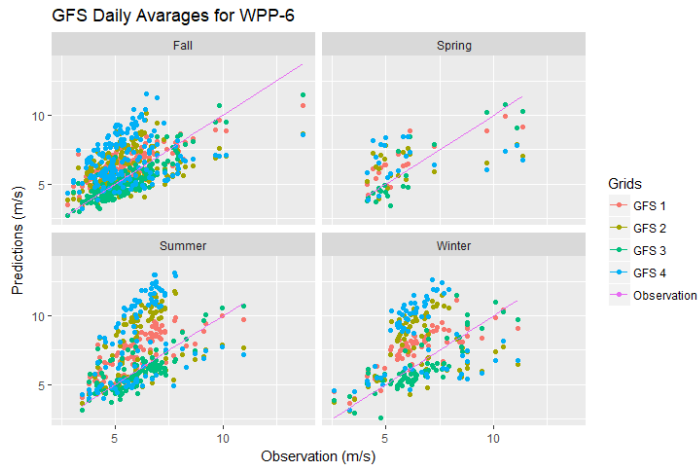


Figure 3.80 Daily Avg. Scatter Plot for GFS Predictions (WPP-6)

A similar prediction performance like in GFS seems to appear in ECMWF predictions at each season (Figure 3.81). The distribution is more scattered but the level of underestimation is more reduced with ECMWF results.

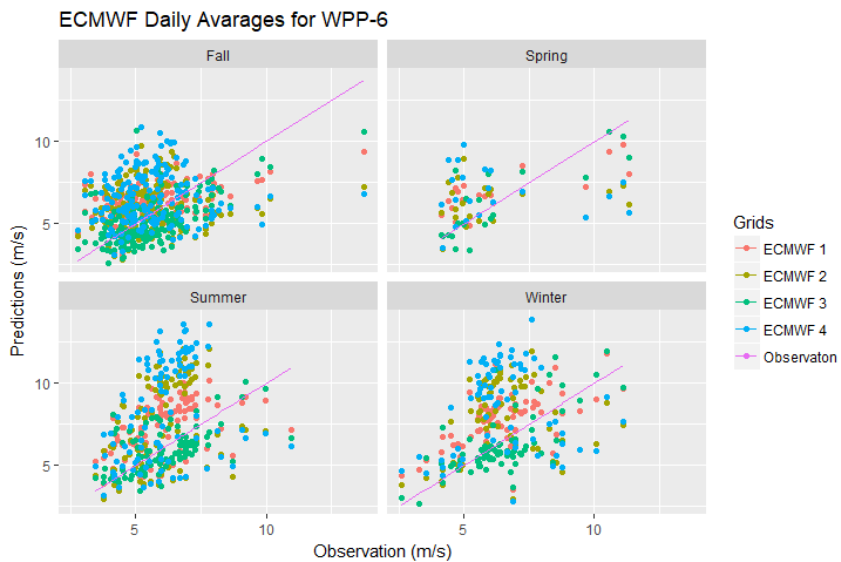


Figure 3.81 Daily Avg. Scatter Plot for ECMWF Predictions (WPP-6)

According to the analysis of averaged daily wind speed provided in these scatter plots (Fig 3.79, 3.80, and 3.81) all models showed similar performance for each season. GFS and ECMWF grid points are similar to each other and ALADIN is better for different grid points. Monthly average observed wind speeds are lower at fall and spring seasons.

The time series of daily average wind speeds calculated from all data period from ALADIN, GFS and ECMWF for 4 grids are compared with observed wind speed in Figure 3.82. It can be observed that there is a significant rising and fluctuation in winter and early spring months for observed values. All models are overestimated for these period. However GFS and ECMWF are distributed better than ALADIN during the last quarter of the year. Overestimation occurs during the summer months for all models. However, ALADIN grid 2 and ECMWF and GFS grid 3 are showed better distribution for these periods.

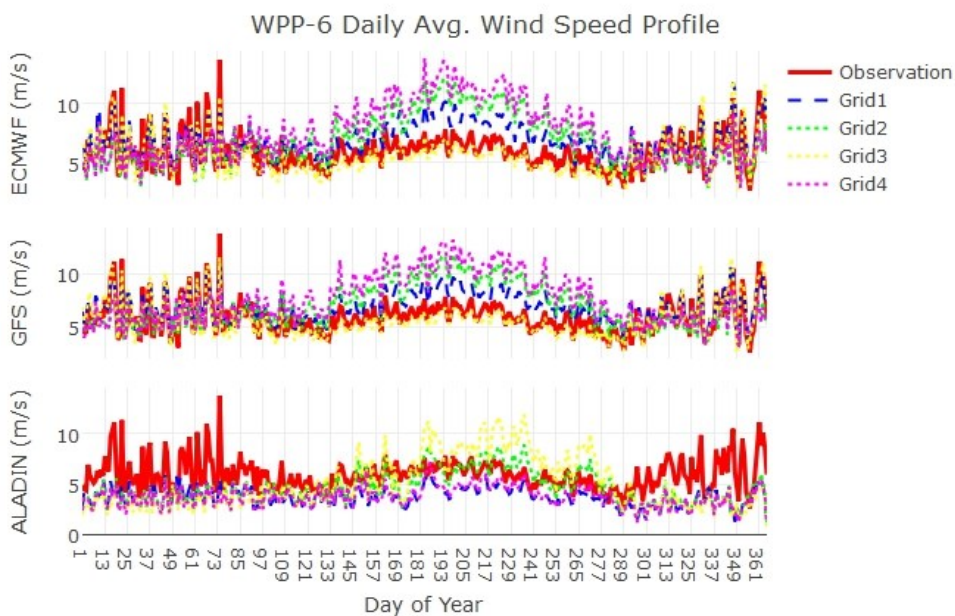


Figure 3.82 Time Series of all NWP and Observation data (WPP-6)

Hourly statistics of bias, RMSE and Correlation Coefficients are calculated for each season and model grid points from ALADIN, GFS and ECMWF in Table 3.6. The table indicates that all four grids of ALADIN and grid 3 for ECMWF and GFS show significant underestimation indicated with negative bias values for all seasons. ALADIN has the highest bias and lowest correlation for all seasons among the other models. GFS and ECMWF grid 1, 2 and 4 has positive Bias (overestimation) for all seasons. GFS correlations better than other models and RMSE values of GFS is lower than other models. Based on the statistical measures available in this table, the most preferable grid that yields lowest bias and RMSE and high correlation coefficient is selected with respect to each season and model as follows: ALADIN 4, GFS 3, and ECMWF 3 for fall, ALADIN 2, GFS 3, and ECMWF 1 for spring, ALADIN 2, GFS 3, and ECMWF 3 for summer, and ALADIN 1, GFS 3, and ECMWF 3 for winter. The evaluations provided in the following sub-sections are made according to these grids for each season. The optimum grid selection that provides lowest bias and RMSE, and highest correlation coefficient for each model is highlighted and underlined in the table (blue for fall, yellow for spring, red for summer and purple for winter).

Table 3-6 Seasonal bias, RMSE and Correlation Coefficients for all models and grids from hourly data

bias	SEASON	ALADIN-1	ALADIN-2	ALADIN-3	ALADIN-4	GFS-1	GFS-2	GFS-3	GFS-4	ECMWF-1	ECMWF-2	ECMWF-3	ECMWF-4
	Fall	-2,084	-1,120	-0,471	-2,002	0,870	0,715	-0,259	1,337	0,917	0,676	-0,189	1,221
	Spring	-1,973	-1,517	-1,569	-1,940	0,578	0,700	-0,578	1,466	0,509	0,551	-0,653	1,302
	Summer	-2,133	-0,135	1,561	-1,762	1,816	3,277	-0,612	4,271	1,971	3,419	-0,589	4,473
	Winter	-2,557	-2,690	-3,183	-2,856	0,544	-0,655	0,511	-0,534	0,447	-0,798	0,356	-0,637
RMS E	Fall	3,799	3,651	4,259	3,698	2,701	3,138	2,460	3,772	3,471	3,649	3,386	4,169
	Spring	3,799	3,795	4,171	3,822	2,585	3,203	2,464	4,018	3,423	3,789	3,433	4,326
	Summer	3,453	3,029	4,371	3,106	2,705	4,111	2,023	5,312	3,054	4,363	2,486	5,486
	Winter	4,705	4,778	5,149	4,820	3,319	3,486	3,384	3,774	4,588	4,521	4,618	4,762
CC	Fall	0,092	0,082	0,045	0,114	0,557	0,391	0,616	0,325	0,266	0,165	0,326	0,142
	Spring	0,255	0,200	0,133	0,226	0,622	0,461	0,668	0,370	0,314	0,212	0,368	0,170
	Summer	0,125	0,239	0,236	0,205	0,583	0,541	0,536	0,550	0,395	0,400	0,301	0,463
	Winter	0,362	0,353	0,303	0,378	0,656	0,575	0,670	0,497	0,340	0,239	0,399	0,174

3.6.2. Diurnal Variation

Figure 3.83 shows mean diurnal temperature profile from observation, ALADIN, GFS, and ECMWF at fall, spring, winter and summer. In a typical diurnal cycle of temperature the peak value occurs around 2 p.m. in the afternoon. All models shows this feature in all seasons. ALADIN shows 1-hr lag shift to earlier in the occurrence time of the peak in fall and summer. ECMWF and GFS show overestimation during the day and it is substantially high (6-8 °C) at peak time. Night time differences between model and observations are smaller for all seasons for ECMWF and GFS. ALADIN shows overestimation during fall and winter. ALADIN predicts the temperature according to smaller difference between day and night temperatures. However other models predicts bigger differences. Summer and spring predictions of ALADIN is underestimated for all hours of day except from nocturnal hours of summer. During these hours for summer, ALADIN overestimates like GFS and ECMWF. However, the difference between model and observed values are smaller for these seasons.

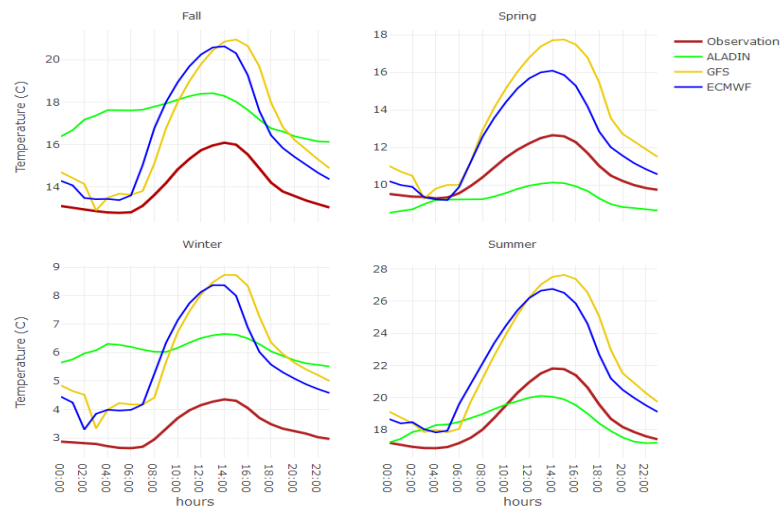


Figure 3.83 Diurnal Temperature by seasonally for the best grids (WPP-6)

Figure 3.84 indicates mean diurnal cycle of wind speed from observation and three models (ALADIN, GFS, and ECMWF) at fall, spring, winter and summer seasons. The line graphs shows that the observed wind speed has a decreasing trend until the daylight hours and there is an increasing trend until the sunset for all seasons except from winter. In fall, oscillation of models and observations are different from each other during the day. ECMWF and GFS show underestimation during the night and evening hours, overestimation could be seen in day light hours. In winter, GFS and ECMWF has a similar trend with observed wind except from night hours. In addition to this, the predictions of these two model sharply drops at 02:00 am for all seasons. In spring, ECMWF seems better than other models except from night hours. GFS and ECMWF also shows 1-hr lag shift to earlier in the occurrence time of the peak and lowest value of wind. GFS and ECMWF are separated from each other after 16:00. GFS shows underestimation while ECMWF is go on with overestimation. In summer, while the ECMWF and GFS has increasing trend, observed winds has an decreasing trend during the night. These two models are successful for daylight and evening hours for this season. GFS seems closer to observed values than GFS. ALADIN shows underestimation for all hours of day at all seasons except from summer. ALADIN overestimates the wind during the morning hours, underestimates the rest of hours a day.



Figure 3.84 Diurnal Wind Speed by Seasonally for the best grids (WPP-6)

Figure 3.85, 3.86, and 3.87 show the diurnal variation of RMSE, bias, and Correlation Coefficient for ALADIN, ECMWF and GFS at fall, spring, winter and summer seasons.

It is obvious that there is a decreasing trend throughout the range of the hours between 00:00 am and 18:00 for RMSE (see fig. 3.85). In the hours 18:00 to 00:00 all models have increasing trend for RMSE. GFS has lowest RMSE values for all seasons. In fall, GFS and ECMWF shows 1-hr delay shift to later in the occurrence time of the lowest value of RMSE than ALADIN. The variation of RMSE during the entire day are same with all models except from spring. All models have different trend for each hour of day in this season. In summer, ECMWF and GFS are similar to each other, however GFS is better than ECMWF. ALADIN has almost constant RMSE values during the day for this season. In winter, ECMWF and ALADIN are closer to each other. RMSE trend is same with the other seasons.



Figure 3.85 Diurnal Cycles for RMSE of Wind Speed (WPP-6)

All range of diurnal bias values changes between + 1.5 and -5 m/s for all seasons (Fig. 3.86). ECMWF and GFS has similar trend with each other similar to RMSE and wind speed graphics. GFS has lowest bias for all seasons. In fall, ECMWF and GFS has negative Bias (underestimation) during the hours night hours and positive Bias (overestimation) during the daylight. In spring, ECMWF shows overestimation except from the nocturnal hours. GFS show also overestimation in the hours between 08:00 am and 18:00. In winter, GFS and ECMWF has positive Bias during the entire day except from 02:00 am which has a sharp decreasing for all seasons. In summer, ECMWF and GFS has negative Bias during the night hours and positive bias for daylight hours. ALADIN has different fluctuation for all hours of day. Negative Bias is converted to the positive with rising sun and negative bias occurs by the hour of 14:00. ALADIN has negative and the highest bias during fall, spring and winter.

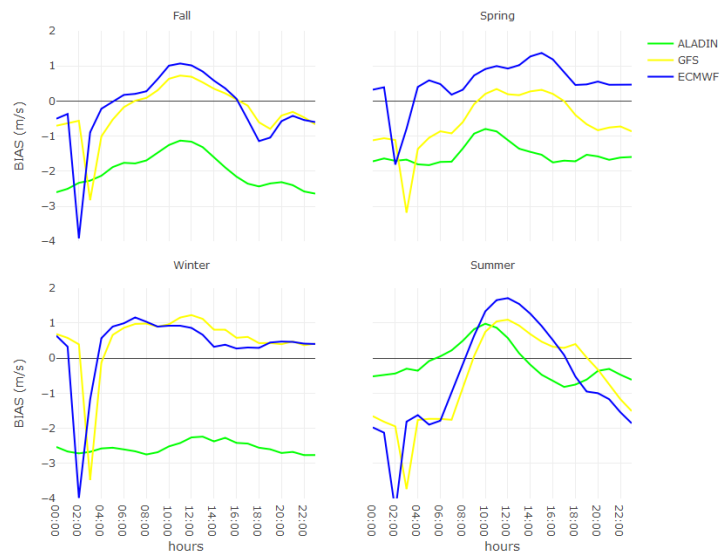


Figure 3.86 Diurnal Cycles for bias of Wind Speed (WPP-6)

As it is illustrated by the figure 3.87, GFS has the highest correlation for all seasons. The correlation coefficient of GFS changes between 0.4 and 0.8 for fall and spring. Sudden plunge in wind speed at 02:00 am are responsible for the lowest correlation. The highest correlations occur from sunrise to sunset. ALADIN has the lowest correlations for all seasons.

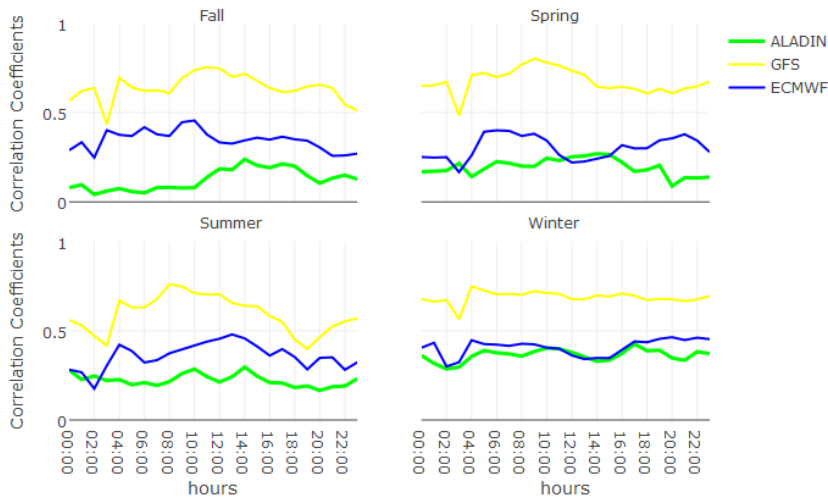


Figure 3.87 Diurnal Cycles for Correlation Coefficient of Wind Speed and Predictions (WPP-6)

3.6.3. Energy Comparison

Figure 3.88 shows the correlation between wind speed and power, and histograms of wind speed and power production values. The “Wind Speed6” graph on the matrix shows the wind speed histogram. Wind speeds are getting intense between 3 and 10 m/s which means wind mostly blows within this range of wind values. The frequency of wind speeds also decreases until 13 m/s. The scatter plot graph on the matrix shows the correlation between wind speed and power. It is similar to power curve (Figure 2.1). The “Power6” graph shows the frequency of power values. The installed capacity of WPP 6 is 135 MW. However 0-50 MW productions are higher than others which means produced electricity is rarely reached full capacity of wind farm due to the lower wind speeds around the 5 m/s. The maximum produced power value for WPP-6 is approximately 120 MW which means the wind farm never produced full capacity electricity. The reason of this might be limitations on the grid in the years that is obtained data. The pearson correlation coefficient between energy and wind speed is

0.72 which is indicated on the top right of the matrix. It proves positive relationship between power and wind speed data.

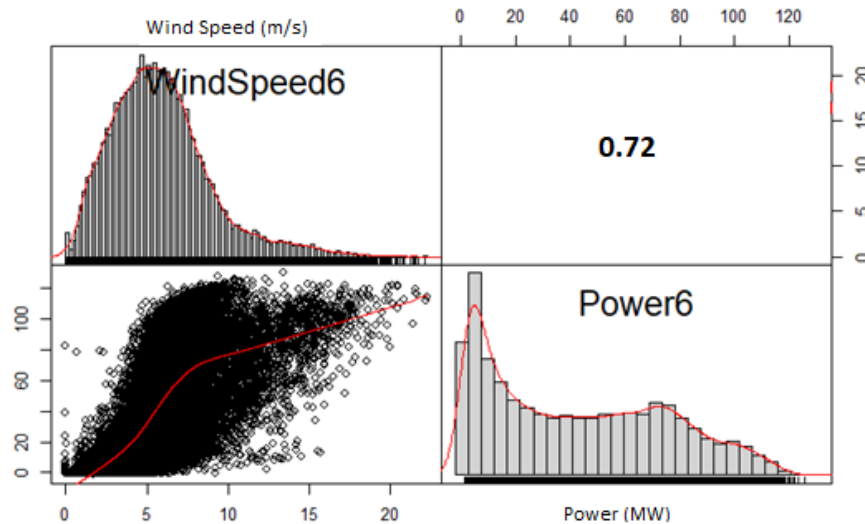


Figure 3.88 The relationship between Observed Wind Speed and Produced Power (WPP-6)

Figure 3.89 shows the diurnal variation of predicted and observed energy and wind speed values at each season. Wind speed values are selected from the final step of RITM forecast system that combines all three NWP (ALADIN, ECMWF and GFS) model outputs. Final products from RITM system also include correction to predicted wind speeds. First row shows produced and predicted power values at each season and the bottom row shows the wind speed prediction and observed values for these seasons. Similar diurnal wind patterns shown in previous section also appear in these figures. Overall underestimation in fall, spring and winter and overestimation in summer seasons appears in these combined final wind product. With the modification performed in the system the weakness in models prediction performance is improved. However, the modification seems not affecting the winter performance. Wind energy

production of WPP starts to decrease from 00:00 am to 12:00. There is an increasing trend after midday for both wind speed and energy.

The difference between energy production and predictions are higher for winter seasons depending on differences in wind speed prediction. Discrepancy in wind estimates also the cause for discrepancy in power estimates. Therefore, the accuracy of power estimates strongly depends on the reliability of wind predictions. It means quality of wind speed predictions directly affects energy predictions. The model shows better production and prediction performance at summer seasons. The produced energy changes between 40 and 80 MW depending on the highest performance among the seasons.

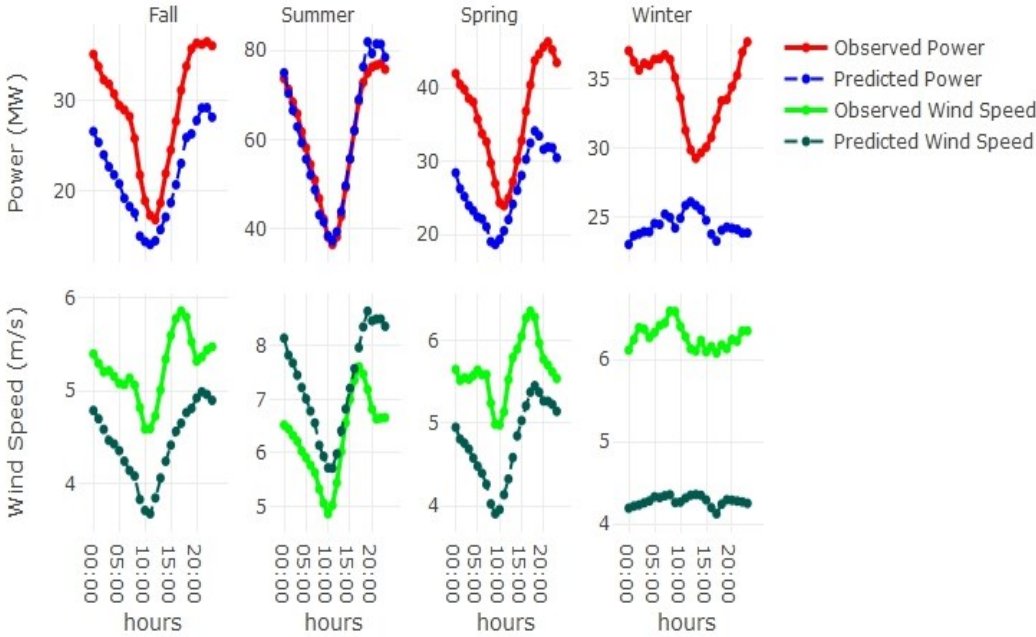


Figure 3.89 Diurnal Cycle for Energy and Wind Speed (WPP-6)

Figure 3.90 shows the monthly RMSE values according to final wind speed predictions and energy predictions for WPP-6. Energy RMSE values are higher at winter and early

spring months and starts to decrease after May. Even if wind speed RMSE values are smaller than the energy, the trend of monthly averages is same with each other. This is a strong indicator how the energy production depends on wind speed. The smaller the wind prediction error the more reliable forecast of energy production. Winter and early spring seasons show the least reliable forecast of power production.

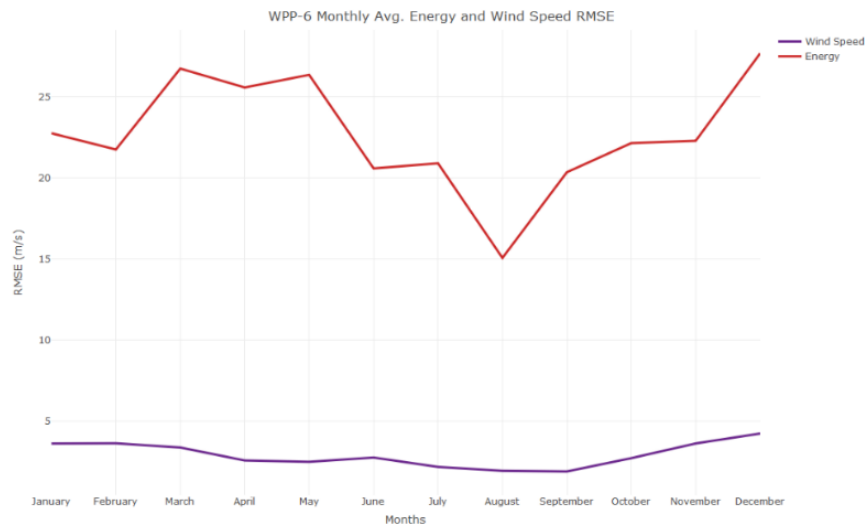


Figure 3.90 Monthly RMSE for Wind Speed and Energy Predictions (WPP-6)

CHAPTER-4

4. REGIONAL AND GENERAL EVALUATION OF ALL WPPS

As it was explained in Chapter 2, all wind power plants had also been selected according to 3 geographical regions. As a result of evaluation of the roughness and elevation maps, it could be done a complexity sequence according to elevation and high roughness length. The complexity of wind farms that are used in this study changes more complex to flat respectively from left to right: WPP-6, WPP-5, WPP-2, WPP-1, WPP-4, and WPP-3.

Figure 4.1 shows mean wind speed, mean temperature, NMAE from hourly data and complexity values. The WPPs have been numbered 1 to 6 according to their geographical location and complexity. All WPPs have different installed capacity, because of that RMSE and bias could not give an idea for energy predictions. Therefore NMAE has been calculated for evaluating at equal level for each WPP. Figure 4.1 indicates that Marmara region has highest mean temperature and lowest complexity. NMAE for energy values is the smallest in Mediterranean region. Aegean Region has the highest NMAE with WPP-1. The lowest mean temperature values could also be seen there. Wind speed values are higher than the other regions as it is expected in REPA [59]. WPP-4 and WPP-5 in Marmara and Mediterranean regions respectively also show high wind speed which are in close values to Aegean Region. This explains that the selection of specific location of WPPs rather than their geographical locations becomes critical for determining the wind potential. It has been determined the most complex terrain is in the Mediterranean Region due to the topographical structure.

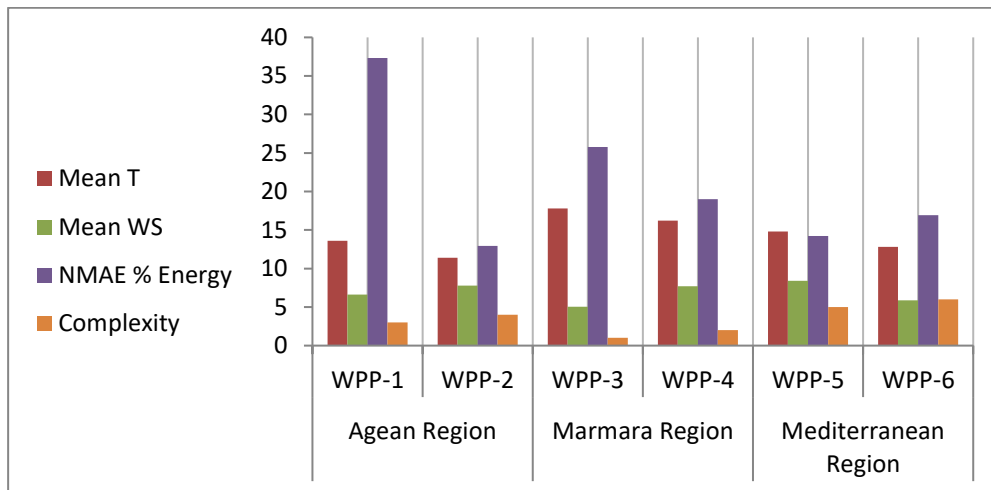


Figure 4.1 Regional Evaluation for all WPPs

Figure 4.2 demonstrates the daily average RMSE values which is calculated for the best grid points that belong to each NWP model and each WPP. The lowest RMSE for wind speed predictions are determined for WPP-4 ECMWF predictions and all models for WPP-2 predictions. ALADIN predictions obviously have the highest RMSE for WPP-4 and 5. GFS predictions has better distribution for WPP-6. WPP-3 has also the highest RMSE among the other WPPs, particularly in winter months. RMSE values are lower at summer for all WPPs except from WPP5. WPP-5 RMSE values increase from spring to summer months and decrease during the fall. GFS for WPP-6, all three models for WPP-2, GFS and ECMWF for WPP-5 and 4 RMSE values changes between 2 and 4 m/s RMSE during the entire year.

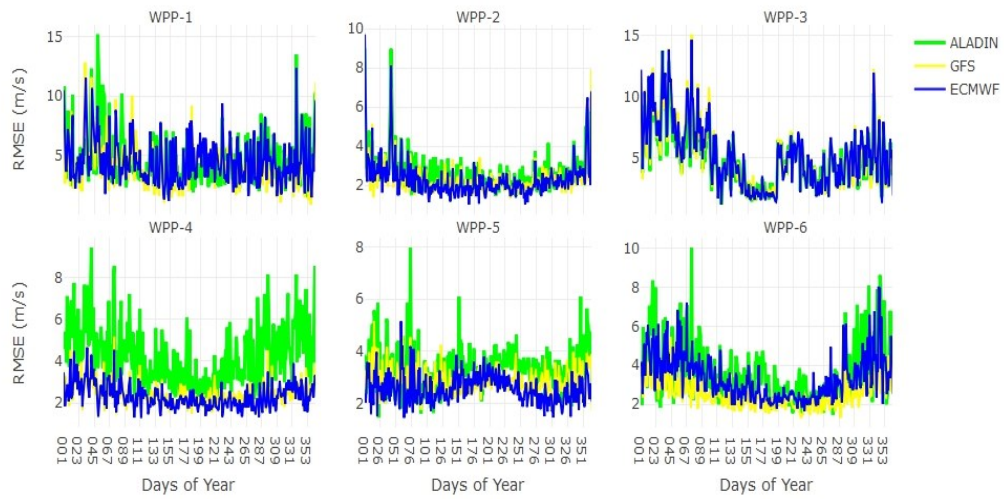


Figure 4.2 Daily Average RMSE for the best grids for all WPPs

Figure 4.3 summarizes all daily bias values that are calculated for best grids among to each WPP. There is a tendency from all models to underestimate (negative bias) wind speed at all WPPs except from WPP-3. Strong underestimation occurs from January to March for WPP-3 all models. ALADIN indicates very strong overestimation especially at WPP-4, 5, and 6. The highest bias were found for WPP-3 (between +5 and +10). GFS has lowest bias values during the entire year for WPP-3 wind speed predictions. WPP-6 prediction models have both positive and negative bias for ECMWF and ALADIN respectively. WPP-1 has positive bias during the January, February and March and negative bias for the rest of the year.

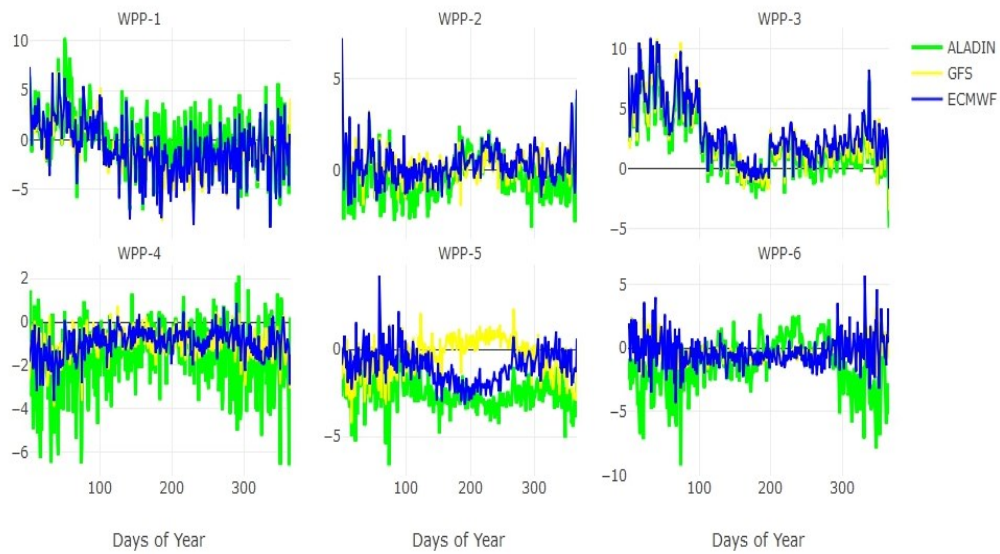


Figure 4.3 Daily Average Bias for the best grids for all WPPs

Figure 4.4 shows all daily average NRMSE values between produced and forecasted power output from hourly data. In order to evaluate equally all WPP, each RMSE values have been divided installed capacities and multiplied with 100 to calculate percentage of the daily error. WPP-3 and 4 (Marmara region) have the highest NRMSE values at all seasons. WPP-1, 2, 6 even 5 have the lowest NRMSE for all seasons. WPP-3 wind speed prediction errors are already worse than others (see Chapter 3.3). Therefore, power predictions are effected by NWP.

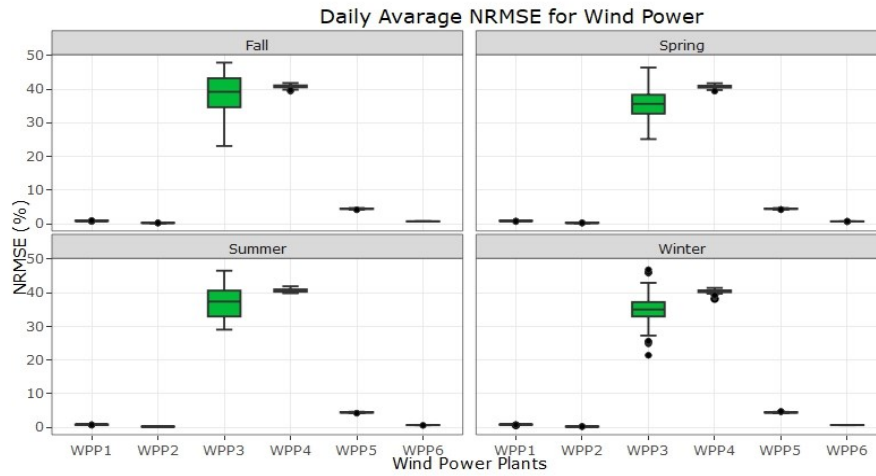


Figure 4.4 Daily Average NRMSE for Wind Power

Figure 4.5 shows the diurnal variation of NRMSE values from hourly data. It should be noted that different installed capacities affects the error. Therefore, each RMSE has been divided to installed capacities of WPPs. The figure explains WPP-2 and WPP-1 have the lowest NRMSE and WPP-3 has the highest NRMSE values. Diurnal variation of NRMSE is not distinctive during the day, all WPPs has nearly constant NRMSE.

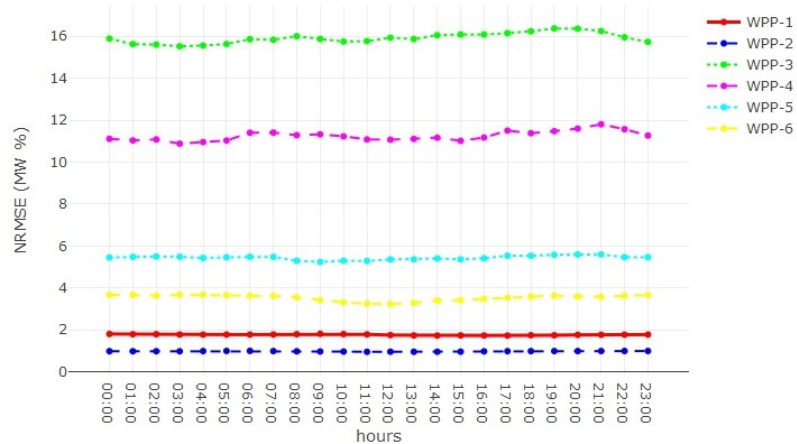


Figure 4.5 Diurnal NRMSE for all WPPs

Figure 4.6 shows diurnal normalized bias (NBias) for all WPP energy production and prediction values. Bias values have been normalized by dividing installed capacities of each WPP. WPP-1 and 2 have the lowest NBias similar to NRMSE. Diurnal variation of NBias belongs to each WPP is more apparent than NRMSE. NBias is starts to decrease after sun rises and starts to increase after sun set for WPP-2 and 6.

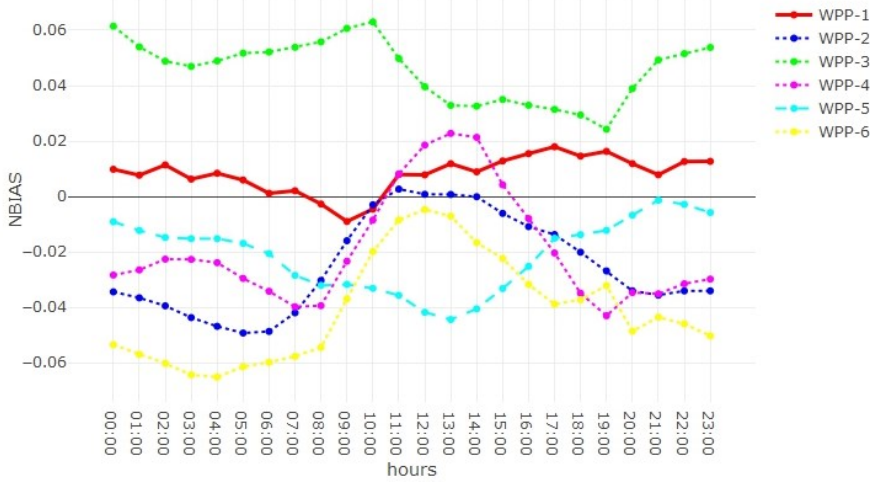


Figure 4.6 Diurnal NBias for All WPPs

The NRMSE values could be sequence changes with highest to lowest respectively: WPP-3, WPP-4, WPP-5, WPP-6, WPP-1, and WPP-2. NBias values could also array as WPP-3, WPP-4, WPP-5, WPP-6, WPP-2, WPP-1 highest to lowest respectively. Same error rate values could be determined for each WPP. These results also show that more flat wind farms such as WPP-3 and 4 have higher NRMSE and NBias than more complex terrain. These two WPP is also located in near the sea. It should be said than power prediction model is unsuccessfull for taking into account sea effects similar to wind speed predictions.

Table 4-1 shows the summary of the results of all WPPs and their determined time scales seasonally. The lowest RMSE, and mean bias and the highest correlation

coefficient values for related time scales have been determined and the best models have been selected among the three NWP models. The table generally explains the model performance of daily and monthly averages indicates same models for same seasons for all WPPs. However, diurnal performance of models could show differences. ECMWF and GFS have almost same performance for all models. ALADIN results are better for WPP-1, 3. ECMWF model results are better for winters. GFS results are mostly less successful than others. WPP-6 diurnal GFS results is interestingly better, while daily and monthly performance of ALADIN and ECMWF better than GFS.

Table 4-1 Summary of all results for each WPP

Diurnal	Fall	Winter	Spring	Summer
WPP-1	GFS	GFS	ECMWF	ALADIN
WPP-2	ECMWF	ALADIN-ECMWF	ECMWF	ECMWF
WPP-3	ALADIN	ALADIN	ALADIN	ALADIN
WPP-4	ECMWF-GFS	ECMWF	ECMWF	ECMWF
WPP-5	ECMWF	ECMWF	ECMWF	ECMWF-GFS
WPP-6	GFS	GFS	GFS	GFS
Daily	Fall	Winter	Spring	Summer
WPP-1	ALADIN	ALADIN	ALADIN	ALADIN
WPP-2	GFS	GFS	GFS-ECMWF	GFS-ECMWF
WPP-3	ALADIN	ALADIN	ALADIN	ALADIN
WPP-4	ECMWF	ECMWF	ECMWF	ECMWF
WPP-5	ECMWF-GFS	ECMWF-GFS	ECMWF-GFS	ECMWF-GFS
WPP-6	ECMWF	ECMWF	ALADIN	ALADIN
Monthly	Fall	Winter	Spring	Summer
WPP-1	ALADIN	ECMWF	ALADIN	ALADIN
WPP-2	GFS	ECMWF	ECMWF	GFS
WPP-3	ALADIN	ALADIN	ALADIN	ALADIN
WPP-4	ECMWF	ECMWF	ECMWF	ECMWF
WPP-5	ECMWF-GFS	ECMWF-GFS	ECMWF-GFS	ECMWF-GFS
WPP-6	ECMWF	ECMWF	ALADIN	ALADIN

CHAPTER-5

5. EVALUATION OF INCOME AND WIND POWER FORECASTS

Wind power affects to market prices. Due to examine behaviors of Turkish Electricity Market according to wind energy, diurnal and monthly variation of errors have been examined in this chapter. Firstly YEKDEM prices and Day Ahead Market Prices (DAMP) have been calculated by using actual power data and formulas that explained in Chapter 1 (Equation 2). These incomes have been compared to power and wind speed averages to define the relationship between wind speed predictions and incomes. Market Clearing Prices, System Marginal Prices and other market values have been taken from EXIST for 2012-2017 years [62]. Exchange rate of dollar has been accepted as constant (1 USD \$ = 3 Turkish Liras) during these years.

5.1. Diurnal Variation of Income

Diurnal variation of wind speed and power had been determined in Chapter 3. Diurnal variation is also important for day ahead markets. Following figure explains the Market Clearing Prices (MCP) and System Marginal Prices (SMP) for diurnal averages. If MCP is higher than the SMP, energy surplus occurs. It should be said that energy surplus is effected Turkish Electricity Market during the day and night for 2012-2017. SMP is important for Balancing Power Markets and MCP represents the day ahead markets [63].



Figure 5.1 Diurnal Variation of Market Prices (2012-2017)

Figure 5.2 explains the diurnal variation of Power, Wind Speed and Incomes (YEKDEM and Day-ahead Market incomes-TL/MWh) for each WPP and prediction values. The topmost graph in the figure indicates to Power (lines) and Power Prediction values (dash), the graph in the middle shows the wind speed (line) and final wind speed predictions (dash) and the graph in the bottom explains the income in terms of YEKDEM and Day Ahead Market Prices (DAMP). It shows that wind speeds start to decrease from midnight to midday depending on wind speed and power diurnal variation. Particularly day ahead market prices affected by wind speed and power as it is expected. The figure also shows the DAMP incomes is higher than the YEKDEM incomes by depending on the higher wind speeds. YEKDEM incomes starts to decrease until morning hours. WPP-2 has the highest income due to the 240 MW installed capacity.

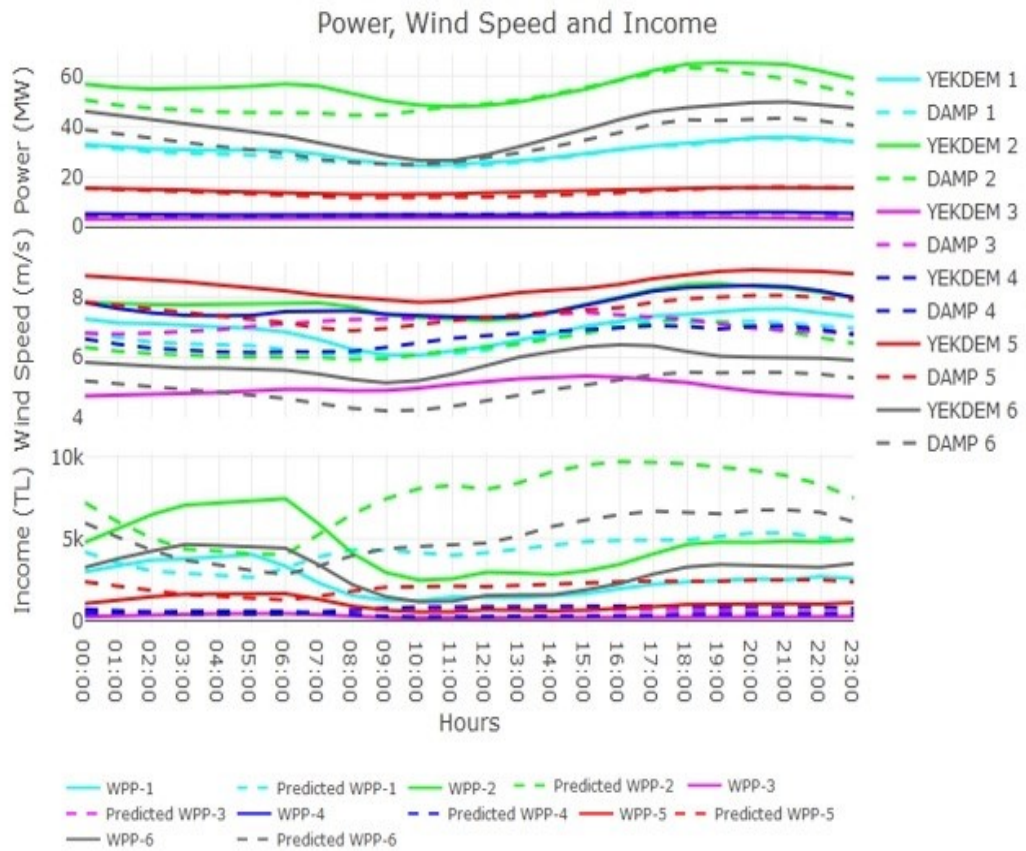


Figure 5.2 Diurnal Variation of Income for all WPPs

5.2. Monthly Variation of Income

Figure 5.3 indicates monthly average Power, Wind Speed and Income (Day Ahead and YEKDEM Prices) for 6 WPPs in this study. The dash lines indicates power predictions, wind speed predictions and day ahead market prices. The lines explains the wind speed, power and MCP. The figure genarraly explains monthly average income for all WPPs is higher at summer months depending on wind speed and power. WPP-2 has highest income due to the heighest installed capacity (240 MW). DAMP monthly avarage incomes are higher than YEKDEM incomes similar to diurnal avarages. YEKDEM incomes are almost constant during the entire year, beacuse of

constant prices. For example YEKDEM prices are higher than DAMP during the March and April for WPP-2. Wind speed monthly averages has lowest for this months (see figure 3.19). It mean, YEKDEM prices are safer then day ahead markets.

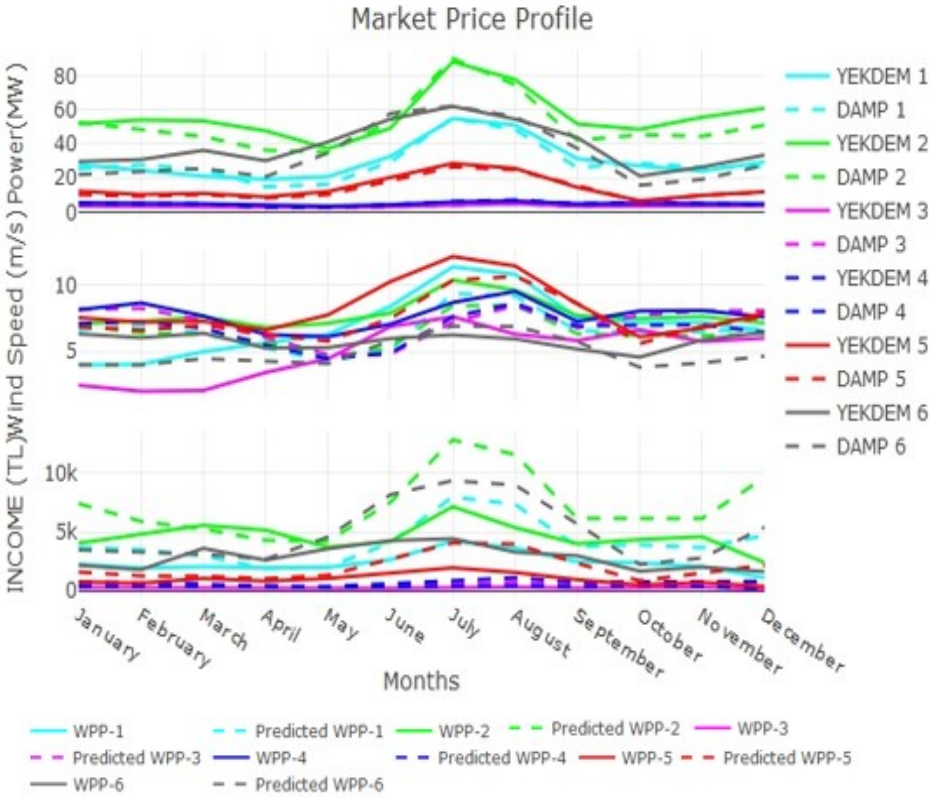


Figure 5.3 Monthly Average Variation of Income

Although diurnal and monthly variation of incomes has advantages for day ahead market, YEKDEM gives sale guarantee to the firms. However income from day ahead market should be better than YEKDEM if the WPP takes the risks due to the wind speed fluctuations. Day ahead market incomes requires well predicted MCP and wind power forecasts due to maximize income.

CHAPTER 6

6. SUMMARY, CONCLUSIONS and RECOMMENDATIONS

In this study, wind speed predictions from two different numerical weather prediction models namely; ALADIN and WRF used in RITM system are evaluated at 6 wind power plants from 3 geographical regions in Turkey. In evaluation, WRF model is configured by two different initial conditions from ECMWF and GFS. First geographical characteristics of each wind power plant has been examined and compared to each other. Secondly, characteristics of WPPs' in terms of energy, wind speed, turbine and installed capacities have been examined. General meteorological conditions of each WPP have also been evaluated. Thirdly, wind speed, direction, temperature and energy production variables belongs to each WPP have been compared in monthly, hourly and daily time scales in terms of RMSE, bias and correlation coefficients. Each NWP has 4 grids around the wind observation station. Therefore, grid performances have been statistically examined to find best grid for each season and model. After finding the best grid for each model, diurnal variation of predictions has been examined for each season. Energy production values have also been compared with the final energy calculated from the combined wind speed prediction in RITM system. The relationship between energy and wind speed along with daily, monthly and seasonal time scales has been determined. Finally, all WPPs have been evaluated at same scales in terms of RMSE and bias to compare the behavior of wind speed errors. In addition to NWP model comparisons, YEKDEM and DAMP income belongs to each WPP have been calculated and compared to wind speed and power values.

Each NWP model has showed different results in different wind farms. According to the site specific conditions at each wind farm, the terrain effects on available wind are different. Therefore, complexity of a terrain also affects to wind power production. Using elevation and roughness data, complexity of each WPP has been ordered more

complex to flat respectively: WPP-6, WPP-5, WPP-2, WPP-1, WPP-4, and WPP-3. Depending on prevailing wind directions and geographical location, seasonality has strong influence on measured and predicted wind speed. Model performances show great variability with seasons. All models and observations have higher wind values in summer. Models also showed better performance in high wind speed measurements in these summer months. Winter prediction errors are generally higher compared to other seasons. WPP-2 showed better performance during all seasons. Winter performance of ECMWF is found better than others almost all WPPs. Monthly analysis are similar to seasonal analysis. GFS had showed better performance for WPP-2 in daily averages. ECMWF is also better for WPP-4, WPP-5 and WPP-6. ALADIN is successful for WPP-1 and WPP-3. In diurnal analysis, nocturnal hours have also more fluctuations than other hours during the day. ECMWF and GFS generally showed similar behaviors for all WPPs. ALADIN is found better in WPP-1 and 3. ECMWF is better for WPP-2 predictions. ECMWF and GFS have better and similar performance for WPP-4 and 5. ECMWF has slightly lower errors than GFS for WPP-4. ECMWF is better for WPP-5 in winter. GFS also has higher performance for WPP-6 unlike ECMWF. Wind speeds are lower during midday and higher from sunset to sunrise. The error rates behaviors during the day are similar to wind speeds. In addition to these results, the reliability of energy prediction strongly depends on the accuracy of predicted and measured wind speed. YEKDEM prices showed lower monthly and diurnal averages than DAMP values belongs to each WPP. However, due to fluctuation and prediction risks all WPPs in this study probably prefers to YEKDEM.

As a result of this study, the importance of numerical weather prediction is found crucial on wind power forecasts. The intermittency in transmission system mostly depends on reliable forecasts. If wind power capacity on an electricity system has to be increased, the performance of wind speed forecasts should be better. From this point of view, it should be noted that, each wind farm has its own characteristics in terms of topographical structure, geographical location and meteorological conditions. Each

NWP model also has its own behavior on different time scales and locations. The model physics such as boundary layer, surface layer and radiation physics that are used in the model configuration affect the wind speed differently at different location and time. Therefore, the sensitivity tests of models for finding proper physics option should be the priority for wind assessment studies. For the simplicity in the current RITM system WRF model is configured with a single domain where initial and boundary conditions are obtained from ECMWF and GFS. However, the model setup can be done with two way interactive nest configuration so that the area of interest can be better resolved and much finer results can be obtained. Long term behavior of wind speeds at each wind farm should be evaluated and specific initial conditions from NWP models should be used in accordance with these evaluations. In addition, the use of ensemble model approach both focusing on number of different initial conditions such as Rapid Update Cycling (RUC) and number of different physics sets could decrease the uncertainty in wind prediction and help better manage the risk associated with wind prediction errors. The importance of long term data from WPPs should also be taken into account. The higher available data gives higher performance evaluation for wind power forecasts. In this way, bias correction method appropriate to each season can be developed to apply in short term forecasts. Wind power forecast systems' NWP predictions should be regulated at specific characteristics belongs to each WPP by using more reliable data. Diurnal and seasonal behavior of wind speed at each WPP should be well determined in a system. Market behavior of predictions also should be examined for long time periods.

REFERENCES

- [1] IPCC, *Renewable Energy Sources and Climate Change Mitigation Special Report of the Intergovernmental Panel on Climate Change*. 2010.
- [2] B. Ernst *et al.*, “Predicting the wind,” *IEEE Power Energy Mag.*, vol. 5, no. 6, pp. 78–89, 2007.
- [3] World Wind Energy Agency Assosiation, “2017 Statistics,” 2018. [Online]. Available: <http://www.wwindea.org/2017-statistics/>. [Accessed: 15-Feb-2018].
- [4] Turkish Wind Energy Assosiation, “Turkish Wind Energy Statistics Summary Report,” 2018.
- [5] Turkey Transmission System Operator, “Genel Günlük İşletme Neticesi,” *Yük Tevzi Bilgi Sistemi*, 2018. [Online]. Available: https://ytbs.teias.gov.tr/ytbs/frm_login.jsf;jsessionid=FB575EA39AC939ACFB5701D1271ACCA4. [Accessed: 02-May-2018].
- [6] Yüksek Planlama Kurulu, *Elektrik Enerjisi Piyasası ve Arz Güvenliği Stratejisi Belgesi*. Türkiye, 2009.
- [7] G. Kariniotakis *et al.*, “What performance can be expected by short-term wind power prediction models depending on site characteristics ?,” *Forecast*, no. November 2016, pp. 22–25, 2004.
- [8] E. L. Petersen, N. G. Mortensen, L. Landberg, J. Højstrup, and H. P. Frank, “Wind Power Meteorology,” *Wind Energy*, vol. 1206, no. December, pp. 2–22, 1997.
- [9] A. L. Manwell, J.F; McGowan, J.G; Rogers, *Wind energy explained: theory, design and application*. John Wiley & Sons, 2010.
- [10] M. Sathyajith, *Wind Energy: Funamentals, Resource Analysis and Economics*. 2006.
- [11] D. Le Gourieres, *Wind Power Plants: Theory and Design*. Elsevier, 2014.
- [12] I. Troen and E. Lundtang Petersen, *European wind atlas*. 1989.
- [13] G. Boyle, *Renewable electricity and the grid: the challenge of variability*. 2012.
- [14] A. M. Foley, P. G. Leahy, A. Marvuglia, and E. J. McKeogh, “Current methods and advances in forecasting of wind power generation,” *Renew. Energy*, vol. 37, no. 1, pp. 1–8, 2012.
- [15] W.-Y. Chang, “A literature review of wind forecasting technology in the

world,” *J. Power Energy Eng.*, vol. 2, no. 4, pp. 161–168, 2014.

[16] K. (2005). Piwko, R., Osborn, D., Gramlich, R., Jordan, G., Hawkins, D., & Porter, “Wind energy delivery issues [transmission planning and competitive electricity market operation].,” *IEEE Power Energy Mag.*, pp. 47–56, 2005.

[17] M. Saguan, “Large - scale wind power in European electricity markets : time for revisiting support schemes and market designs ? Céline Hiroux electricity markets : time for,” *Energy*, no. June, 2009.

[18] L. Vandezande, L. Meeus, R. Belmans, M. Saguan, and J. M. Glachant, “Well-functioning balancing markets: A prerequisite for wind power integration,” *Energy Policy*, vol. 38, no. 7, pp. 3146–3154, 2010.

[19] C. Weber, “Adequate intraday market design to enable the integration of wind energy into the European power systems,” *Energy Policy*, vol. 38, no. 7, pp. 3155–3163, 2010.

[20] J. Jung and R. P. Broadwater, “Current status and future advances for wind speed and power forecasting,” *Renew. Sustain. Energy Rev.*, vol. 31, pp. 762–777, 2014.

[21] X. Zhao, S. Wang, and T. Li, “Review of evaluation criteria and main methods of wind power forecasting,” *Energy Procedia*, vol. 12, pp. 761–769, 2011.

[22] S. S. Soman, H. Zareipour, O. Malik, and P. Mandal, “A review of wind power and wind speed forecasting methods with different time horizons,” *North Am. Power Symp. 2010*, pp. 1–8, 2010.

[23] W.-Y. Chang, “A Literature Review of Wind Forecasting Methods,” *J. Power Energy Eng.*, vol. 2, no. 4, pp. 161–168, 2014.

[24] M. Lei, L. Shiyang, J. Chuanwen, L. Hongling, and Z. Yan, “A review on the forecasting of wind speed and generated power,” *Renew. Sustain. Energy Rev.*, vol. 13, no. 4, pp. 915–920, 2009.

[25] G. Kariniotakis, P. Pinson, N. Siebert, G. Giebel, R. Barthelmie, and others, “The state of the art in short-term prediction of wind power-from an offshore perspective,” *Proc.*, no. OCTOBER, pp. 20–21, 2004.

[26] S. Al-Yahyai, Y. Charabi, and A. Gastli, “Review of the use of numerical weather prediction (NWP) models for wind energy assessment,” *Renew. Sustain. Energy Rev.*, vol. 14, no. 9, pp. 3192–3198, 2010.

[27] General Directorate of Renewable Energy, “Wind Power Monitoring and Forecasting Center (RITM).” .

[28] T.C., *Rüzgar Enerjisi Santrallerinin Rüzgar Gücü İzleme ve Tahmin Merkezine*

Bağlanması Hakkında Yönetmelik. Turkey, 2015.

[29] M. B. Özkan *et al.*, “Verification of a real-time wind power monitoring and forecast system for Turkey,” p. 2.63, 2013.

[30] E. Terciyanli, T. Demirci, D. Küçük, M. Saraç, I. Cadirci, and M. Ermiş, “Enhanced nationwide wind-electric power monitoring and forecast system,” *IEEE Trans. Ind. Informatics*, vol. 10, no. 2, pp. 1171–1184, 2014.

[31] E. Terciyanli *et al.*, “The architecture of a large-scale wind power monitoring and forecast system,” *Int. Conf. Power Eng. Energy Electr. Drives*, vol. 5, pp. 3–8, 2013.

[32] M. Ozkan and P. Karagoz, “A Novel Wind Power Forecast Model: Statistical Hybrid Wind Power Forecast Technique (SHWIP),” *IEEE Trans. Ind. Informatics*, vol. 3203, no. c, pp. 1–1, 2015.

[33] M. B. Özkan, D. Küçük, E. Terciyanli, S. Buhan, T. Demirci, and P. Karagoz, “A data mining-based wind power forecasting method: Results for wind power plants in Turkey,” *Lect. Notes Comput. Sci. (including Subser. Lect. Notes Artif. Intell. Lect. Notes Bioinformatics)*, vol. 8057 LNCS, 2013.

[34] C. E. Koksoy *et al.*, “Improved Wind Power Forecasting Using Combination Methods,” *2015 IEEE 14th Int. Conf. Mach. Learn. Appl.*, pp. 1142–1147, 2015.

[35] S. Buhan and I. Cadirci, “Multistage Wind-Electric Power Forecast by Using a Combination of Advanced Statistical Methods,” *IEEE Trans. Ind. Informatics*, vol. 11, no. 5, pp. 1231–1242, 2015.

[36] S. Buhan *et al.*, “Verification of a very short term wind power forecasting algorithm for Turkish transmission grid,” *Int. Conf. Power Eng. Energy Electr. Drives*, vol. 5, pp. 1217–1221, 2013.

[37] S. Buhan, Y. Özkazanç, and I. Çadirci, “Wind Pattern Recognition and Reference Wind Mast Data Correlations With NWP for Improved Wind-Electric Power Forecasts,” *IEEE Trans. Ind. Informatics*, vol. 12, no. 3, pp. 991–1004, 2016.

[38] T.C., *Elektrik Piyasası Kanunu*. Turkey, 2013.

[39] T.C., *Elektrik Piyasası Dengeleme ve Uzlaştırma Yönetmeliği*. Turkey, 2018.

[40] T.C., *Yenilenebilir Enerji Kaynaklarının Elektrik Enerjisi Üretimi Amaçlı Kullanımına İlişkin Kanun*. Turkey, 2005.

[41] EMRA, *Yenilenebilir Enerji Kaynaklarının Desteklendirilmesi ve Belgelendirilmesine İlişkin Yönetmelik*. Turkey, 2013.

[42] Energy Market Regulatory Authority, *Board Decision*. Turkey, 2018.

- [43] M. Dabernig, “Comparison of different numerical weather prediction models as input for statistical wind power forecasts,” University of Innsbruck, 2013.
- [44] M. F. Bielecki, “Statistical Characterization Of Errors In Wind Power Forecasting,” 2010.
- [45] U. Sīle, T., Beķere, L., Cepīte-Frišfelde, D., Seņņikovs, J., & Bethers, “Verification of Numerical Weather Prediction Model Results for Energy Applications in Latvia,” *Energy Procedia Eur. Geosci. Union Gen. Assem.*, vol. 59, pp. 213–220, 2014.
- [46] S. Alessandrini, S. Sperati, and P. Pinson, “A comparison between the ECMWF and COSMO Ensemble Prediction Systems applied to short-term wind power forecasting on real data,” *Appl. Energy*, vol. 107, no. August 2015, pp. 271–280, 2013.
- [47] M. Lange, “On the Uncertainty of Wind Power Predictions—Analysis of the Forecast Accuracy and Statistical Distribution of Errors,” *J. Sol. Energy Eng.*, vol. 127, no. 2, p. 177, 2005.
- [48] H. Holttinen, J. Miettinen, and S. Sillanpää, *Wind power forecasting accuracy and uncertainty in Finland*. 2013.
- [49] “ALADIN.” [Online]. Available: <http://www.umr-cnrm.fr/spip.php?article122>. [Accessed: 02-May-2018].
- [50] W. C. Skamarock *et al.*, “A Description of the Advanced Research WRF Version 3,” *Tech. Rep.*, no. June, p. 113, 2008.
- [51] “Corine 2006.” [Online]. Available: <https://www.eea.europa.eu/data-and-maps/data/clc-2006-raster>. [Accessed: 15-Apr-2017].
- [52] “WASP Map Editor.” [Online]. Available: <http://www.wasp.dk/dataandtools#map-editor>. [Accessed: 15-Feb-2018].
- [53] “Global Mapper.” [Online]. Available: <http://www.bluemarblegeo.com/products/global-mapper.php>. [Accessed: 12-Feb-2018].
- [54] “WindSIM.” [Online]. Available: <https://windsim.com/>. [Accessed: 15-Feb-2018].
- [55] “R Project.” [Online]. Available: <https://www.r-project.org/>. [Accessed: 10-Mar-2017].
- [56] “Windographer.” [Online]. Available: <https://www.windographer.com/download>. [Accessed: 06-Sep-2017].

- [57] S. Erinç, *Climatology and its methods*. Istanbul University Press, 1984.
- [58] MGM, “İklim Sınıflandırmaları,” *Meteoroloji Genel Müdürlüğü, Klimatoloji Şube Müdürlüğü*, p. http://www.mgm.gov.tr/FILES/iklim/iklim_siniflandi, 2015.
- [59] GDRE, “Wind Energy Potential Atlas of Turkey (REPA),” 2006.
- [60] S. Sensoy, M. DEMİRCAN, Y. ULUPINAR, and İ. BALTA, “Climate of Turkey,” *Repub. Turkey Minist. Environ. For. Turkish state Meteorol. Serv. Retrieved December*, vol. 10, p. 2007, 2008.
- [61] EPDK, “Çeyrek Tarife Tabloları,” 2018.
- [62] EXIST, “General Reports.” [Online]. Available: <https://rapor.epias.com.tr/rapor/xhtml/ptfSmfListeleme.xhtml>. [Accessed: 19-Jan-2018].
- [63] EXIST, “Sistem Marjinal Fiyatı.” [Online]. Available: <https://www.epias.com.tr/dengeleme-guc-piyasasi/smf-hesaplanmasi>.